LOW NONLINEARITY OPTICAL FIBERS FOR BROADBAND AND LONG-DISTANCE COMMUNICATIONS

Haroldo T. Hattori

Dissertation submitted to the Faculty of the
Virginia Polytechnic Institute and State University
in partial fulfillment of the requirements for the degree of

Doctor of Philosophy

in

Electrical and Computer Engineering

Ahmad Safaai-Jazi, Chair

Ioannis M. Besieris

Lee W. Johnson

Ting-Chung Poon

Wayne A. Scales

February 11, 1998

Blacksburg, Virginia

Key words: Low nonlinearity fiber designs, fiber-optics communications

LOW NONLINEARITY OPTICAL FIBERS FOR BROADBAND AND LONG-DISTANCE COMMUNICATIONS

Haroldo T. Hattori

(ABSTRACT)

A class of low nonlinearity dispersion-shifted and dispersion-flattened fibers for broadband and long haul applications is presented. The refractive index profiles of these fibers assume a depressed-core multi-clad geometry in order to achieve effective-areas much larger than those in conventional optical fibers.

A systematic approach for designing large effective-area dispersion-shifted fibers, using a reference W-index profile to initiate the design, is presented. Transmission properties, including effective-area, mode-field-diameter, dispersion, dispersion slope, cutoff wavelength, and bending, microbending and splice losses are evaluated for several design examples. To ascertain that the proposed fibers can be practically fabricated, the effects of varying fiber dimensions and indices on effective-area, mode-field-diameter and dispersion are assessed.

It is shown that there is a trade-off between effective-area and mode-field-diameter and, generally, larger effective-areas are associated with larger mode-field-diameters. In other words, less signal distortion due to fiber nonlinearity (larger effective-area) is associated with higher power loss due to bending of fiber (larger mode-field-diameter). Thus, a large effective-area and low bending loss are conflicting requirements. A parameter Q is defined as a performance indicator, considering effective-area and mode-field-diameter.

Dispersion-shifted single-mode fiber designs with effective-areas of 78 mm^2 to 210 mm^2 and the corresponding mode-field-diameter of 8.94 mm to 14.94 mm, dispersion less than

0.07 ps/nm.km, and dispersion slope of about 0.05 ps/ nm^2 .km are presented. Numerical simulations for propagation of pulses in few designed fibers are performed.

Designs of large effective-area dispersion-flattened fibers are also presented, for the first time we believe. These fibers provide large effective-area and low dispersion over an extended range of wavelengths. For our design, over the wavelength range of 1.48 mm < l < 1.58 mm, the effective-area is 75 mm^2 to 100 mm^2, while the dispersion remains below 0.7 ps/nm.km.

Acknowledgments

I would like to thank Dr. Ahmad Safaai-Jazi for his guidance, advice and support during my Ph.D. research at Virginia Tech. I appreciated the opportunity of exploring the area of optical fiber design which helped me to expand my knowledge horizon.

I also acknowledge the advice and teachings of my committee members: Drs. Besieris, Lee Johnson, Poon and Scales. Their suggestions for improving the quality of this work are sincerely appreciated. Additionally, I would like to recognize the teachings and advices of Dr. Jacobs.

Finally, I would like to dedicate this dissertation to my family, specially to my wife Maria Conceição Nogueira Hattori. Without their patience and support, none of this work would have been possible. Also, I would like to remember my father who would be very glad to see his second son obtaining a Ph.D. degree.

Table of Contents

List of Tables

List of Figures

Chapter 1

Introduction

With the advent of Erbium-doped optical fiber amplifiers, a major obstacle for the transmission of optical signals over long distances without electronic repeaters, namely attenuation, has been removed [1-4]. However, apart from fiber losses that can be compensated by optical amplifiers, the signal also suffers distortions from dispersion and nonlinearities. Dispersion can be avoided by employing ordinary dispersion-shifted or dispersion-flattened fibers [5], but the harmful effects of nonlinearities remain a limiting factor for long distance transmission [6]. Nonlinearities play a particularly important role in very long links where their effects cannot be neglected.

Many researchers have analyzed the effects of nonlinearities in long-distance optical fiber links. Marcuse [7] has discussed the effects of nonlinearities in single-channel systems. For negative dispersion, nonlinearities help dispersion to broaden pulses and cause inter-symbol interference (ISI) among these pulses. When the system is operating under positive dispersion, the sequence of pulses tends to break into solitons, leading to broadening of the spectrum and consequently resulting in pulse distortion. This is in contrast to pico-second soliton pulse propagation in which fiber nonlinearity perfectly compensates dispersion and no distortion results. Under zero-dispersion condition and in the absence of noise, no pulse distortion would occur even if nonlinearity exists. However, simulations have shown that when noise is present, nonlinearity pumps up the noise generated by optical fiber amplifiers at the expense of the signal power [7].

Marcuse et al. [8] have also studied the effects of Kerr nonlinearities in WDM systems. They have derived a pseudo-spectral method for analyzing nonlinear fiber optics systems. Various systems are considered in their analysis, but of special interest are single-channel and multi-channel systems. For single-channel systems, they obtained similar conclusions as in [7]. For a two-channel ASK (Amplitude Shift-Keying) system, they predicted error-free transmission at 2.5 Gb/s per channel for distances up to 7500 km, provided that both channels operate under negative dispersion and spaced 2 to 3 nm apart. Li [9] also has discussed long-distance systems with

optical fiber amplifiers. For multi-channel wavelength division multiplexed systems, he has determined that dispersion and nonlinearity are the major limiting factors for transmission over very long links. He has presented several examples of long-distance systems that have already been implemented.

Fiber nonlinearity is due to weak dependence of the refractive index of glass on light intensity [10-11]. This dependence may be expressed as $n = n_L + n_{NL}$, where n_L and n_{NL} are the linear and nonlinear parts of the refractive index, respectively. The nonlinear term may be described by $n_{NL} = \hat{N}P / A_{eff}$, where $\hat{N}$ is a property of fiber material, P is the power of the optical signal inside the fiber, and A_{eff} is the effective-area [11]. From this expression, it is clear that the larger the effective-area the weaker is the power density inside a fiber. By decreasing the power density inside a fiber, nonlinear effects become weaker. Therefore, in order to minimize the effects of nonlinearities, large effective-area fibers should be used.

Several research groups have investigated low-nonlinearity dispersion-shifted fibers. Effective-areas ranging from 70 mm^2 to 90 mm^2 have been reported in the literature [12-17]. Nouchi et al. in a pioneering work [12] reported a 70 mm^2 effective-area dispersion-shifted fiber with bending losses lower than 0.005 dB/m for 30 mm bending radius. Using such fibers, they demonstrated improvement in the transmission of 10 Gb/s-19 Mm soliton waves. Typical amplifier spacing for soliton systems is 26km to 46 km, but by using a 70 mm^2 effective-area fiber, they were able to increase the repeater spacing up to 63 km [13]. Liu et al. [14] have designed large effective-area dispersion-shifted fibers with effective-areas as large as 91 mm^2. They have used a dual-ring index profile structure to increase the effective-area. Their design also prevents large bending losses and maintains a dispersion slope of nearly 0.1 $ps / nm^2 . km$. They have fabricated these large effective-area fibers by employing the 'outside vapor deposition' method (OVD) and measured effective-areas on the order of 80 mm^2 to 91 mm^2. Arai et al. [15] have employed a dual-shape core structure to design low nonlinearity dispersion-shifted fibers. Effective-areas as large as 90 mm^2 and mode-field-diameters on the order of 9.1 mm were obtained. For a bending diameter of 30 mm, they have measured bending losses as low as 0.05

dB/m. They have used the 'vapor axial deposition' (VAD) process to fabricate their fibers. Kato et al. [16] slightly changed the dual-core structure in [15] by introducing a depressed cladding. They achieved effective-areas as large as 85 mm^2 with mode-field-diameters of about 10.6 mm. Their designs provide a dispersion slope of about 0.11 $ps/nm^2.km$ and bending losses of 0.1 dB/m for a bending diameter of 30 mm. Also, they state that tolerable bending losses are obtained for mode-field-diameters less than 11 mm with bending radii of 30 mm or more [16]. The vapor axial deposition process was also employed to fabricate these fibers. Research on large effective-area fibers is actively pursued nowadays, and the scope of work is expanding to include other dispersion-altered fibers such as dispersion-flattened and non-zero dispersion-shifted fibers [17-21].

An exhaustive survey of literature revealed that, so far, there has not been a comprehensive investigation on the design and analysis of large effective-area fibers. Much of the work reported in recent years amount to preliminary experimental research on these fibers. Furthermore, some of the conflicting design requirements necessitate a trade-off analysis and development of a scheme for optimization of the design. It is the aim of this research to present a thorough and comprehensive study of large effective-area fibers for broadband and long distance communications.

There are several design requirements for low nonlinearity single-mode fibers, including low dispersion in the wavelength range of operation, larger effective-area than in conventional fibers, low losses (intrinsic, splice, microbending, and bending losses), and cutoff wavelength well below the wavelength of operation. However, the design requirements cannot be satisfied independently; for example, a larger effective-area generally implies a larger bending loss, and satisfactory designs must provide a reasonable value of bending loss. Thus, a trade-off between effective-area and bending loss is unavoidable.

The structures used to design the large effective-area fibers consist of a depressed central core and several claddings. The cladding layer surrounding the central core assumes the highest refractive index. The motivation in choosing this index profile is to let the electromagnetic fields spread more into the claddings and hence increase the effective-area of the fiber. The approach

adopted here is to start with a reference fiber that provides zero dispersion at 1.55 mm and reduce the refractive index of a central portion of the core region. A W-index fiber is chosen as the reference fiber. Reducing the index of a portion of its core region, a depressed-core triple-clad structure is created in which the first inner cladding assumes the highest refractive index. This modification of index profile moves the zero-dispersion wavelength away from 1.55 mm. Then, indices and dimensions of different layers are adjusted so that the zero-dispersion wavelength is shifted back to 1.55 mm.

The proposed depressed-core multi-clad large effective-area fibers are analyzed using the weakly guiding approximation. This approximation is justified by the fact that all materials used in the fiber fabrication have small refractive index differences. In the weakly guiding approximation, the electromagnetic fields are quasi-TEM, with longitudinal components of the fields being very small compared to the transverse components. The field solutions are then obtained by solving the scalar wave equation. Boundary conditions result in a characteristic equation from which the propagation constant at a certain wavelength can be determined. To enhance the accuracy of results, a vector correction term is added to the scalar propagation constant. The wavelength dependence of the refractive index is directly accounted for by expressing each refractive index in terms of a third-order Sellmeier equation. With the knowledge of the propagation constant and field solutions, second and third order dispersions, effective-area, and extrinsic losses can be calculated.

Dispersion-shifted fibers with effective-areas several times larger than those in conventional dispersion-shifted fibers have been designed based on the depressed-core index profile [21]. These fibers provide dispersion less than 0.06 ps/nm.km and a dispersion slope less than 0.06 $ps/nm^2.km$ at 1.55 mm. Their splice and microbending losses are comparable to those in conventional fibers. The intrinsic losses are also expected to be low due to the fact that index differences are very small (less than 1%). The cutoff wavelengths for the designed fibers are well below 1.55 mm. The bending losses of these fibers can be kept at a tolerable level if the bending radius is made sufficiently large (say > 30 mm).

In designing large effective-area dispersion-shifted fibers, it was noted that there exists many possibilities for achieving both large effective-area and negligible dispersion at l = 1.55 mm. Now, the question is which fiber offers a better performance; namely, less signal distortion and less loss. The design data indicate that there is a trade-off between the effective-area that provides a measure of signal distortion due to nonlinearity and the mode-field-diameter that is an indicator for bending loss. Assuming that all other losses such as intrinsic and microbending losses are about the same for all designed fibers, the performance of a design may be assessed in terms of a quality factor defined as the ratio of effective-area over the square of mode-field-diameter. This factor is a dimensionless quantity that can be used to determine the tradeoff between mode-field-diameter and effective-area. Then, among several designs satisfying certain limits on effective-area and mode-field-diameter the fiber that provides the largest quality factor is the best design. The quality factor for conventional dispersion-shifted fibers is about 0.741 [22] and for the large effective-area dispersion-shifted fibers designed here varies on the range of 0.78 to 1.03.

Wavelength-division-multiplexed systems have been rapidly developing in recent years. These systems allow many-fold increases in information carrying capacity using a single optical fiber. WDM systems with 32 channels are envisioned to be implemented in the near future. However, with many optical channels present in the fiber, the overall power density is many times larger than that in a single-channel fiber-optic communication system. This makes the effect of nonlinearities even more important. These effects have been studied in WDM systems using dispersion-shifted fibers [23-25]. Apart from dispersion-shifted fibers, dispersion-flattened fibers have been considered a potential candidate for WDM systems.

Prior to 1998, research on large effective-area fibers was limited to dispersion-shifted fibers only. The depressed-core multi-clad fiber geometry can also be employed to design large effective-area dispersion-flattened fibers. For the first time, we presented large effective-area dispersion-flattened fibers for wavelength-division-multiplexing applications [26]. These fibers provide large effective-area and low dispersion over an extended range of wavelength. For our design, over the wavelength range of 1.48 mm < l < 1.58 mm, the effective-area is 75 mm^2 to 100 mm^2, while the dispersion remains below 0.7 ps/nm.km [26]. Very recently, other researchers

have also reported preliminary results of their investigations on large effective-area dispersion-flattened fibers [18].

Although larger effective-areas imply less signal distortion, to obtain a quantitative assessment of the improvement in the performance of the system, numerical simulations of pulse propagation in several designed fibers are performed. In these simulations, the increase in transmission distance compared to conventional dispersion-shifted fibers, is determined for error-free transmission. The input power, fiber loss, and dispersion are assumed to be the same for the conventional and designed large effective-area fibers. Pseudo-spectral methods, such as the split-step Fourier method, are used to numerically solve the nonlinear Schrödinger equation. These methods are highly efficient because they employ fast Fourier transform algorithms, and are much faster than finite element and finite difference methods.

Chapter two presents a formulation of principal propagation characteristics of depressed-core multiple clad fibers. The scalar wave method is used to determine the field solutions. The formulation is sufficiently general to accommodate any five-layer cylindrical dielectric waveguide with an arbitrary multi-step index profile. Expressions for dispersion relation, vector correction term for scalar propagation constant, dispersion, effective-area and mode-field-diameter are derived. Finally, the formulation of the extrinsic losses of the fiber, including splice, microbending, and bending losses, is addressed in this chapter.

Chapter three summarizes nonlinear effects in optical fibers. A short introduction to stimulated scattering is presented, but special attention is devoted to the nonlinear refraction. The nonlinear Schrödinger equation is derived. A brief description of the first-order soliton is presented.

Chapter four addresses the design of large effective-area dispersion-shifted and dispersion-flattened fibers. An iterative approach is used to determine the dimensions and indices (material compositions) of fibers which satisfy the desired design requirements. The process involves numerical solution of the dispersion relation and subsequent evaluation of various propagation properties including dispersion, dispersion-slope, cutoff wavelength, effective-area, mode-field-diameter, and fiber losses (splice, microbending and bending losses) are assessed.

Chapter five presents a tolerance analysis for the designed large effective-area fibers. The effects of small variations in fiber parameters on the propagation characteristics, particularly on dispersion, effective-area, and mode-field-diameter are presented. Tolerance analysis are very important to determine the viability of fabricating a certain optical fiber. Large changes in propagation properties due to small variations in the fiber parameters are quite undesirable.

Chapter six examines the propagation of optical pulses inside a fiber. Simulation results for pulse propagation in designed large effective-area dispersion-shifted fibers are obtained by numerically solving the nonlinear Schrödinger equation. The analysis is performed for different power levels and dispersion values.

The conclusions of the dissertation and directions of further work are summarized in Chapter 7. The significance of this work and the impact of large effective-area on long-haul terrestrial and submarine fiber-optic links are pointed out in this chapter.

Chapter 2

Propagation Characteristics of Depressed-core Multiple-Clad Optical Fibers

In this chapter, the principal transmission properties of an optical fiber are addressed. These properties describe how light is coupled from one fiber into another and how pulses are attenuated and distorted in optical fibers. In particular, dispersion, cutoff wavelength, effective-area, mode-field-diameter, and fiber losses are addressed. A scalar-wave analysis will be employed. This analysis is sufficiently accurate if fiber materials have small index differences. The accuracy of results is enhanced by adding a correction term to the scalar propagation constant.

2.1 Scalar-Wave Analysis

It is well known that the constituent materials of practical optical fibers have nearly equal refractive indices, so that the waveguiding region of a fiber appears like a nearly homogeneous medium. In this case, the fields inside the optical fiber are quasi-TEM (Transverse ElectroMagnetic) and have only small components along the direction of propagation [27]. The polarization effects due to different layers are small and the fields may be described as a linear combination of scalar modes oriented along transverse Cartesian coordinates (x or y direction). These considerations allow us to examine the propagation properties inside a fiber based on the scalar wave analysis.

The materials constituting the fiber are assumed to be isotropic, homogeneous, and low loss dielectrics. Initially, it is assumed that fiber is a linear medium and nonlinearities will be accounted for as a perturbation to the "linear state" in a later chapter. These nonlinearities are weak in general and the principal nonlinearity to be considered here is the Kerr effect.

Assuming that fields are time-harmonic with angular frequency w and travel in the +z direction, the expressions for electric and magnetic fields in a cylindrical coordinate system (r, f, z) are given by, [28]

$$\vec{E}(r,f,z) = y(r,f)\begin{Bmatrix}\hat{a}_x\\ \hat{a}_y\end{Bmatrix}e^{j(wt-bz)}e^{-az} \tag{2.1a}$$

$$\vec{H}(r,f,z) = Y_0 n(r)\hat{a}_z \times \vec{E}(r,f,z) \tag{2.1b}$$

where $\vec{E}$ is the transverse electric field, $\vec{H}$ is the transverse magnetic field, $y(r,f)$ is a scalar function describing the transverse distribution of fields, b is the propagation constant, w is the radian frequency of the light, a is the attenuation constant, n(r) is the refractive index as a function of the radial coordinate, $Y_0 = \sqrt{e_0 / m_0}$ is the free-space admittance, and $\hat{a}_x$ and $\hat{a}_y$ are unit vectors in the x and y directions, respectively.

Figure 2.1 shows the geometry and coordinates for a multi-layer cylindrical dielectric waveguide. The z-axis is assumed to coincide with the optical fiber waveguide. In an ith region with refractive index n_i, the function $y(r,f)$ is the solution of the following scalar-wave equation [29]:

$$\frac{1}{r}\frac{\partial}{\partial r}\left(r\frac{\partial y}{\partial r}\right)+\frac{1}{r^2}\frac{\partial^2 y}{\partial f^2}+\left[\left(\frac{2p}{l}n_i\right)^2 - b^2\right]y = 0 \tag{2.2}$$

Using the method of separation of variables, the solution to (2.2) is obtained as, [29,30]

$$y(r,f) = \left[A_i J_n(x_i r) + \overline{A}_i Y_n(x_i r)\right]Q(f) \qquad if\ \ b < \frac{2p}{l}n_i \tag{2.3a}$$

or

$$y(r,f) = \left[A_i I_n(x_i r) + \overline{A}_i K_n(x_i r)\right]Q(f) \qquad if\ \ b > \frac{2p}{l}n_i \tag{2.3b}$$

with

$$x_i = \sqrt{\left|b^2 - \left(\frac{2p}{l}\mathrm{n_i}\right)^2\right|} \qquad (\mathrm{i}= 1, 2, \ldots, \mathrm{N}) \tag{2.3c}$$

$$Q(f) = \begin{Bmatrix}\cos(nf)\\ \sin(nf)\end{Bmatrix} \tag{2.3d}$$

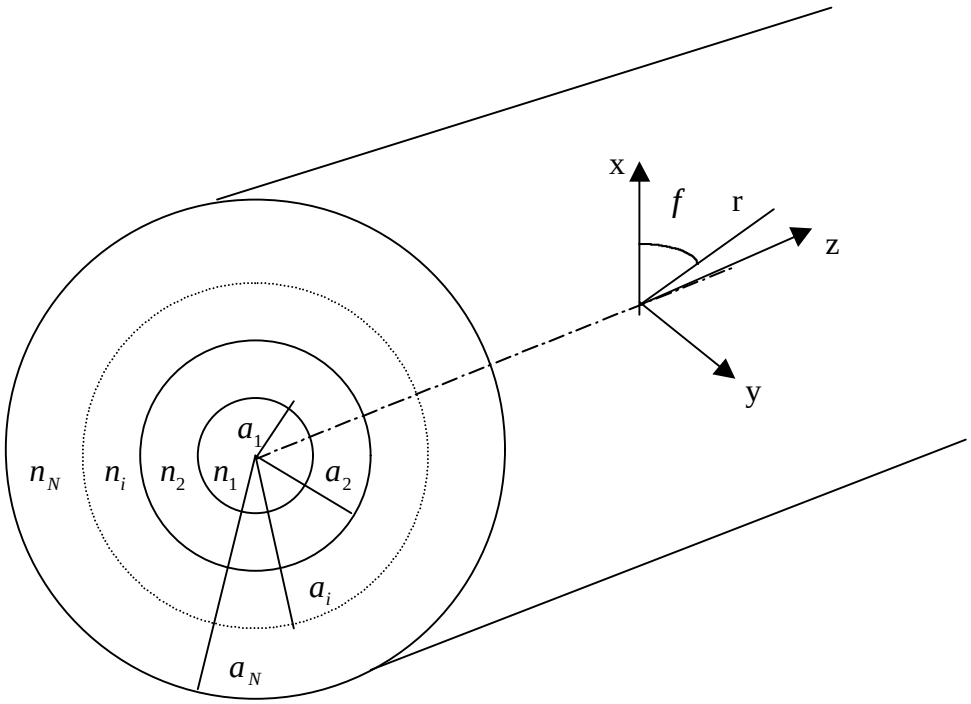

Figure 2.1 Geometry and coordinates for a cylindrical multi-layer optical fiber waveguide.

and A_i and $\overline{A}_i$ are arbitrary constants, n is an integer, J_n is the Bessel function of first kind of order n, Y_n is the Bessel function of second kind of order n, I_n is the modified Bessel function of first kind of order n, and K_n is the modified Bessel function of second kind of order n. In the region that includes the origin (r=0), Y_n and K_n functions must be excluded from the solution because they are undefined at the origin. Also, in the outer cladding layer the solutions involve only K_v functions to ensure that fields remain bounded as r approaches infinity.

The discrete "approximate solutions" derived from the scalar wave equation are called linearly polarized modes and are designated as LP_{nm}, where m is the order of mode for a given value of n; m=1, 2, 3, …. The fundamental mode is the LP_{01} mode, while the next propagating mode is the LP_{11} mode.

The index profiles of the structures to be analyzed here are shown in Figure 2.2. They include three to five layers, a central core and several claddings. In most of the fibers designed

here, the second layer (first cladding) assumes the highest refractive index. The most external cladding is assumed to have an infinite thickness (in practice, the most external layer has a finite but sufficiently large radius a_N such that $y(a_N, f) \approx 0$).

For an N-layer fiber, the solution of the scalar function y is summarized as (after dropping the common term $Q(f)$):

$$y(r) = \begin{cases} A_1 Z_{n1}(x_1 r), & 0 \le r \le a_1, \\ A_i Z_{ni}(x_i r) + \bar{A}_i \bar{Z}_{ni}(x_i r), & a_{i-1} < r \le a_i;\ i = 2,3,\ldots,N-1, \\ \bar{A}_N K_n(x_N r), & r > a_{N-1}, \end{cases} \tag{2.4}$$

where

$$Z_{ni} = \begin{cases} J_n, & if\ b < k_0 n_i, \\ I_v, & if\ b > k_0 n_i, \end{cases} \tag{2.5a}$$

$$\bar{Z}_{ni} = \begin{cases} Y_n, & if\ b < k_0 n_i, \\ K_v, & if\ b > k_0 n_i, \end{cases} \tag{2.5b}$$

and $k_o = 2p / l$, A_i and $\bar{A}_i$ are constant amplitude coefficients.

For guided modes, it is required that $n_N \le \bar{b} \le n_{\max}$, where $n_{\max}$ is the maximum refractive index in the fiber and $\bar{b} = b / k_0$. Continuity of the tangential field components is maintained if $y(r, f)$ and its radial derivative $dy(r, f)/dr$ are continuous at the boundaries. The boundary conditions result in a system of 2N-2 equations with 2N-2 unknowns. In order to avoid a trivial solution, the determinant of coefficients for this system of equations must be zero. This results in a relation which is a function of frequency, propagation constant, and fiber parameters. In the remainder of this chapter, the discussion is limited to fibers with five or less layers. For a five-layer fiber, the dispersion relation is summarized as,

$$\frac{(h_1 - h_3)(h_7 - h_4) - h_{15}(h_1 - h_2)(h_7 - h_5)}{(h_1 - h_3)(h_6 - h_4) - h_{15}(h_6 - h_5)(h_1 - h_2)} = h_{16} \frac{(h_{14} - h_{13})(h_9 - h_{10}) - h_{17}(h_9 - h_{11})(h_{14} - h_{12})}{(h_{14} - h_{13})(h_8 - h_{10}) - h_{17}(h_8 - h_{11})(h_{14} - h_{12})} \tag{2.6}$$

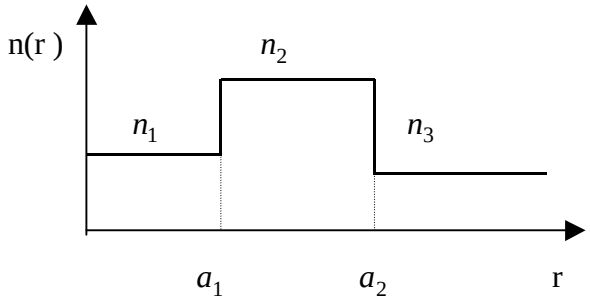

(a)

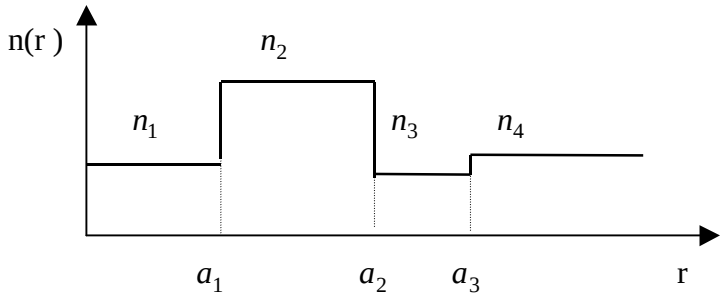

(b)

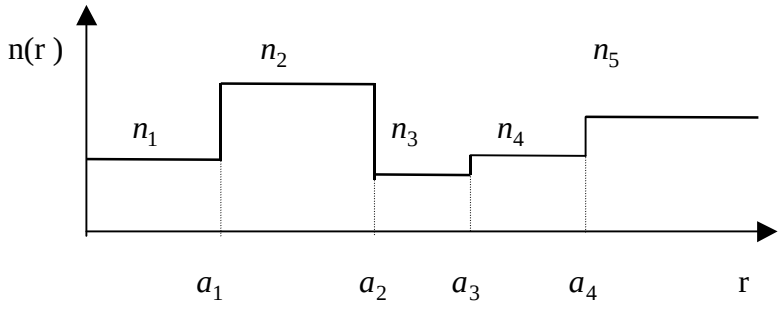

(c)

Figure 2.2 - Index profiles for several multiple-clad fibers. In all fibers, the first cladding assumes the highest refractive index.

where $h_i; i = 1, \ldots 17,$ are found in Appendix A. For four-layer fibers, we can shrink layer 4 to have zero thickness and for three-layer fibers, layers 3 and 4 can be shrunk to have zero thickness. For the LP_{01} dominant mode n =0.

From equation (2.6), the normalized scalar propagation constant $\bar{b}$ is obtained for given fiber parameters and for a desired mode versus wavelength. In order to determine $\bar{b}$, a numerical root search technique such as the bisection method is employed. The numerical results will be presented in Chapter 4.

2.2 Vector Correction to the Scalar Propagation Constant

The weakly guiding approximation based on the scalar-wave analysis is sufficiently accurate when the refractive indices of the fiber are slightly different. This approximation for most cases of practical interest is adequate. However, the solution is not exact and may not provide the required accuracy for predicting the information capacity of ultra wideband fibers. Thus, to improve the accuracy a "vector correction" term is added to the normalized propagation constant. The vector-corrected normalized propagation constant $\bar{b}_n$ is obtained from the following equation [28],

$$\bar{b}_n^{\,2} - \bar{b}^{\,2} = -\frac{l^2}{4p^2}\frac{\iint \left(\nabla_t . \vec{E}\right)\left\{\vec{E}.\nabla_t \ln\left[\mathrm{n}^2(r)\right]\right\} dS}{\iint \left|\vec{E}\right|^2 dS} = -\frac{l^2}{4p^2}\frac{\sum_{i=1}^{N-1}\left[ry(r)\frac{dy(r)}{dr}\right]_{r=a_i} \ln\left(\frac{n_{i+1}}{n_i}\right)}{\int_0^\infty y^2(r) r dr} \tag{2.7}$$

where the electric field $\vec{E}$ is defined in (2.1a), ∇_t is the transverse part of 'del' operator (in the cylindrical coordinate system, $\nabla_t = \frac{\partial}{\partial r}\hat{a}_r + \frac{1}{r}\frac{\partial}{\partial f}$), the double integrals are over the cross section of the fiber.

Substituting for $\vec{E}$ and evaluating the integrals in (2.7), the expression for the vector corrected propagation constant $\overline{b}_v$, for the LP_{01} mode in a five-layer fiber, is found to be equal to:

$$\overline{b}_v^2 = \overline{b}^2 - \frac{l^2}{4p^2 P}\{c_1 + c_2 + c_3 + c_4\} \tag{2.8}$$

where the expressions for c_i, i=1, 2, 3 and 4 and for P are found in Appendix B. As the system of equations has a nontrivial solution, all A_i i=2, 3, …, 8 can be expressed in terms of A_1.

2.3 Material Compositions

The dependence of the refractive indices on the wavelength can be expressed in terms of Sellmeier's relation, [31]

$$n_k^2 = 1 + \sum_{p=1}^{3} \frac{A_{kp}\, l^2}{\left(l^2 - l_{kp}^2\right)} \tag{2.9}$$

where n_k is the refractive index of material k, A_{kp} are the Sellmeier's coefficients, l_{kp} are the wavelength resonances, and l is the operating wavelength. Equation (2.9) accurately describes the behavior of the refractive indices when the operating wavelengths are far from resonance [31]. At the resonances, the refractive indices don't go to infinity, because the resonance peaks are finite due to the fiber losses.

The materials used in designing large effective-area fibers are summarized in Table C.1 in Appendix C. In this table, an integer k is assigned to each material. The corresponding Sellmeier's coefficients for the materials shown in Table C.1 are given in Table C.2. The data in Tables C.1 and C.2 are extracted from [31].

With the knowledge of the Sellmeier's coefficients, the refractive indices can be expressed in terms of wavelength. Then, the propagation characteristics (dispersion, cutoff wavelength, effective-area and extrinsic losses) of a fiber with given parameters can be determined as discussed below.

2.4 Dispersion

The propagation constant varies with wavelength, thus the group velocity depends on wavelength too and, consequently, different spectral components of the signal will travel with different group velocities. This phenomenon is called chromatic dispersion and the medium in which this occurs is called dispersive [32,33]. If different spectral components arrive at a certain position at different times, the signal will be distorted. In digital communication systems, the pulses representing information bits spread and overlap with neighboring pulses. If pulse spreading is beyond an acceptable level, erroneous detection of information bits becomes probable which, in turn, imply degradation of quality of transmitted signal.

To determine an expression for dispersion, the propagation constant $b(w)$ is expanded in terms of a Taylor series around the operating radian frequency w_o. Doing so, the following expression is obtained,

$$b(w) = b_o(w_o) + b_1(w_o)(w - w_o) + \frac{1}{2} b_2(w_o)(w - w_o)^2 + \frac{1}{6} b_3(w_o)(w - w_o)^3 + ... \tag{2.10}$$

where $b_i(w_o) = \dfrac{d^i b(w_o)}{dw^i}$. Usually, the terms b_o, b_1, b_2, and b_3 are sufficient for assessing the fiber dispersion in a range of frequencies centered about $w_o = 2pc / l_o$. This is because the signals are generally narrowband at optical frequencies ($\Delta w / w_o << 1$, Δw being the signal bandwidth). Having determined b versus wavelength (or frequency), the terms b_o, b_1, b_2, b_3 are readily evaluated. These terms are expressed in terms of the normalized propagation constant $\bar{b}$ as given below:

$$b_1 = \frac{1}{v_g} = \frac{1}{c}\left(\bar{b} - l\,\frac{d\bar{b}}{dl}\right) \tag{2.11a}$$

$$b_2 = \frac{l^3}{2pc^2}\frac{d^2\bar{b}}{dl^2} \tag{2.11b}$$

$$b_3 = -\frac{3l^4}{4p^2c^3}\frac{d^2\bar{b}}{dl^2} - \frac{l^5}{4p^2c^3}\frac{d^3\bar{b}}{dl^3} \tag{2.11c}$$

where c is the velocity of light in free space. The second and third order dispersions are defined as (the dispersion slope is twice the third order dispersion):

$$D = -\frac{l}{c}\frac{d^2\bar{b}}{dl^2} \tag{2.12a}$$

$$D_3 = -\frac{1}{2c}\left(\frac{d^2\bar{b}}{dl^2} + l\,\frac{d^3\bar{b}}{dl^3}\right) \tag{2.12b}$$

Another variable of interest is the dispersion length, defined as:

$$L_D = \frac{T_0^2}{|b_2|} \tag{2.13}$$

where T_0 is the initial pulse width. The dispersion length gives us an idea of how important is dispersion for a given link. If the total link distance is much less than L_D, dispersion effects can be ignored; otherwise they must be taken into account.

A common way of transmitting optical pulses is on-off keying. For a given bit rate, it is easy to estimate the maximum transmission distance that the signal can be transmitted without much degradation due to dispersion. For a Gaussian light source (LED or laser) with RMS spectral width s_w and for an initially transmitted Gaussian optical pulse with initial RMS width s_0 and chirp C_0, the RMS width of the pulse after traveling a distance L is obtained from [34]:

$$\frac{s}{s_0} = \left[\left(1 + \frac{C_0 b_2 L}{2s_0^2}\right)^2 + \left(1 + V_1^2\right)\left(\frac{b_2 L}{2s_0^2}\right)^2 + \left(1 + C_0^2 + V_1^2\right)^2 \frac{1}{2}\left(\frac{b_3 L}{4s_0^3}\right)^2\right]^{0.5} \tag{2.14}$$

where $V_1 = 2s_w s_0$. A rule of thumb to determine the maximum distance is given as [35]:

$$sB \le 0.25 \tag{2.15}$$

where B is the bit rate.

2.5 Cutoff Wavelength

The cutoff wavelength of a guided mode is that when the mode becomes a radiation mode and its power leaks out the fiber and is absorbed by the jacket. In simple terms, this means that total reflection at the most external boundary of the fiber ceases to exist and the wave is partially transmitted into the external cladding region.

All fiber designs presented in Chapter four are required to be single-mode. This means that a fiber must support only one propagating mode in the wavelength range of operation, $l_1 < l < l_2$. This is accomplished if the first propagating mode has a cutoff wavelength greater than l_2 and the second propagating mode has a cutoff wavelength less than l_1. The first mode to propagate in a multi-clad structure is the LP_{01} mode and the second one is the LP_{11} mode. Then, single-mode operation is guaranteed if $l_{c,11} < l < l_{c,01}$, where $l_{c,01}$ and $l_{c,11}$ are cutoff wavelengths of LP_{01} and LP_{11} modes, respectively.

The cutoff occurs at the wavelength that normalized propagation constant $\bar{b}$ becomes equal to the refractive index of the most external layer, n_{ext}. To determine the cutoff wavelength of a mode, it is sufficient to set $\bar{b} = n_{ext}$ in the dispersion relation and solve it for wavelength. A simpler, but less accurate way is to execute the dispersion program and find the wavelength for which $\bar{b} \cong n_{ext}$. In this dissertation, the cutoff wavelength refers to the cutoff wavelength of the LP_{11} mode, unless otherwise specified [36].

2.6 Effective-Area

The effective-area is a property of optical fibers that appears when the nonlinear Schrödinger equation is derived [11]. Intuitively, the power divided by the effective-area is a measure of power density inside the fiber. The larger the effective-area, the lower is the power density inside a fiber. Fiber nonlinearities strongly depend on the power density inside a fiber,

thus an increase in the effective-area results in a decrease in fiber nonlinearities and their effects on signal transmission.

As mentioned before, fiber nonlinearities are detrimental for very long links, even at moderate power levels. For this reason, it is important to design optical fibers with large effective-areas. However, as will be shown later, a larger effective-area is achieved at the expense of a higher bending loss. It is necessary to provide designs with large effective-areas and tolerable bending losses. The effective-area is defined as [11]:

$$A_{eff} = \frac{\left[\int_0^{2p}\int_0^{\infty} |y(r,f)|^2 \, r dr df\right]^2}{\int_0^{2p}\int_0^{\infty} |y(r,f)|^4 \, r dr df} \tag{2.16a}$$

where $y(r,f)$ is the scalar field of the propagating mode. It should be noted that for the LP_{01} mode, $y(r,f)$ depends only on the coordinate r and (2.16a) is further simplified to:

$$A_{eff} = 2p \frac{\left[\int_0^{\infty} |y(r)|^2 \, r dr\right]^2}{\int_0^{\infty} |y(r)|^4 \, r dr} \tag{2.16b}$$

2.7 Fiber Losses

2.7.1 Loss Mechanisms

Fiber attenuation is one of the most important limitations in optical fiber communication links. It limits the maximum distance that information can be sent without use of repeaters. Although fiber losses do not distort optical pulses, they can reduce the amplitude of a pulse to the extent that the initial information cannot be recovered in presence of noise.

The basic attenuation mechanisms in optical fibers are absorption, scattering and bending losses. In addition to these losses, there is the splice loss that occurs when two fibers are concatenated. Splice loss occurs due to fiber misalignments, differences in the numerical apertures, etc. Three mechanisms contribute to absorption [37]: absorption by atomic defects in

the glass composition, extrinsic absorption by impurity atoms in the glass material and intrinsic absorption by the basic constituents of fiber materials.

Every material has defects in its atomic structure. These defects cause absorption of the optical radiation incident on it. In optical fibers, the losses caused by these defects are in general negligible compared with other sources of absorption. They are only important when the fiber is exposed to intense nuclear radiation levels [38, 39].

The extrinsic absorption by impurity atoms occurs when light is absorbed by these atoms causing energy transitions or charge transitions between their ions. They are present in the range of 0.6-1.6 mm and are generated by metal impurities and water vapors [35].

The intrinsic absorption is related to the electronic resonances (in the ultraviolet region) and the vibrational resonances (in the infrared region) of silica glass. The electronic resonances occur when a photon interact with an electron in the valence band and excites it to a higher energy level; whereas the vibrational resonances are associated to the chemical bonds of the silica glass [37].

Light is scattered when it encounters variations of the material caused by density fluctuations, defects, etc. When scattering occurs, part of the light leaves the fiber and is absorbed by the jacket. The scattering losses due to density fluctuations, known as Rayleigh scattering losses, are proportional to l^{-4}. These scattering losses are more important at shorter wavelengths. The Rayleigh scattering and, ultraviolet and infrared absorption losses are intrinsic to the fiber materials. The combination of these losses has a global minimum in the region around 1550 nm and that is why most long distance systems are operated at this wavelength [40,41].

A different kind of loss which must be taken into account in fiber design is the bending loss. Everytime an optical fiber is bent, radiation occurs. When a bend occurs, a portion of the power propagating in the cladding is lost through radiation (if not, the wave propagating in this portion should travel at speeds higher than the light speed to "keep track" with the field in the core). There are two types of bending losses: macrobending and microbending losses. Macrobending loss occurs when the bends are large compared to the fiber diameter, while microbending loss is caused by random bends of the fiber axis when the fiber is made into a

cable. In general, macrobending loss is simply referred to as bending loss and this term will be used throughout this dissertation.

2.7.2 Splice Loss

When two fibers are concatenated, some loss of power occurs due to the imperfect coupling of light from one fiber into another. This imperfect coupling of light may be a result of mechanical misalignments, differences in the geometries of the fibers and mismatches of index profiles. There are, basically, four types of mechanical misalignments: lateral, longitudinal, angular and a combination of the three misalignments. Lateral misalignment occurs when two fibers have no longitudinal separation, but their axes are separated by a distance d (see Figure 2.3). Longitudinal misalignment occurs when two fibers are separated longitudinally from each other, but their axes are aligned with each other. Angular misalignment occurs when the two fiber axes form an angle so that the fiber end faces are no longer parallel. A combination of these misalignments occurs when two or more of different misalignments occur at the same time (lateral and angular displacements, for example).

With the availability of modern splice tools, splice loss is no longer a critical problem. Nevertheless, an estimation of splice loss, particularly the one due to lateral misalignment, is useful for designing fiber-optic links.

For two fibers with their axes separated by a distance d, as shown in Fig. 2.3, the coupling efficiency may be evaluated as [28],

$$h_s = 4\frac{\int_0^{\infty}\int_0^{\infty} y\left[\sqrt{\left(x-\frac{d}{2}\right)^2+y^2}\right] y\left[\sqrt{\left(x+\frac{d}{2}\right)^2+y^2}\right] \mathrm{dx\ dy}}{\int_0^{2p}\int_0^{\infty}\left|y\,(r,f)\right|^2\ \mathrm{r\ dr}} \qquad (2.17a)$$

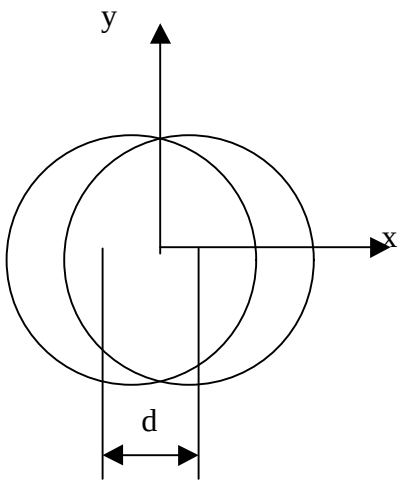

Figure 2.3- Lateral offset between two identical fibers.

As $y(r,f) = y(r)$ for the LP_{01} mode, a further simplification is obtained:

$$h_s = \frac{2}{p} \frac{\int_0^\infty \int_0^\infty y\left[\sqrt{\left(x-\frac{d}{2}\right)^2 + y^2}\right] y\left[\sqrt{\left(x+\frac{d}{2}\right)^2 + y^2}\right] \text{dx dy}}{\int_0^\infty |y(r)|^2 \text{ r dr}} \qquad (2.17b)$$

where the expressions for $y(r,f) = y(r)$ were given in section 2.1 and $r = \sqrt{x^2 + y^2}$. The denominator $\int_0^\infty |y(r)|^2 r dr$ is calculated in Appendix B. Power loss in dB is given by:

$$L_s = -10 \log_{10}(h_s) \qquad (2.18)$$

2.7.3 Microbending Loss

Microbendings are random bends of the fiber axis that occur when fibers are made into cables. The microbending loss occurs when light from a guided mode is coupled into a radiation mode and leaks out of the fiber. Eventually, the jacket absorbs the portion that is radiated away from the fiber.

Among several works in microbending loss [42-45], the theory presented in this section is based on the works of Marcuse [42] and Bjarklev [43]. In the absence of microbendings, the refractive indices in conventional circular fibers depend only on the radial distance r. However, this is not the case when microbending occurs, because the fields magnitude become dependent on coordinates z and f. Let us denote the refractive indices of a perfect fiber (without microbendings) and that with microbendings as $n_o(r)$ and $n(r,f,z)$, respectively, and express $n(r,f,z)$ as a first-order Taylor expansion [42]:

$$n(r,f,z) = n_o(r) + \frac{\P n_o}{\P r} f(z)\cos f \tag{2.19}$$

where f(z) describes the random deformation of the fiber axis. For step-index fibers, the term $\P n_o / \P r$ in (2.19) is expressed as,

$$\frac{\P n_o}{\P r} = \sum_{k=1}^{L} (n_{k+1} - n_k) d(r - a_k) \tag{2.20}$$

where L=N-1 for an N-layer fiber (L=2, 3 and 4 for the fibers considered in this work), n_k is the refractive index of the kth layer, $d(.)$ is the Dirac's delta function and a_k is the kth radius (k=1,2,...N-1) for a N-layer fiber.

Following Marcuse's approach, the cladding mode field profile is defined as,

$$y_{c,vs} = A_{vs} J_v\left(g_{vs} \frac{r}{b}\right)\cos(vf) e^{-jb_{vs}z} \tag{2.21}$$

where A_{vs} is an arbitrary constant, $y_{c,vs}$ is the field profile for the cladding mode, v is an integer , b is the radius of the external cladding-jacket boundary and b_{vs} is the propagation constant of the cladding mode. The variable g_{ns} is given by:

$$\left(\frac{g_{vs}}{b}\right)^2 + b_{vs}^2 = \left(\frac{2p}{l} n_p\right)^2 \tag{2.22}$$

where n_p is the index of the outer cladding region (p =3, 4, 5 for the three, four or five layer fiber). The cladding field must vanish at the cladding-jacket boundary. Thus,

$$J_v(g_{vs}) = 0 \tag{2.23}$$

Due to the symmetry of the fiber geometry, the LP_{01} mode couples to the cladding mode with n =1. Normalizing the cladding mode field to unity, A_{1s} is given by:

$$A_{1s} = \sqrt{\frac{-2}{b^2 J_0(g_{1s}) J_2(g_{1s})}} \tag{2.24}$$

Assuming a Gaussian auto-correlation function for *f(z)* with an rms deviation s and a correlation length L_c, Bjarklev [43] calculated the average power loss coefficient due to microbending loss as:

$$\langle a \rangle = 0.5\left(\frac{2p}{l}\right)^2 \sqrt{p}\, s^2 L_c \sum_{k=1}^{G} \exp\left\{-\left[\frac{1}{2}\left(\bar{b}\,\frac{2p}{l} - b_{1k}\right)L_c\right]^2\right\} \left[\sum_{j=1}^{p-1}\left(n_{j+1} - n_j\right) y\left(a_j\right) a_j \bar{y}_{c,1s}\left(a_j\right)\right]^2 \tag{2.25}$$

where b_{1k} is the propagation constant for the kth cladding mode, it is real for all values of $k \le G$; $\bar{y}_{c,1s}$ is the cladding mode field profile without the z and f dependence and p represents the number of layers of the fiber.

For a five-layer fiber, the microbending loss is given by (after normalizing all field profiles):

$$\langle a \rangle = \frac{1}{2}\left(\frac{2p}{l}\right)^2 \sqrt{p}\, s^2 L_c \sum_{k=1}^{G} \exp\left\{-\left[\frac{1}{2}\left(\bar{b}\,\frac{2p}{l} - b_{1k}\right)L_c\right]^2\right\} \left[(n_2 - n_1)x_1 a_1 + (n_3 - n_2)x_2 a_2 + (n_4 - n_3)x_3 a_3 + (n_5 - n_4)x_4 a_4\right]^2 \tag{2.26}$$

where

$$x_1 = \begin{cases} A_1 I_o(x_{11}) A_{1k} J_1\left(g_{1k}\,\dfrac{a_1}{b}\right) & \text{if } \bar{b} > \mathrm{n}_1 \\ A_1 J_o(x_{11}) A_{1k} J_1\left(g_{1k}\,\dfrac{a_1}{b}\right) & \text{if } \bar{b} \le \mathrm{n}_1 \end{cases}$$

$$x_2 = \begin{cases} \left[A_2 I_o\left(x_{22}\right) + \overline{A}_2 K_o\left(x_{22}\right)\right] A_{1k} J_1\left(g_{1k}\dfrac{a_2}{b}\right) & \text{if } \bar{b} > \mathrm{n}_2 \\ \left[A_2 J_o\left(x_{22}\right) + \overline{A}_2 Y_o\left(x_{22}\right)\right] A_{1k} J_1\left(g_{1k}\dfrac{a_2}{b}\right) & \text{if } \bar{b} \le \mathrm{n}_2 \end{cases}$$

$$x_3 = \begin{cases} \left[A_3 I_o\left(x_{33}\right) + \overline{A}_3 K_o\left(x_{33}\right)\right] A_{1k} J_1\left(g_{1k}\dfrac{a_3}{b}\right) & \text{if } \bar{b} > \mathrm{n}_3 \\ \left[A_3 J_o\left(x_{33}\right) + \overline{A}_3 Y_o\left(x_{33}\right)\right] A_{1k} J_1\left(g_{1k}\dfrac{a_3}{b}\right) & \text{if } \bar{b} \le \mathrm{n}_3 \end{cases}$$

$$x_4 = \overline{A}_5 K_o\left(x_{54}\right) A_{1k} J_1\left(g_{1k}\frac{a_4}{b}\right)$$

A typical value for the RMS deviation of *f(z)* is 1 nm. There is no reliable information about the correlation length [42], so in our simulations, it is varied from 1 mm to 500 mm.

2.7.4 Mode-Field-Diameter, Bending Loss

On a straight fiber, the electromagnetic fields at any point, in the phase plane perpendicular to its axis, travel at the same speed. When a fiber is bent, the electromagnetic fields at some points should travel faster than the speed of light in the medium to maintain the integrity of the fields along a planar arc of constant radius. This is not possible and consequently the fields in these regions radiate. This is the mechanism of power losses caused by bending.

The concept of mode-field-diameter was introduced by Petermann [46] to provide a measure of how high the bending and microbending losses are in a fiber. Two mode-field-diameters have been defined, but here we employ only Petermann II definition which is better applicable to multi-clad fibers used in this work. The Petermann II mode-field-diameter, denoted as d_o, is given by:

$$d_o^2 = 8\frac{\int_0^\infty |y(r)|^2 r dr}{\int_0^\infty \left|dy(r)/dr\right|^2 r dr} \tag{2.27}$$

It is emphasized that this formula is not a substitute for bending loss calculations. It only gives a qualitative information about the bending loss. Kato et al. [16] have stated that, in general, tolerable bending losses are obtained for mode-field-diameters less than 11 mm (for a bending radius equal to 30 mm).

The bending loss analysis is much more complicated than simple calculation of mode-field-diameter. Different studies of bending loss are available in the literature [28, 47-52]. Here, we use a reasonably accurate approach presented by Snyder [28]. In his approach, the fiber core and inner claddings are substituted by an equivalent current-carrying antenna irradiating in an infinite medium of index equal to n_{ext} (the refractive index of the most external layer, $n_{ext} = n_N$ for a N-layer fiber; N=3, 4 or 5). To a first approximation and using the Maxwell's equation $\nabla x\vec{H} = \vec{J} + jwe\vec{E}$, it can be shown that the current density of the equivalent radiating antenna is given by the following expression,

$$\vec{J}(r) = -j\sqrt{\frac{e_o}{m_o}}\frac{2p}{l}\left[n_{ext}^2 - n^2(r)\right]\vec{E}(r) \tag{2.28}$$

where $\vec{E}(r)$ is the exact electric field of the fiber. As an approximation, it is sufficient to assume that this field is the same as the field of the straight fiber, given by (2.1a), provided that the bending radius is large enough compared with the fiber dimensions. Without loss of generality, the electric field vector is assumed to be along the x direction (refer to Figure 2.1), hence the equivalent current is along this direction, as illustrated in Figure 2.4. The equivalent current is expressed as,

$$\vec{I}_a = \hat{a}_x \iint \vec{J} dA = I_{co}\hat{a}_x e^{j(wt-bz)} \tag{2.29}$$

In Figure 2.4, the equivalent current is along the Z direction, which coincides with the x direction in Fig. 2.1. The fiber irradiates in an infinite medium of refractive index n_{ext}. The

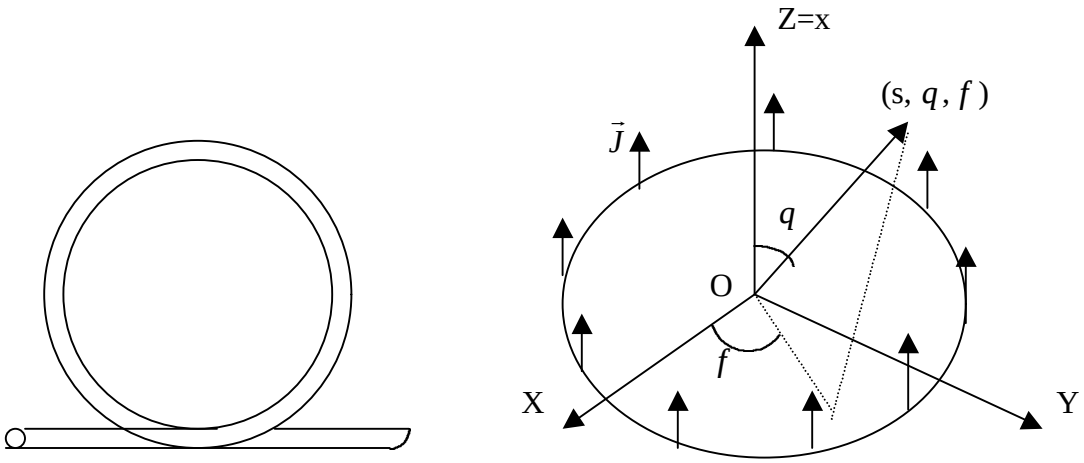

(a) (b)

Figure 2.4 (a) Lateral view of the bent fiber, (b) Systems of coordinates X,Y and Z to analyze the bending loss of a fiber.

coordinates (r, f, q) are used to describe a general point in space, while (r', f', q') describe a source point. The angles and distances are always measured relative to the origin O. The fiber is assumed to be bent at a constant radius R_C. The current amplitude I_{co} can be expressed as,

$$I_{co} = -j\frac{(2p)^2}{l}\sqrt{\frac{e_o}{m_o}}\int_0^{\infty}\left[n_{ext}^2 - n^2(r')\right]y(r')\, I_0\left(\frac{u_{ext}}{a_{ext}}r'\right)r'dr' \tag{2.30}$$

where $\frac{u_{ext}}{a_{ext}} = \frac{2p}{l}\sqrt{\bar{b}^2 - n_{ext}^2}$. Appendix D presents the formula for this current amplitude for a five-layer fiber. Following the steps of Snyder, the radiated power is expressed as,

$$P_{rad} = \frac{p}{2l}n_{ext}\sqrt{\frac{m_o}{e_o}}R_c\left|I_{co}\right|^2 F_{rad}\exp\left\{-\frac{2}{3}\frac{2p\, n_{ext}R_c}{l}\left[\left(\frac{\bar{b}}{n_{ext}}\right)^2 - 1\right]^{1.5}\right\} \tag{2.31a}$$

where

$$F_{rad} = \frac{1}{\left(\bar{b}^2 - n_{ext}^2\right)^{0.5}}\sqrt{\frac{1}{\frac{8}{3}l\, n_{ext}R_c\sqrt{\left(\bar{b}/n_{ext}\right)^2 - 1}\left[2\left(\bar{b}/n_{ext}\right)^2 + 1\right]}}. \tag{2.31b}$$

The loss coefficient is calculated as,

$$g = \frac{P_{rad}}{2p\, R_c\, P(0)} \tag{2.32}$$

where $P(0) = p\sqrt{\frac{e_o}{m_o}}\int_0^\infty n(r)\left|y\,(r)\right|^2 rdr$ is the power carried by the wave at the fiber input.

From (2.31) it is clear that the closer is $\bar{b}$ to n_{ext}, the higher will be the bending loss for a fixed bending radius. This implies that large effective-area fibers should be designed with ratios $\bar{b}/n_{ext}$ as high as possible to obtain small bending losses. However, as the fields need to penetrate inside the external cladding to achieve a large effective-area, it is expected that larger effective-area fibers will have also larger bending losses. Also, it is clearly noticed that an increase in the bending radius brings about smaller bending losses. Therefore, if the bending loss is large for a given bending radius, a tolerable loss can be obtained by increasing the radius sufficiently.

Chapter 3

Nonlinear Effects in Optical Fibers

3.1 Introduction

In this chapter, nonlinear effects in optical fibers are described, with particular attention paid to the Kerr effect. In conventional fiber optic links, nonlinearities are undesired and contribute to signal distortion, especially in very long-distance links. On the other hand, there is a special case in which nonlinearities counterbalance dispersion, in such a way that pulses propagate undistorted over very long distances. These pulses are called solitons, pulses with duration on the order of femtoseconds. However, solitons are still far away from commercial implementation and, for this reason, are not of major concern in this work.

Nonlinear phenomena in optical fibers operated at typical power levels are generally weak, but not negligible. As mentioned before, the strength of nonlinear effects is proportional to the power density inside the fiber. In spite of small values for nonlinear coefficients in fused silica at moderate power levels, the very small spot size, extremely low loss and long length of optical fibers provide a ground for nonlinear effects to have a significant impact on signal transmission. This means that even at low power levels, the power density inside a fiber can be high enough to cause signal distortions due to nonlinearities over long distances.

In very long links that use optical amplifiers, nonlinearities cannot be neglected. For pulses with hundreds of picoseconds or few nanoseconds duration, nonlinearities help dispersion in distorting the optical pulses that travel inside a fiber. Even in the absence of dispersion, nonlinearities can drastically amplify the spontaneous emission noise resulting from optical amplifiers to the extent that the bit error rate becomes unacceptably high.

Nonlinear effects in optical fibers can be divided into elastic and inelastic processes. Elastic processes do not exchange energy between the electromagnetic fields and the dielectric

medium and are generally caused by the nonlinear refractive index. On the other hand, inelastic processes exchange energy with the medium and are caused by stimulated scattering [11]. The focus of this chapter is on elastic processes, but a short description of inelastic processes is presented in the next section.

3.2 Stimulated Scattering in Optical Fibers

In stimulated inelastic scattering, optical fields transfer part of their energy to their constituent materials. There are two inelastic processes: Stimulated Brillouin Scattering (SBS) and Stimulated Raman Scattering (SRS). In both processes, a photon is annihilated to create another photon and a phonon (acoustic phonon for the SBS and optical phonon for the SRS). In other words, a pump wave transfers part of its energy to a lower frequency wave (Stokes wave) and the rest to an acoustic wave generated in the medium.

Although both processes seem to be identical, they have some differences. SRS is a broadband process with line-widths on the order of few THz, while SBS is narrow-band with line-widths of few MHz. In the Stimulated Raman Scattering, the Stokes and the pump waves can either propagate in the same or opposite directions, but in Stimulated Brillouin Scattering, the incident and scattered waves propagate in the opposite directions.

For the SRS, the evolution of the Stokes and pump waves is governed by the following pair of equations [11]:

$$\frac{dI_s}{dz} = g_r I_p I_s - a_s I_s \tag{3.1a}$$

$$\frac{dI_p}{dz} = -\frac{w_p}{w_s} g_r I_p I_s - a_p I_p \tag{3.1b}$$

where I_s is the intensity of the Stokes wave, I_p is the intensity of the pump wave, g_r is the Raman gain, a_s and a_p are the losses of the Stokes and pump waves and w_s, w_p are the

frequencies of the Stokes and pump waves, respectively. These equations are valid only for a quasi-cw regime (low bit rates).

If the pump transfers only a small amount of energy to the Stokes wave, then the solutions for (3.1) are obtained as,

$$I_p(z) \approx I_p(0)\exp(-a_p z) \tag{3.2a}$$

$$I_s(z) = I_s(0)\exp\left\{g_r I_p(0)\left[1-e^{-a_p z}\right]/a_p - a_s z\right\} \tag{3.2b}$$

It is clearly observed from equations (3.1 and 3.2) that some energy is transferred from the pump wave to the Stokes wave. This may be beneficial in some cases such as in Raman amplifiers. In Raman amplifiers, a pump wave is injected in the fiber in such a way that it transfers energy to a Stokes wave. This transfer of energy produces an amplification of the Stokes wave that carries the information.

Stimulated Raman scattering (SRS) is significant for peak powers greater than $P_o^{cr} \approx 16A_{eff}/z_{eff}g_r$, where A_{eff} is the effective-area of the fiber and z_{eff} is the fiber effective length [11]. If polarization is not preserved, the factor 16 in the above relation is increased to a value between 16 and 32. Typical values of this critical power are in the range of hundreds of milliwatts to few watts, unlikely to occur in single-channel fiber optic systems. However, SRS is important to WDM systems, because the power of each channel contributes to the total power of the system. Intermediate channels transfer their energy to longer wavelength channels but also receive energy from shorter wavelength channels. The shortest wavelength channel is most affected because it transfers power to all other channels in the Raman bandwidth [11]. SRS is a limiting factor in WDM systems with a very large number of channels, while for a small number of channels its effects are, in general, negligible.

For the Stimulated Brillouin Scattering, the Brillouin gain has a Lorentzian spectral profile given by [11]:

$$g_b(f) = \frac{(\Delta f_b/2)^2}{(f-f_b)^2 + (\Delta f_b/2)^2} g_b(f_b) \tag{3.3}$$

where $g_b(f)$ is the Brillouin gain, f_b is the peak gain frequency, Δf_b is the full-width at half maximum ($\approx 10\,MHz$) and $g_b(f_b)$ is the peak gain that can be related to the acoustical and optical properties of fiber materials. If the pump wave has a Lorentzian spectral profile with spectral width (FWHM) Δf_p, the peak gain reduces to $\tilde{g}_b = \dfrac{\Delta f_b}{\Delta f_b + \Delta f_p} g_b(f_b)$.

Under cw or quasi-cw modulation, the equations that describe the behaviors of the pump and Stokes waves are given by [11]:

$$\frac{dI_s}{dz} = -g_b I_p I_s + aI_s \tag{3.4a}$$

$$\frac{dI_p}{dz} = -g_b I_p I_s - aI_p \tag{3.4b}$$

where a is the fiber loss coefficient for the Stokes and pump waves, which is assumed to be the same at the pump and Stokes wavelengths because of the narrowband characteristic of Stimulated Brillouin Scattering. The solutions of the above equations are obtained as, [11]

$$I_s(z) = \frac{b_o(1-b_o)}{G(z)-b_o} I_p(0) e^{az} \tag{3.5a}$$

$$I_s(z) = \frac{G(z)(1-b_o)}{G(z)-b_o} I_p(0) e^{-az} \tag{3.5b}$$

where $b_o = I_s(L)/I_p(0)$, $g_o = g_b I_p(0)$ and $G(z) = \exp\left[(1-b_o)(g_o/a)(1-e^{-az})\right]$. Stimulated Brillouin Scattering is significant for peak powers greater than $P_o^{cr} \approx 21 A_{eff}/z_{eff}\, g_b(f_b)$. If polarization is not preserved, the factor 21 in the above relation is increased to values between 21 and 42. Typical values of this critical power are few mW. Although SBS has a low threshold power, SBS is a narrow-band process and for this reason it is not important for high bit rate signals.

SBS, as a result of pump depletion, can transfer power from the wave that carries the information (acting as a pump wave) to a Stokes wave that can be built up even from noise if it does not already exist. Also, a Stokes wave can cause destabilization of the transmitting laser. For

coherent systems such as ASK and FSK, the threshold increases by a factor of 2 and 4, respectively, while for PSK, the peak gain decreases with the bit rate as,

$$g_b^{PSK} = \frac{\Delta f_b}{B + \Delta f_b} g_b^{CW} \tag{3.6}$$

In WDM systems that employ bi-directional transmission, SBS can cause inter-channel cross-talk by increasing the power of a channel at the expense of a counter-propagating channel. On the other hand, SBS can increase the receiver sensitivity by injecting a counter-propagating pump signal in the fiber. This pump signal transfers energy to the signal and amplifies it. Also, SBS can be used as a tunable narrow-band optical filter for densely packed multi-channel systems.

3.3 Elastic Processes in Optical Fibers

Whenever nonlinear effects are discussed, the primary idea that comes to mind is the generation of new frequencies. Phenomena such as third-harmonic generation and four-wave mixing which generate new carrier frequencies occur in optical fibers, but are very weak and require special efforts to achieve phase matching [11]. Another elastic effect occurs due to the nonlinear refraction that does not cause a change in the carrier of the wave. In this nonlinear process only the envelope of the carrier wave is affected. This type of nonlinearity will be the main focus of discussion in this dissertation. The pulses considered here have widths much greater than 0.1 ps, so that the simplified version of the nonlinear Schrödinger equation can be used. Also, the power levels considered here will be low enough to neglect other nonlinear effects such as the stimulated Raman scattering.

3.3.1 The Nonlinear Schrödinger Equation

The electric polarization of any dielectric material may be represented as [11]:

$$\vec{P} = e_o\left[c_1.\vec{E} + c_2:\vec{E}\vec{E} + c_3:\vec{E}\vec{E}\vec{E} + ...\right] \tag{3.7}$$

where c_j is the jth order susceptibility tensor. Strictly speaking, this formula is valid only in the frequency domain. However, the optical signals considered here have envelopes that vary slowly compared to the optical frequency, so that this formula can be extended to the time domain as an approximation.

Most optical fibers are made of silica glass. Because silica glass is a symmetric molecule, c_2 is zero. Thus, the major source of nonlinearity in glass fibers is the third order susceptibility. The molecular symmetry of silica glass also implies that conventional optical fibers are isotropic, hence the electric displacement vector may be expressed as,

$$\vec{D} = e_o\left(n^2 + c_3\left|\vec{E}\right|^2\right)\vec{E} \tag{3.8}$$

where n is the linear part of the refractive index of the fiber material.

If the optical wave propagating in the fiber is monochromatic with angular frequency w_0, the electric field can be expressed as (in the absence of nonlinearities), [53]

$$\vec{E} = y(x,y,w_0)e^{j(w_0 t - b_0 z)}\begin{Bmatrix}\hat{a}_x \\ \hat{a}_y\end{Bmatrix} \tag{3.9}$$

where b_0 is the propagation constant at $w = w_0$, $y(x,y,w_0)$ is the transverse field function defined in (2.4), with $r = \sqrt{x^2 + y^2}$. If the wave is not monochromatic, the guided mode can be represented as a superposition of monochromatic waves [53]. For optical signals with narrow spectra centered on frequency w_0, the time-domain representation of $y(x,y,w)$ can be expressed as,

$$\vec{E}(x,y,z,t) = A(z,t)y(x,y,w_0)e^{j(w_o t - b_0 z)}\begin{Bmatrix}\hat{a}_x \\ \hat{a}_y\end{Bmatrix} \tag{3.10}$$

where A(z, t) represents the envelope of the optical field. The small spectral width of the optical signal implies slow variation of A(z, t) with respect to time compared with the optical carrier. The spectrum of A(z, t) is given by,

$$f(z,w) = e^{j(b-b_o)z}\int_{-\infty}^{\infty} A(z,t)e^{-j(w-w_o)t}dt \tag{3.11}$$

Expanding $b(w)$ in a Taylor series around w_0 and retaining the first three terms of the expansion, (3.11) can be expressed as,

$$f(\Omega,z) = \exp\left[j\left(b_1\Omega + \frac{1}{2}b_2\Omega^2 + \frac{1}{6}b_3\Omega^3 \right)z \right] \int_{-\infty}^{\infty} A(z,t)e^{-j\Omega t}dt \tag{3.12a}$$

where $\Omega = w - w_o$. Using the inverse Fourier transform, $A(z,t)$ is given as

$$A(z,t) = \int_{-\infty}^{\infty} f(\Omega,z)e^{j\Omega t} \exp\left[-j\left(b_1\Omega + \frac{1}{2}b_2\Omega^2 + \frac{1}{6}b_3\Omega^3 \right)z \right] d\Omega \tag{3.12b}$$

It can be shown that A(z, t) satisfies the following partial differential equation [53]:

$$\frac{\partial A}{\partial z} + b_1\frac{\partial A}{\partial t} - \frac{j}{2}b_2\frac{\partial^2 A}{\partial t^2} - \frac{1}{6}b_3\frac{\partial^3 A}{\partial t^3} = 0 \tag{3.13}$$

Following Marcuse's approach [53], nonlinearities and losses can be incorporated into (3.13) to obtain a more general equation. Doing so, the equation that governs the evolution of the optical wave in a nonlinear medium is obtained as,

$$\frac{\partial A}{\partial z} + b_1\frac{\partial A}{\partial t} - \frac{j}{2}b_2\frac{\partial^2 A}{\partial t^2} - \frac{1}{6}b_3\frac{\partial^3 A}{\partial t^3} + aA = -j\frac{2p}{l}\hat{n}|A|^2 A \tag{3.14a}$$

where

$$\hat{n} = \frac{c_3}{2n}\frac{\langle y^4 \rangle}{\langle y^2 \rangle} \tag{3.14b}$$

$$\langle y^p \rangle = \int_{-\infty}^{\infty}\int_{-\infty}^{\infty} y(x,y)^p \, dxdy \tag{3.14c}$$

Equation (3.14a) is the well-known nonlinear Schrödinger equation and is valid for pulses with durations greater than 0.1 ps. This equation governs the evolution of the envelope of the optical wave as it propagates in a nonlinear medium. Based on this analysis, the transverse field profile $y(x,y)$ essentially does not change as the pulse propagates inside the fiber. Only the envelope of the wave is affected. As typical optical signals have frequencies on the order of $10^{14}\,Hz$, their period is on the order of 0.01 ps. If these pulses last more than 0.1 ps, the envelope will vary slowly compared with the optical signal. For optical pulses with durations less than 0.1

ps, the approximation described above does not hold and three more terms must be included in (3.14a) [11].

The right-hand-side of (3.14a) may be also written as,

$$-j\frac{2p}{l}\hat{n}|A|^2 A = -j\frac{2p}{l}\hat{N}\frac{P}{A_{eff}}A \tag{3.15}$$

where A_{eff} is the effective-area as defined in (2.16), P is the peak power carried by the wave given by,

$$P = \frac{1}{2}\sqrt{\frac{e_o}{m_o}}\langle n y^2\rangle |A|^2 \quad , \tag{3.16}$$

and $\hat{N}$ is defined as [53],

$$\hat{N} = \sqrt{\frac{m_o}{e_o}}\frac{c_3}{n}\frac{\langle y^2\rangle}{\langle n y^2\rangle} \cong \sqrt{\frac{m_o}{e_o}}\frac{c_3}{n^2} \tag{3.17}$$

Strictly speaking, $\hat{N}$ depends upon the field profile, but in most cases it can be considered constant for a given material. Usually, the refractive indices inside a fiber are very close to each other, such that n(r) has small variations in the radial direction. This makes the ratio $\langle y^2\rangle / \langle n y^2\rangle$ nearly constant ($\approx 1/n$). For pure silica glass, $\hat{N} = 3.2X10^{-20} m^2/W$.

The nonlinear term in the Schrödinger equation is proportional to the peak power carried by the wave and inversely proportional to the effective-area. This indicates that nonlinear effects depend on the power density inside the fiber. An increase in the effective-area of a fiber implies that nonlinearities become weaker and cause less distortion of pulses propagating inside it. Conventional optical fibers have effective-areas on the order of 50 mm^2. In order to reduce the harmful effects of fiber nonlinearities in long-distance links, new optical fibers with larger effective-areas need to be designed. The design of large effective-area fibers constitute the main thrust of research carried out in this work

3.3.2 Solitons

Although, the main interest of this dissertation is in fiber-optic communication systems in which pulses have bit periods on the order of hundreds of picoseconds, a particular type of pulses with durations of femtoseconds to few picoseconds, called soliton, can propagate inside an optical fiber without distortion. These pulses are the result of a perfect balance between dispersion and nonlinearity. Soliton waves have been analyzed extensively in the past as is evidenced by the wealth of literature in this subject [see for example 11, 53-56]. The goal of this subsection is only to illustrate how the nonlinear Schrödinger equation can be used to study nonlinear pulses. A general approach to studying soliton waves is to use the inverse scattering method [11]. However, first order solitons can be analyzed more simply as described below.

Neglecting the fiber losses and the third order dispersion term in (3.14a), a solution of the type $A(z,t) = A_o H(t - b_1 z)e^{ja_o z}$ is assumed, where A_o is an arbitrary constant and H is a real function. In order to find a solution whose power spectrum does not depend on z, a_o cannot depend on time and so is assumed to be constant.

Following this procedure, the Schrödinger nonlinear equation is converted into the following ordinary differential equation:

$$\frac{d^2 H}{dt^2} - \frac{2a_o}{b_2} H - \frac{4p}{l}\hat{n}A_o^2 H^3 = 0 \tag{3.18}$$

The solution of this nonlinear differential equation has been obtained as [53]

$$A(z,t) = A_o \operatorname{sec} h\left[(t - b_1 z)\sqrt{\frac{2a_o}{b_2}}\right] \tag{3.19}$$

As $a_o < 0$, b_2 must also be negative for this solution to exist. Therefore, bright solitons exist only for $b_2 < 0$ and positive second-order dispersion.

The electric field is given by [53]:

$$E = A_o y\,(x,y)e^{j(w_o t - (b_o - a_o)z)} \operatorname{sec} h\left[(t - b_1 z)/T_o\right] \tag{3.20}$$

where $T_o = \sqrt{\frac{b_2}{2a_o}}$.

For describing higher order solitons, the inverse scattering method must be employed. Practical implementation of optical solitons requires further research and development work and it may take many years to become commercial.

Chapter 4

Design of Low Nonlinearity Dispersion-Shifted and Dispersion- Flattened Fibers

Silica glass optical fibers have minimum intrinsic loss at 1.55 mm. Earlier generation of optical fibers provide nearly zero second-order dispersion at 1.31 mm, but the trend in recent years has been to shift to 1.55 mm in order to take advantage of the lower attenuation at this wavelength. However, fibers designed for operation at 1.31 mm present a large dispersion at this wavelength. Special fiber designs are required to achieve nearly zero dispersion at 1.55 mm. Fibers that provide zero dispersion at 1.55 mm are called dispersion-shifted fibers. A more advanced design; namely, the dispersion-flattened fiber provides low dispersion over an extended range of wavelengths. This feature makes dispersion-flattened fibers useful for applications in broadband communication systems, particularly those incorporating WDM (Wavelength Division Multiplexing). Both dispersion-shifted and dispersion-flattened fibers must be single-mode in the wavelength range of operation to avoid inter-modal dispersion.

Commercial dispersion-shifted and dispersion-flattened fibers have effective-areas on the order of 50 mm^2. With effective-areas in this range, nonlinearities play a strong role in very long links, covering distances over 1000 km, and cause several kinds of signal distortion. Therefore, dispersion-shifted and dispersion-flattened fibers intended for all optical long links should not only provide low dispersion and low loss in their wavelength range of operation, but should also provide larger effective-areas than conventional fibers in order to minimize the detrimental effects of nonlinearities. However, a larger effective-area is achieved at the expense of a higher bending loss. Thus, novel single-mode fiber designs are needed to achieve larger effective-area, tolerable bending loss, and nearly zero dispersion at 1.55 mm.

In this chapter, new low-nonlinearity dispersion-shifted and dispersion-flattened fibers based on depressed-core multi-step index profiles are presented. A systematic approach for

designing these fibers, using a reference W-index profile to initiate the design, is adopted. The transmission properties of example designed fibers are evaluated.

4.1 Designs for Dispersion-Shifted Fibers

The principal design requirements are large effective-area, small dispersion, low losses, and single-mode operation in the 1.55 mm window. The latter three requirements are met in conventional dispersion-shifted fibers. To achieve a larger effective-area, the index profile of the fiber is modified such that the fields become less confined to its central core region. The approach adopted is to start with a reference fiber that provides zero dispersion at 1.55 mm and reduce the refractive index of a central portion of the core region. Here, a W-index fiber is chosen as the reference fiber. [57] Reducing the index of a portion of its core region, a depressed-core triple-clad structure is created in which the first inner cladding assumes the highest refractive index. This modification of index profile moves the zero-dispersion wavelength away from 1.55 mm. Then, indices and dimensions of different layers are adjusted so that the zero-dispersion wavelength is shifted back to 1.55 mm.

The design of large effective area dispersion-shifted fibers may evolve from known profiles, which provide zero dispersion at $l = 1.55\,mm$. Here, a simple profile as that shown in Fig. 4.1a is chosen as the reference profile. Obviously, this choice is not unique and other profiles might be considered in initiating the design. Material compositions for the reference W-fiber and other profiles in Fig. 4.1 (M_1, M_2, etc.) are given in Table 4.3. The reference W-fiber with $a_2 = 2.58\,mm$ and $a_3 = 5\,mm$ provides a negligible -0.0713 ps/nm.km dispersion and an effective-area of about 32 mm^2 at $l = 1.55\,mm$. To increase the effective-area, the central core is modified by adding a lower-index region to it. Doing so, a profile such as that shown in Fig. 4.1b is created which allows the fields to be less confined to the core region and, as a result, the effective-area will increase. Although lowering the index of a portion of the core of reference fiber brings the benefit of larger effective area, but moves the zero-dispersion wavelength away from 1.55 mm. To bring the zero-dispersion wavelength back to 1.55 mm, the dimensions and/or

the indices of the cladding regions must be altered. To what extent and which dimensions or indices need to be modified are dictated by several factors, including the size and index of the depressed-core region, the requirement that the fiber remain single-mode in the 1.55 mm window, and the designer's choice. Here, we initially choose to keep the indices (that is, the material compositions), and the radius of the outer cladding of the reference W-fiber unchanged. Then, the thickness of the lowest index cladding is adjusted to achieve nearly zero dispersion at $l = 1.55\ mm$.

The radius of the depressed-index core region, a_1, is varied from $2.0\ mm$ to $3.57\ mm$. Table 4.1 (rows 2 to 8) summarizes the dimensions and transmission properties at $l = 1.55\ mm$. The first row in this table gives the data for the reference W-fiber. Next, field distributions, effective-areas, mode-field-diameters, and dispersion for the reference fiber ($a_1 = 0$) and four of the depressed-core fibers with $a_1 = 2.0\ mm$, $2.7\ mm$, $3.01\ mm$, and $3.57\ mm$ are examined in more details. As indicated in Table 4.1, these fibers are labeled as fiber 'a', 'b', …. and 'e'. Figure 4.2 illustrates normalized radial field distributions, $y(r)$, at $l = 1.55\ mm$. It is observed that the confinement of field to the core is reduced as the radius of the depressed-index core is increased. This results in an increase in the effective-area. Figure 4.3 shows variations of effective-area versus wavelength in the 1.55 mm window for these fibers. As expected, fiber 'e' provides the largest effective-area, and, in general, the larger the radius of the depressed-index core region the larger the effective-area. The effective-area at $l = 1.55\ mm$ varies from 78 mm^2 for fiber 'b' to about 190 mm^2 for fiber 'e'. A larger effective-area, however, is achieved at the expense of a larger mode-field-diameter which, in turn, implies higher bending losses. This loss, however, is not serious if the bending radius is sufficiently larger than a critical radius. A mode-field-diameter about 10 mm or less has been considered reasonable in the literature. [16] Plots of mode-field-diameter versus wavelength are shown in Fig. 4.4. The mode-field-diameter at $l = 1.55\ mm$ varies from about 8.9 mm for fiber 'b' to 13.4 mm for fiber 'e'. It is now clear that a satisfactory design should maintain a balance between the effective-area and mode-field-diameter. Finally, the fundamental requirement of nearly zero dispersion at $l = 1.55\ mm$ is met by all fibers. This is seen in Fig. 4.5 which depicts variations of dispersion versus wavelength.

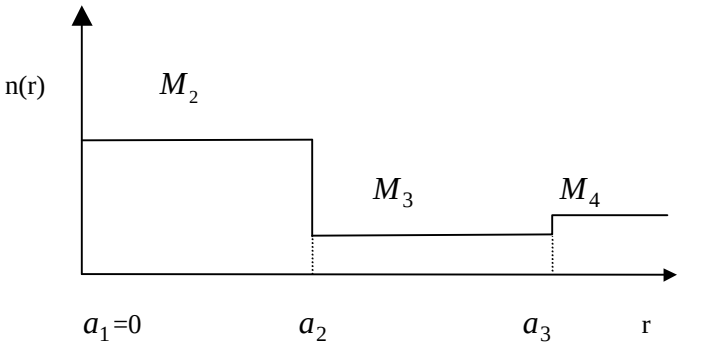

(a)

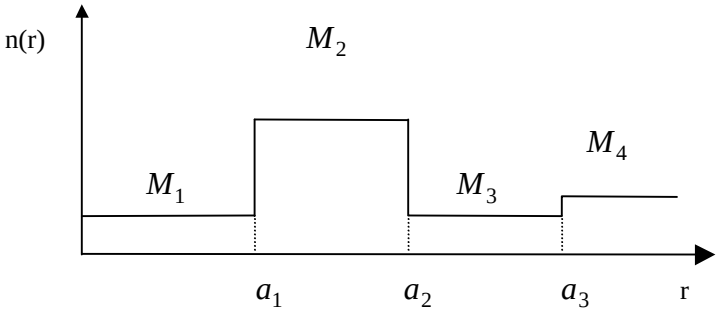

(b)

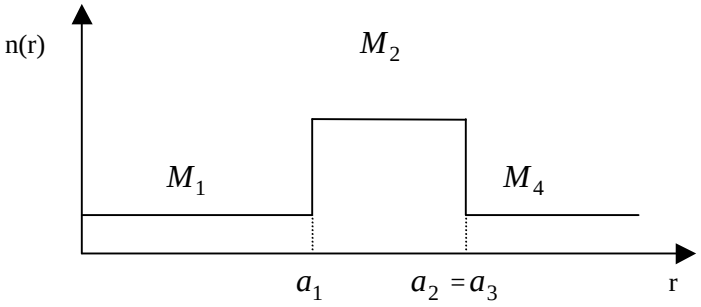

(c)

Figure 4.1 Refractive index profiles for (a) a reference dispersion-shifted W-fiber, and (b and c) depressed-core large effective-area dispersion-shifted fibers. Fiber dimensions and material compositions are given in Tables 4.1 and 4.3.

Table 4.1 Effective-area, mode-field-diameter, dispersion, dispersion slope (all at $l = 1.55\,mm$), cutoff wavelength and quality factor for a reference W-type and several triple-clad depressed-core fibers. All fibers have the same material compositions as indicated in Fig. 4.1.

a_1 mm)	a_2 (mm)	a_3 (mm)	A_{eff} (mm^2)	(mm)	(ps/nm.km)	(ps/ nm^2 .km)	(mm)	
0 [a]	2.58	5.0	31.97	6.47	0.029	0.035	1.08	0.764
2.0 [b]	3.5	5.0	78.04	8.94	0.028	0.045	1.33	0.976
2.4	3.8	5.0	96.40	9.65	0.054	0.050	1.38	1.04
2.7 [c]	4.0	5.0	113.18	10.30	-0.045	0.051	1.39	1.07
2.85	4.1	5.0	122.51	10.66	-0.010	0.052	1.41	1.08
3.01[d]	4.2	5.0	133.64	11.08	0.023	0.052	1.41	1.09
3.37	4.4	5.0	165.57	12.36	0.068	0.050	1.39	1.08
3.57[e]	4.5	5.0	189.84	13.34	0.054	0.049	1.37	1.07
2.7	3.9	4.35	118.93	10.75	0.015	0.055	1.39	1.03
2.7	3.8	4.0	123.42	11.10	-0.005	0.056	1.36	1.00
2.7	3.7	3.71	128.28	11.46	-0.032	0.056	1.31	0.977
2.8	4.0	4.6	123.60	10.85	-0.032	0.054	1.40	1.05
3.0	4.0	4.3	147.18	12.06	-0.050	0.053	1.34	1.01
3.2	4.0	4.1	183.38	13.78	-0.034	0.052	1.25	0.966
3.3	4.0	4.0	210.17	14.94	0.017	0.053	1.21	0.942

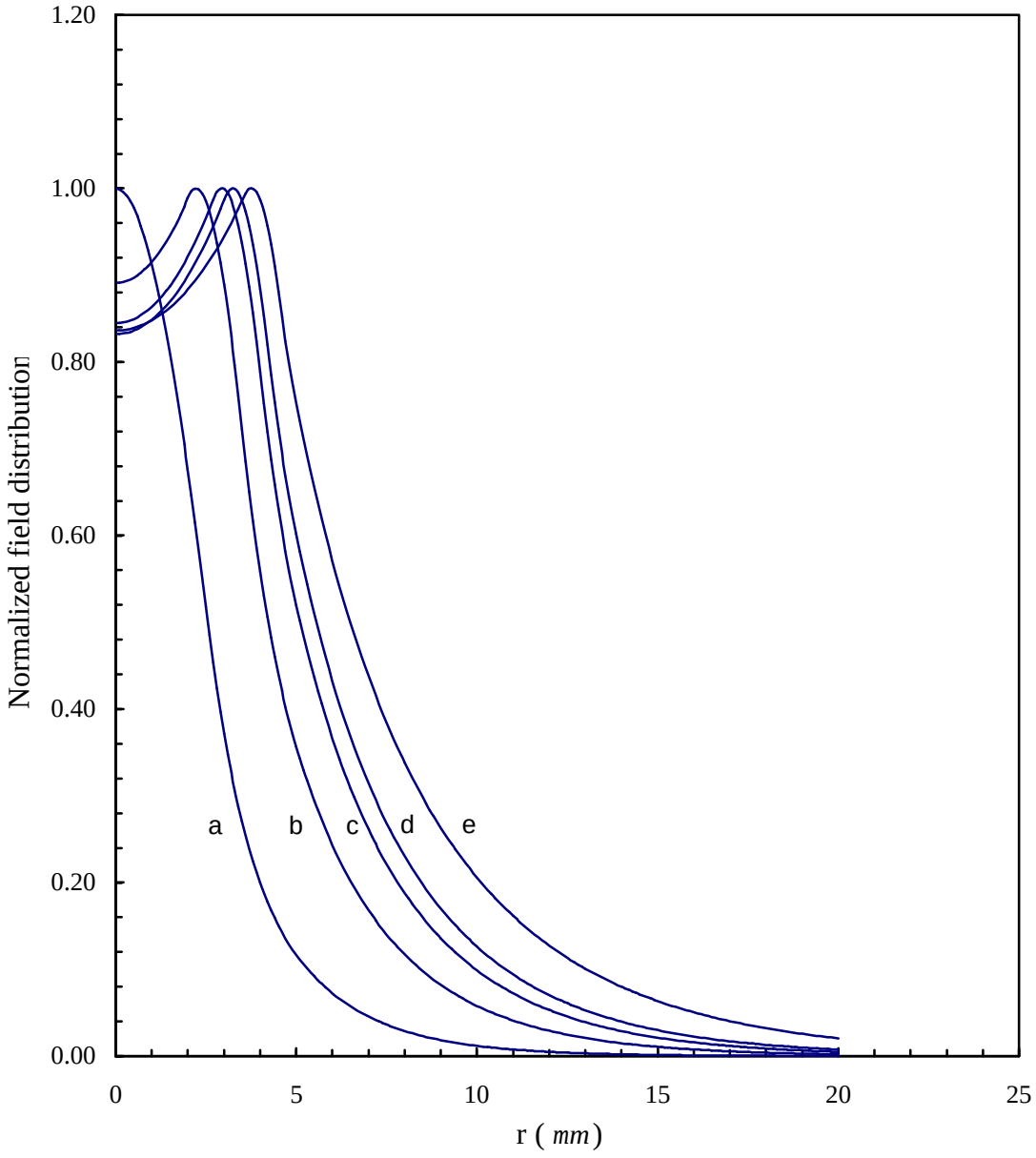

Figure 4.2 Normalized field distributions at $l = 1.55\,mm$ for (a) the reference W-fiber, and (b to e) large effective-area depressed-core fibers.

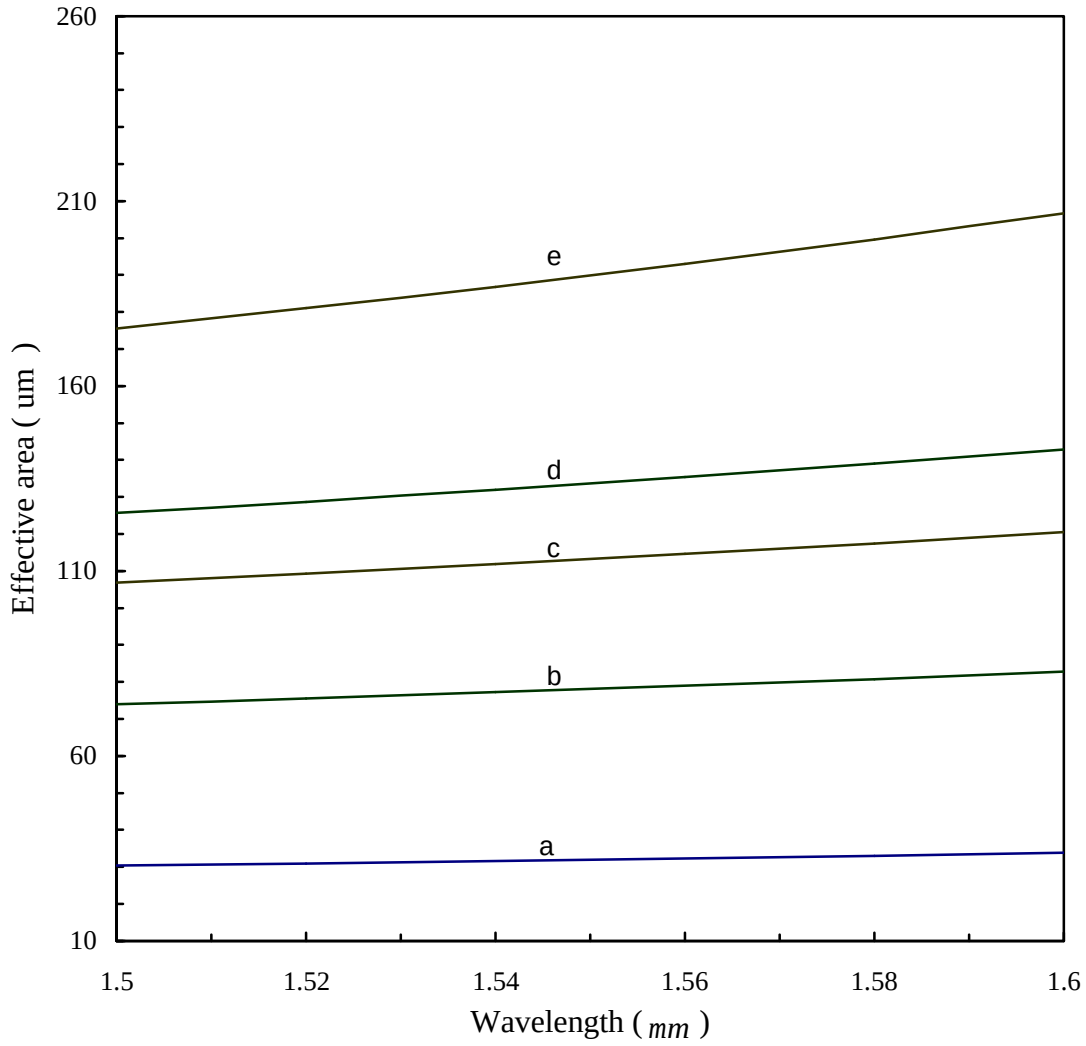

Figure 4.3 Variations of effective-area versus wavelength for fibers a to e with parameters given in Table 4.1

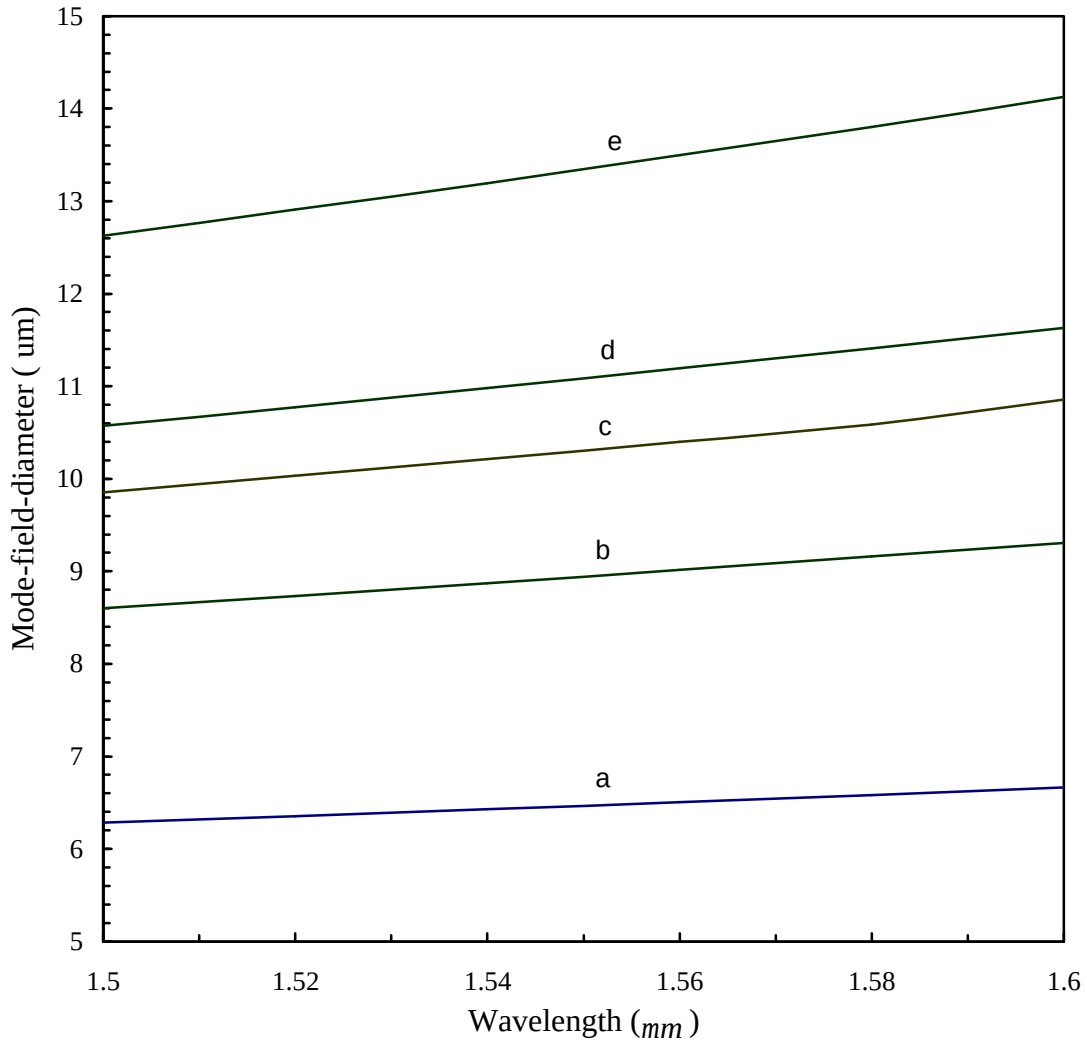

Figure 4.4 Variations of mode-field-diameter versus wavelength for fibers a to e with parameters given in Table 4.1.

Apart from negligible dispersion at $l = 1.55\ mm$, the dispersion slope is also an important property. As noted from Fig. 4.5 and Table 4.1, all four depressed-core fibers have nearly equal dispersion slope of about 0.05 ps/nm^2.km at $l = 1.55\ mm$. The wavelength range for single-mode operation is determined from the cutoff wavelength (l_c) of the second propagating mode. As noted from Table 4.1, l_c is less than 1.41 mm, indicating that all fibers are single-mode in the 1.55 mm window. This table also shows how transmission properties are affected when a_1 or a_2 is kept constant and the other two radii are varied. Rows 9 to 11 in Table 4.1 give the results for the case of a_1 kept constant at 2.7 mm, while rows 12 to 16 show the transmission properties when a_2 is kept constant at 4.0 mm. For $a_1 = 2.7\ mm$, it is observed that reducing the thickness of the second cladding, $a_3 - a_2$, results in larger effective-area and larger mode-field- diameter. In the limiting case of $a_3 - a_2 \to 0$, the fiber reduces to a double-clad depressed-core structure with index profile as that shown in Fig. 4.1c; see row 11. For $a_2 = 4.0\ mm$, corresponding to last four rows in Table 4.1, it is noted that increasing the core radius, a_1, and decreasing the thickness of the second cladding, $a_3 - a_2$, must occur simultaneously in order to maintain nearly zero dispersion at $l = 1.55\ mm$. In this case, sharp increases in both effective-area and mode-field-diameter occur. Again, a limiting case of $a_3 = a_2 = 4\ mm$ (last row) occurs which corresponds to a double-clad structure (Fig. 4.1c).

Refractive indices, which, so far, have been kept constant, may also be changed to vary the effective-area. To illustrate how index variations influence the effective-area, we choose fiber 'c' in Table 4.1 and replace its core material (M_1) once with a lower-index material (M_3) and once with a higher-index material (M_4). In doing so, the radius of the outer cladding (a_3) is kept unchanged and the other dimensions (a_1 and a_2) are adjusted to achieve zero dispersion at $l = 1.55\ mm$. These lower and higher core-index fibers are labeled as 'g' and 'f', respectively. Their dimensions and transmission properties are summarized in Table 4.2. It is noted that the fiber with higher core-index provides larger effective-area and mode-field-diameter than the fiber with lower core-index. The larger effective-area for fiber 'f' may be attributed to its flatter field distribution as shown in Fig. 4.6. Increasing the core index further and further eventually

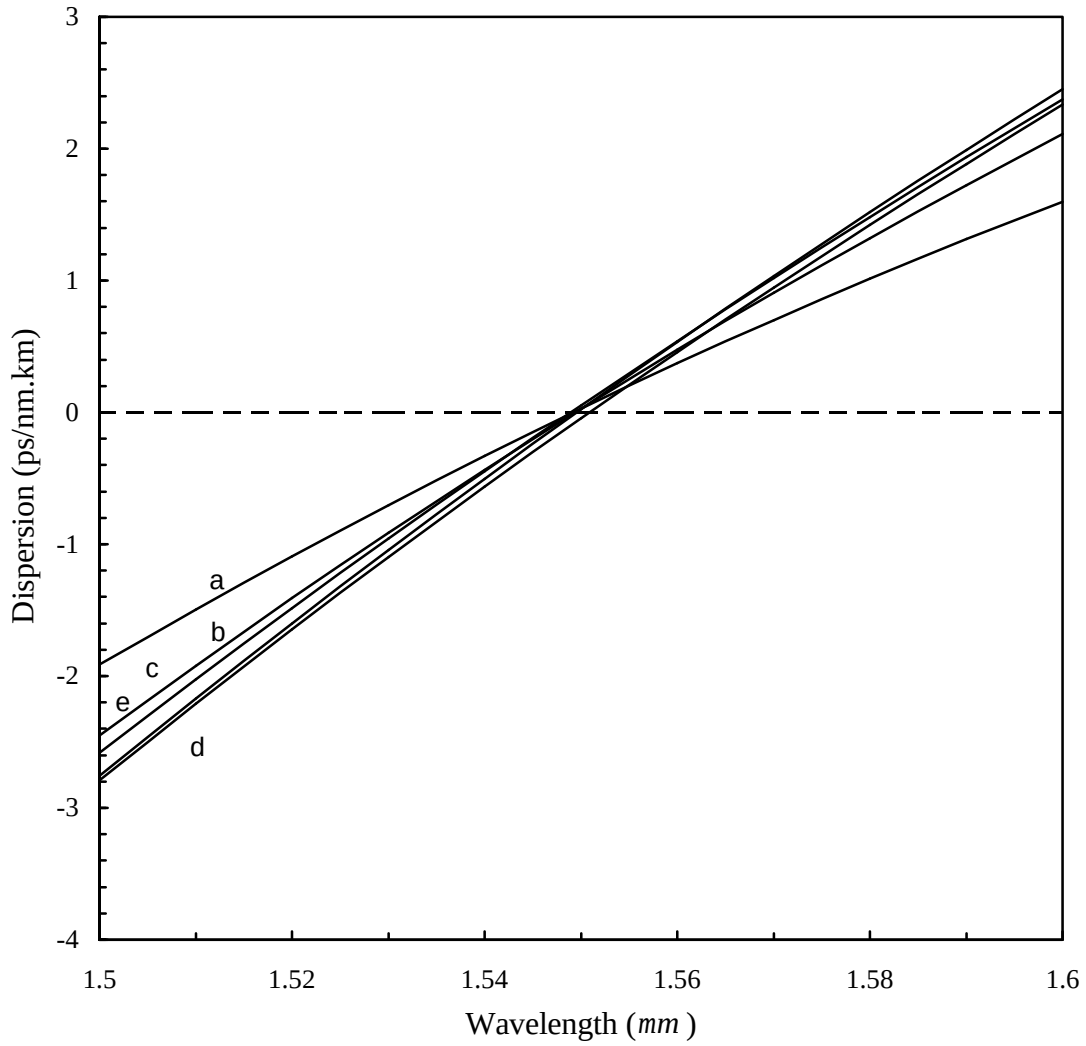

Figure 4.5 Variations of second-order dispersion versus wavelength for fibers a to e.

results in reduction of effective-area as the profile becomes closer and closer to that of the W-fiber in Fig. 4.1a for which the effective-area is about $32\,mm^2$. A smaller index difference between the core and first cladding may be maintained by lowering the index of this cladding. As an example, material M_2 in fiber 'c' may be replaced with material M_5 to obtain a dispersion-shifted fiber. The parameters and properties of this fiber, labeled as 'h', are given in Table 4.2 (row 3). The result is even flatter field distribution compared to that of fiber 'f' and larger effective-area and mode-field-diameter.

The data in Tables 4.1 and 4.2 clearly indicate that there exist many possibilities for achieving both large effective-area and negligible dispersion at $l = 1.55\,mm$. Now, the question is which fiber offers a better performance; namely, less signal distortion and less loss. The data in these tables clearly indicate the trade-off between the effective-area that provides a measure of signal distortion due to nonlinearity and the mode-field-diameter that is an indicator for bending loss. Assuming that all other losses such as intrinsic and microbending losses are about the same for all fibers in Tables 4.1 and 4.2, the performance of a design may be assessed in terms of a quality factor defined as $Q = A_{eff} / d_0^2$. This factor is a dimensionless quantity that can be used

Table 4.2 Effective-area, mode-field-diameter, dispersion, dispersion slope (all at $l = 1.55\,mm$), cutoff wavelength and quality factor for triple-clad depressed-core fibers with different material compositions.

a_1 (mm)	a_2 (mm)	a_3 (mm)	A_{eff} (mm^2)	d_0 (mm)	D (ps/nm.km)	D' (ps/nm^2.km)	l_c (mm)	Q
2.7 [f]	3.77	5.0	124.04	11.30	0.016	0.057	1.24	0.971
2.1 [g]	3.88	5.0	88.02	8.82	0.036	0.059	1.50	1.13
1.2 [h]	4.65	5.0	130.02	12.87	0.049	-0.0036	1.27	0.785

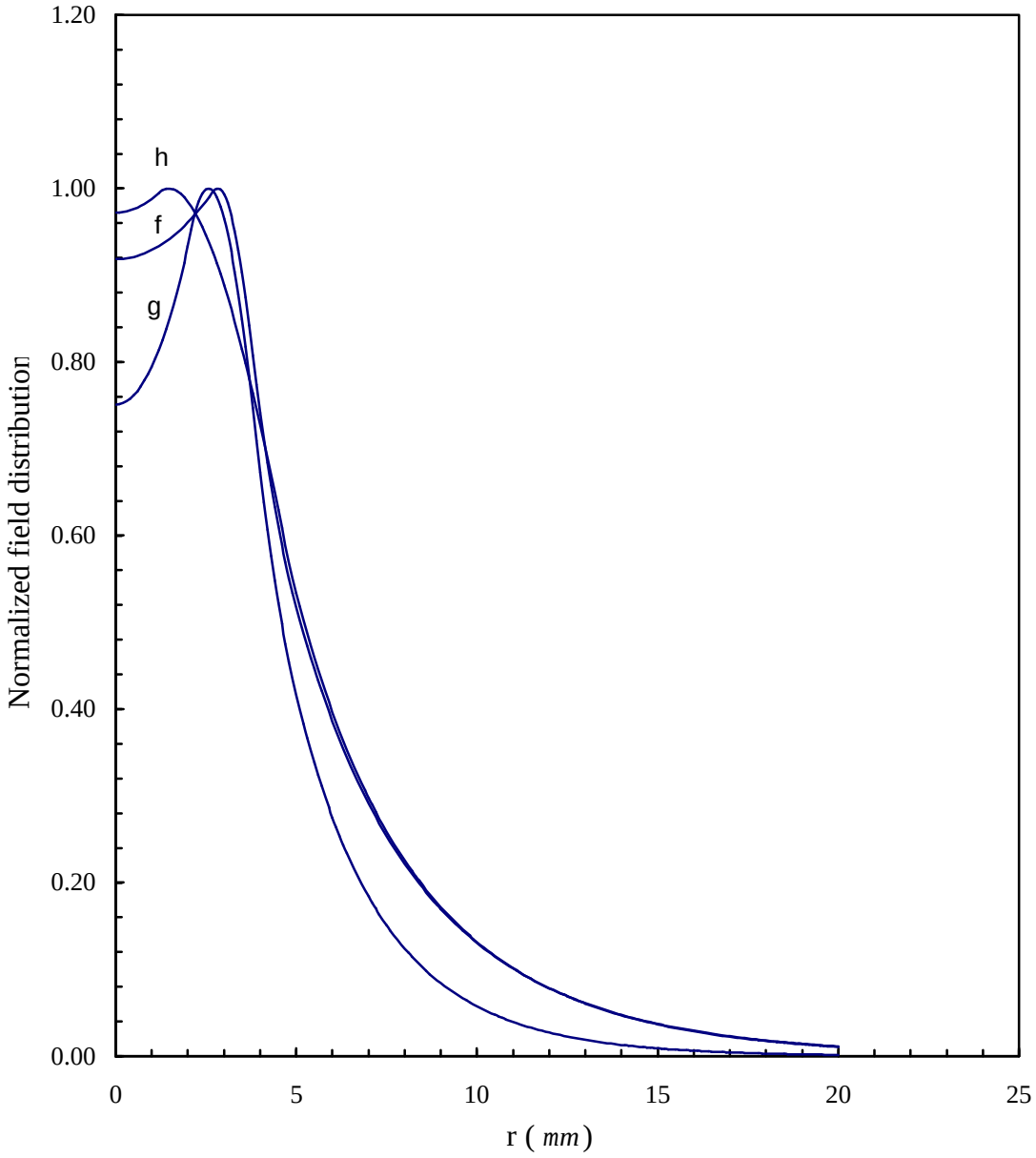

Figure 4.6 Normalized field distributions at $l = 1.55\ mm$ for fibers f, g and h.

to determine the tradeoff between mode-field-diameter and effective-area. Then, among several designs satisfying certain limits on effective-area and mode-field-diameter, say A_{eff} about 80 mm^2 or larger and d_o about 10 mm or smaller, the fiber that provides the largest quality factor is the best design. Accordingly, fiber 'g' among all fibers in Tables 4.1 and 4.2 meets the design requirements for maximum effective-area and minimum mode-field-diameter and provides the largest quality factor (Q=1.13). The quality factor for conventional dispersion-shifted fibers is about 0.741. [22] A comprehensive optimization of index profile for large effective-area fibers is an important and challenging task, which should be based on a more broadly defined quality factor accounting for all losses, and is beyond the scope of this paper. In summary, the trade-off between effective-area and mode-field-diameter is an important deciding factor in selection of a design.

The intrinsic losses of large effective-area fibers due to material properties of doped and pure silica glass are expected to be about the same as those in conventional dispersion-shifted fibers. This is based on the fact that the index differences are very small. The low-loss single-mode large effective-area fibers reported in the literature have $\Delta n < 0.015$. [12] The largest Δn in the profiles of Fig. 4.1 is that between the central core and the first cladding which, at $l = 1.55\,mm$, is equal to 0.0109. Bending and microbending losses are significant contributing factors to overall fiber losses. The amount of bending loss depends on the bend radius and the mode-field-diameter of the fiber. Fiber designs with mode-field-diameters about 10 mm or less result in negligible bending losses (with bending radius $\geq$ 30 mm). [12, 16] Using the method outlined in reference 28 (ch.23), bending losses were calculated at $l = 1.55\,mm$. The results are presented in Fig. 4.7 which illustrates variations of bending loss versus bending radius for fibers 'a' to 'e'. It is emphasized that the accuracy of this method is subject to sufficiently large bending radii so that the attenuation of local-mode power can be ignored. It is clearly observed from Fig. 4.7 that fibers with larger effective-area and hence larger mode-field-diameter suffer larger bending losses. However, for bending radii greater than 30 mm, the bending loss for fiber 'c' (as representative of a large effective-area fiber) is less than 0.021 dB/m.

Microbending loss occurs when fibers are gathered in a cable. The analysis of microbending loss presented here is based on the work of Marcuse. [42] In this analysis,

microdeformations are assumed to be Gaussian with an r.m.s. deviation s and a coherence length L_c. Figure 4.8 shows variations of microbending loss coefficient for $s = 1\,nm$ and several values of coherence length versus wavelength for fiber 'c' as a representative case. There are no reliable information on s and L_c, and for purpose of comparison, the same values as those in reference 42 are used here. The jacket inner diameter is assumed to be 125 mm. Comparison of these results with those for ordinary step-index fibers presented by Marcuse [42] indicates that microbending losses of the low nonlinearity fiber proposed here and those of the conventional fibers are in the same range. For example, microbending losses at $l = 1.55\,mm$ for fiber 'c' with $L_c = 1$, 10, 100, and 500 mm are 5.78, 7.17, 1.07, and 0.0135 dB/km, while the corresponding losses for fiber 'a' (as an example of conventional dispersion-shifted fiber) are 3.30, 10.6, 2.24, and 2.22×10^{-6} dB/km. It is noted that for coherence lengths 1, 10, and 100 mm, the microbending losses of both fibers are comparable, and for $L_c = 500\,mm$, both microbending losses are negligible although the microbending loss of fiber 'a' is much smaller than that of fiber 'c'. This observation together with small index differences between adjacent layers (<1%) and small bending losses for bending radii greater than 30 mm suggests that the total loss of the fibers with mode-field-diameters about $10\,mm$ or less should be in the same range as those of existing low-loss dispersion-shifted fibers. The multiple-clad low nonlinearity fibers presented here can be fabricated using the existing techniques such as modified-chemical-vapor-deposition (MCVD) [58] and inside-vapor deposition (IVD). [59]

Finally, variations of splice losses versus wavelength for fibers a to e are shown in Figure 4.9. The splice loss that is calculated here is caused by a lateral misalignment between two identical fibers, the transmitting and receiving fibers. From Fig. 4.9, it is noted that the larger is the effective-area of a fiber, the lower is the splice loss. This is explained by the fact that, when a fiber has a large effective-area, its electromagnetic fields are more spread throughout the claddings, resulting in less sensitivity to lateral misalignments.

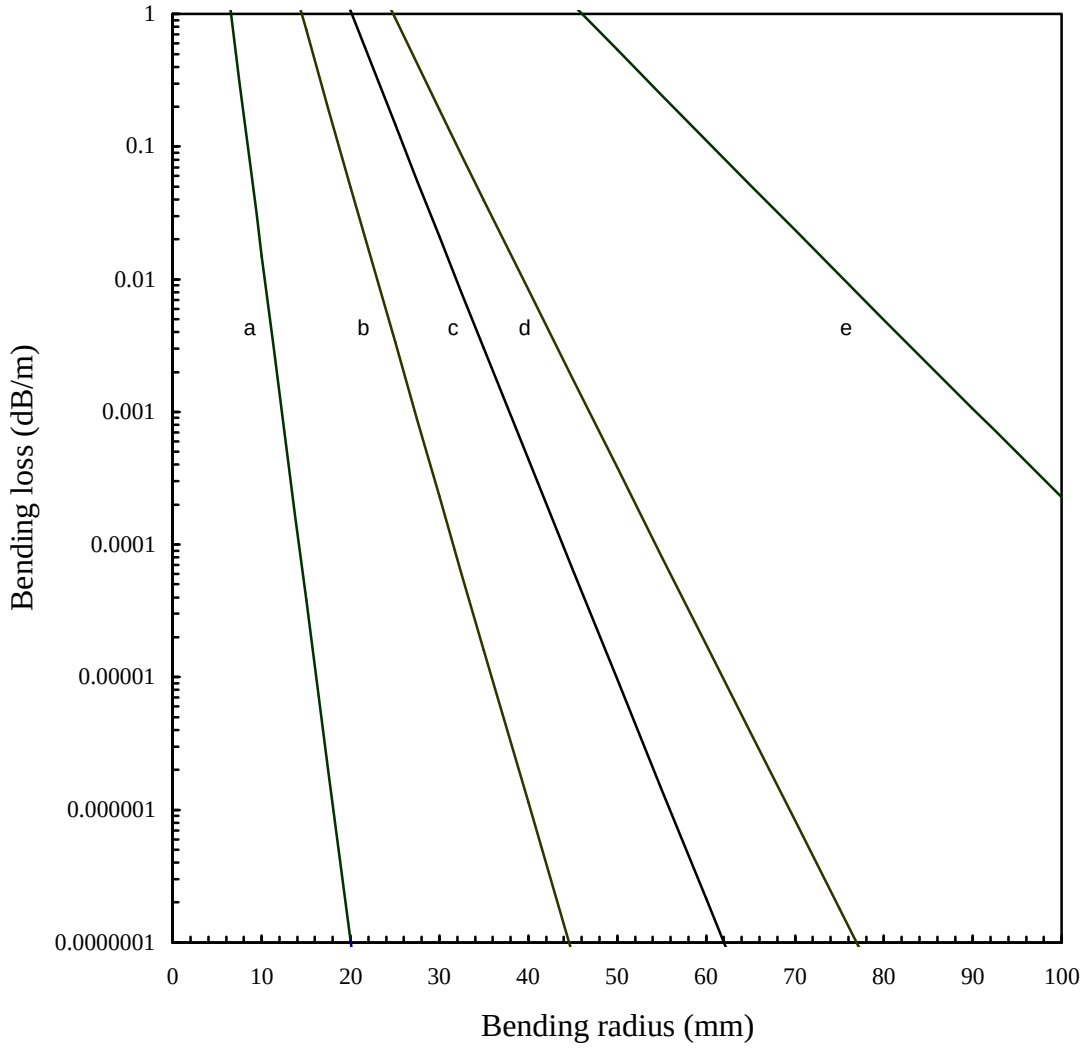

Figure 4.7 Variations of bending loss versus bending radius, at $l = 1.55\,mm$, for fibers a to e.

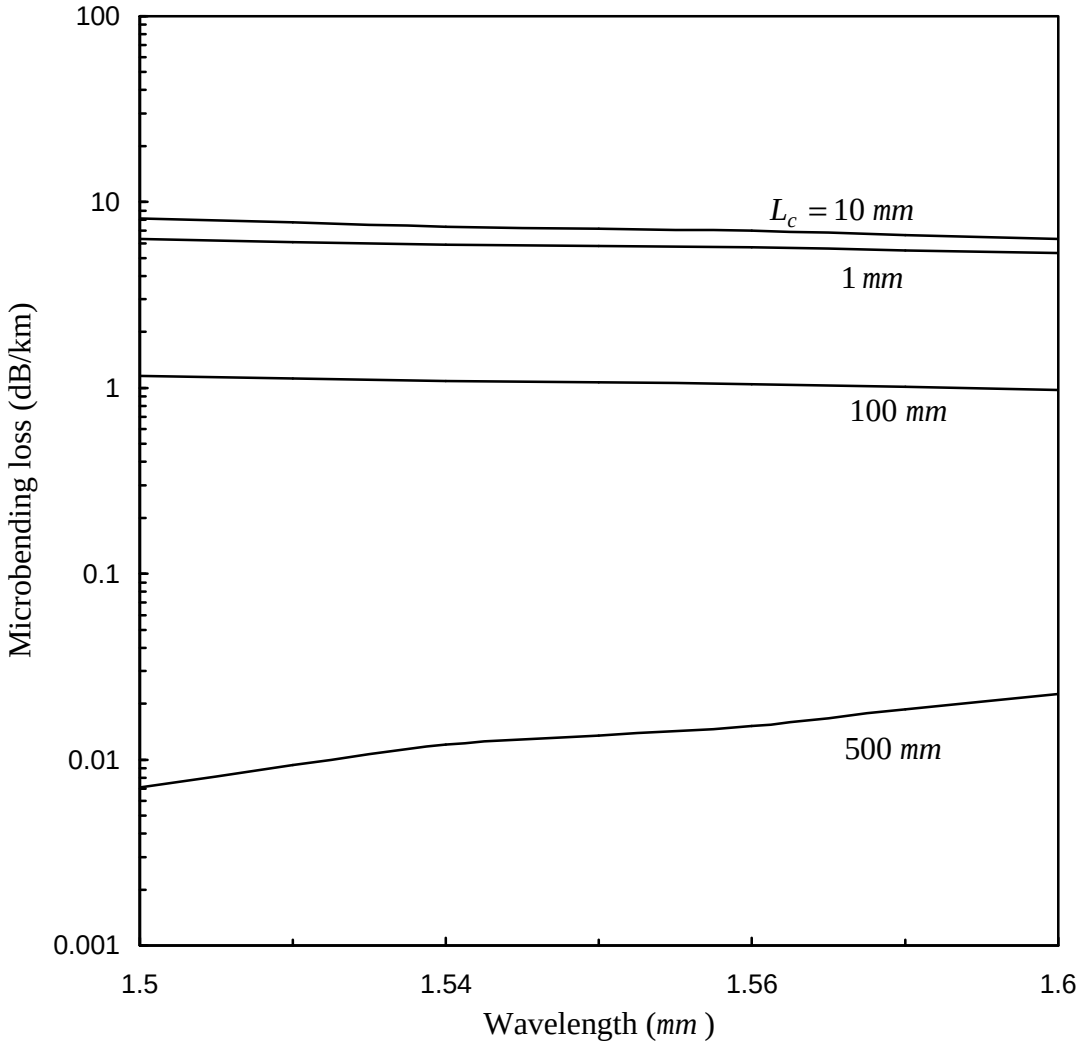

Figure 4.8 Variations of microbending loss of fiber c versus wavelength for several values of correlation lengths.

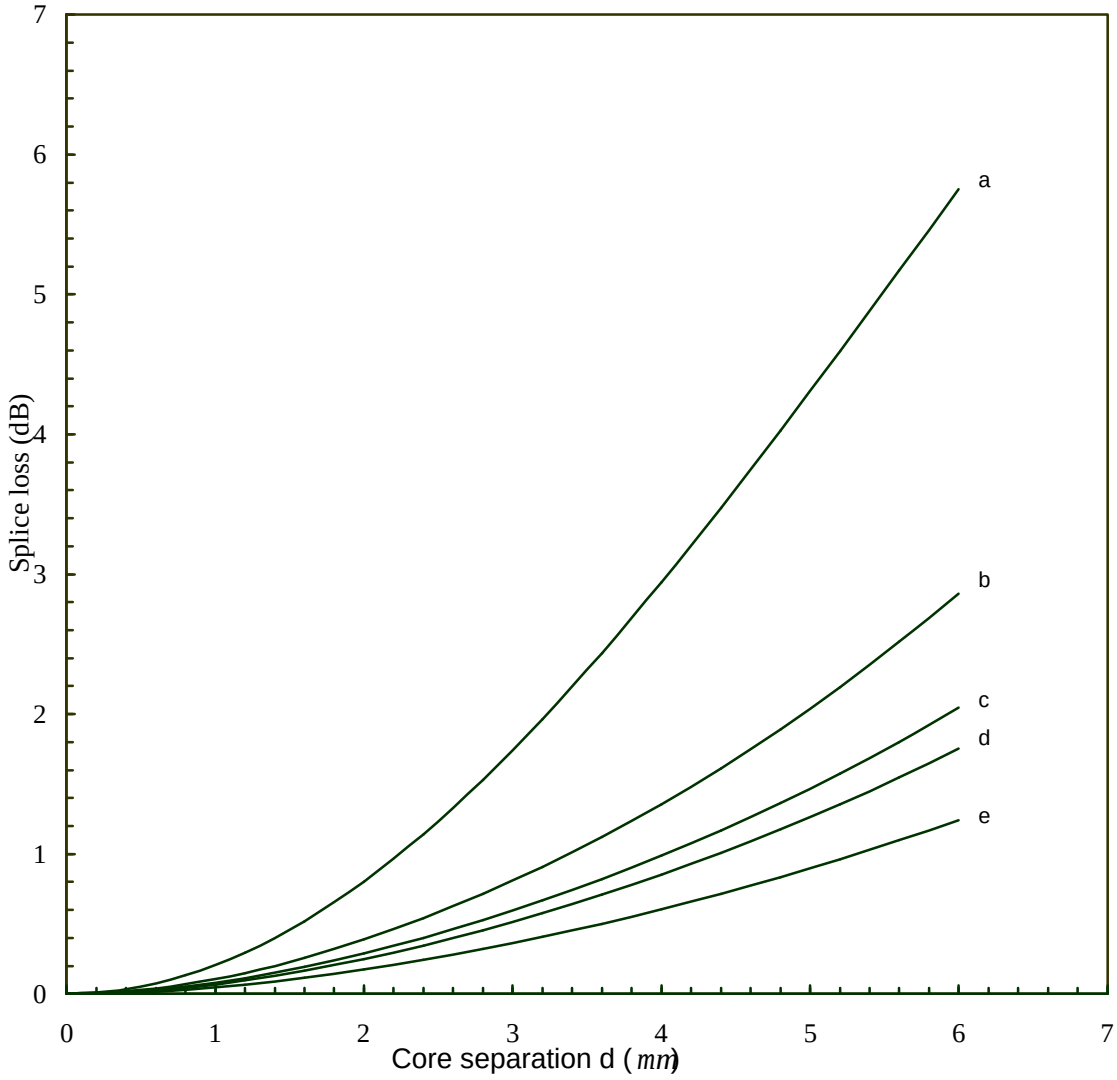

Figure 4.9 Variations of splice loss versus wavelength for fibers a to e.

Table 4.3 Material compositions and index difference $\Delta = \left[\left(n_{M2} \right)^2 - \left(n_{Mi} \right)^2 \right] / 2 \left(n_{M2} \right)^2$ for fibers in Tables 4.1 and 4.2.

Material	Material compositions	Index difference, Δ
M_1	$9.1\,m/o\ GeO_2, 83.2\,m/o\ SiO_2, 7.7\,m/o\ B_2O_3$	0.743 %
M_2	$13.5\,m/o\ GeO_2, 86.5\,m/o\ SiO_2$	0 %
M_3	$5.8\,m/o\ GeO_2, 94.2\,m/o\ SiO_2$ (*Chilled*)	0.888 %
M_4	$7.0\,m/o\ GeO_2, 93.0\,m/o\ SiO_2$	0.719 %
M_5	$9.1\,m/o\ P_2O_5, 90.9\,m/o\ SiO_2$ (*Quenched*)	0.479 %

4.2 Designs for Dispersion-Flattened Fibers

Dispersion-flattened fibers are special fibers that provide small dispersion over an extended range of wavelengths. The dispersion-flattened fibers discussed here must exhibit larger effective-areas than conventional dispersion-flattened fibers and have low losses (microbending, bending, intrinsic and splice losses). The large effective-area can be very useful to broadband WDM (Wavelength Division Multiplexing) systems involving very long distances.

The dispersion-flattened fibers presented here are four- or five-layer circular dielectric waveguides. The central core is depressed in order to increase the effective-area. All design requirements for losses and dispersion must be satisfied at the same time, while a large effective-area is sought. Dispersion-flattened fibers with effective-areas on the order of 90 mm^2 at 1.55 mm are designed. Their dimensions and material compositions are summarized in Table 4.4.

Fibers i and j are very similar, but provide slightly different dispersion at 1.55 mm. They have about the same effective-areas, mode-field-diameters, bending, microbending and splice losses.

The second-order dispersions for fibers i, j and k are 0.0305, 0.3847 and 0.0740 ps/nm.km, respectively, at 1.55 mm. The third-order dispersions for these three fibers, at 1.55 mm, are equal to -1.52×10^{-2}, -9.26×10^{-3} and -3.95×10^{-3} ps/nm^2.km. For these three fibers, Figures 4.10 and 4.11 illustrate variations of second-order and third-order dispersion versus wavelength, respectively.

The effective-areas for fibers i, j and k are equal to 89, 90.5 and 93.4 mm^2, respectively, at 1.55 mm. Note that these values are about 1.8 times greater than those in conventional dispersion-shifted fibers. Figure 4.12 shows variations of effective-area versus wavelength for these three fibers.

The effective-areas of the above three fibers are smaller than those of the dispersion-shifted fibers in Tables 4.1 and 4.2. This is due to the fact that the third layer in dispersion-flattened fibers generally has a much smaller refractive index than the second layer and this causes the field to decay more rapidly. However, to achieve larger effective-areas, the fields must decay as slowly as possible in the claddings. In other words, flattened dispersion characteristic and larger effective-area seem to be opposing requirements and hence a trade-off.

The cutoff wavelengths of fibers i, j, and k are 0.92, 0.94 and 0.96 mm, respectively. The splice and microbending losses are comparable to those in conventional fibers. The splice losses due to lateral separation for these fibers are illustrated in Figure 4.13. As fibers i and j are expected to exhibit similar microbending losses, only microbending loss for fiber i is presented. Figures 4.14 and 4.15 illustrate microbending losses for fibers i and k for several values of correlation lengths L_c. In these Figures, the jacket radius is assumed to be 62.5 mm and $s = 1\,nm$. It is noted that the microbending losses for fibers i and k are on the same order of magnitude, reinforcing the idea that these designs have similar transmission properties.

Finally, variations of mode-field-diameter versus wavelength are shown in Figure 4.16. It is noted that the largest effective area fiber, k, exhibits the largest mode-field-diameter and thus a higher bending loss. The mode-field-diameters for fibers i, j, and k, at 1.55 mm, are equal

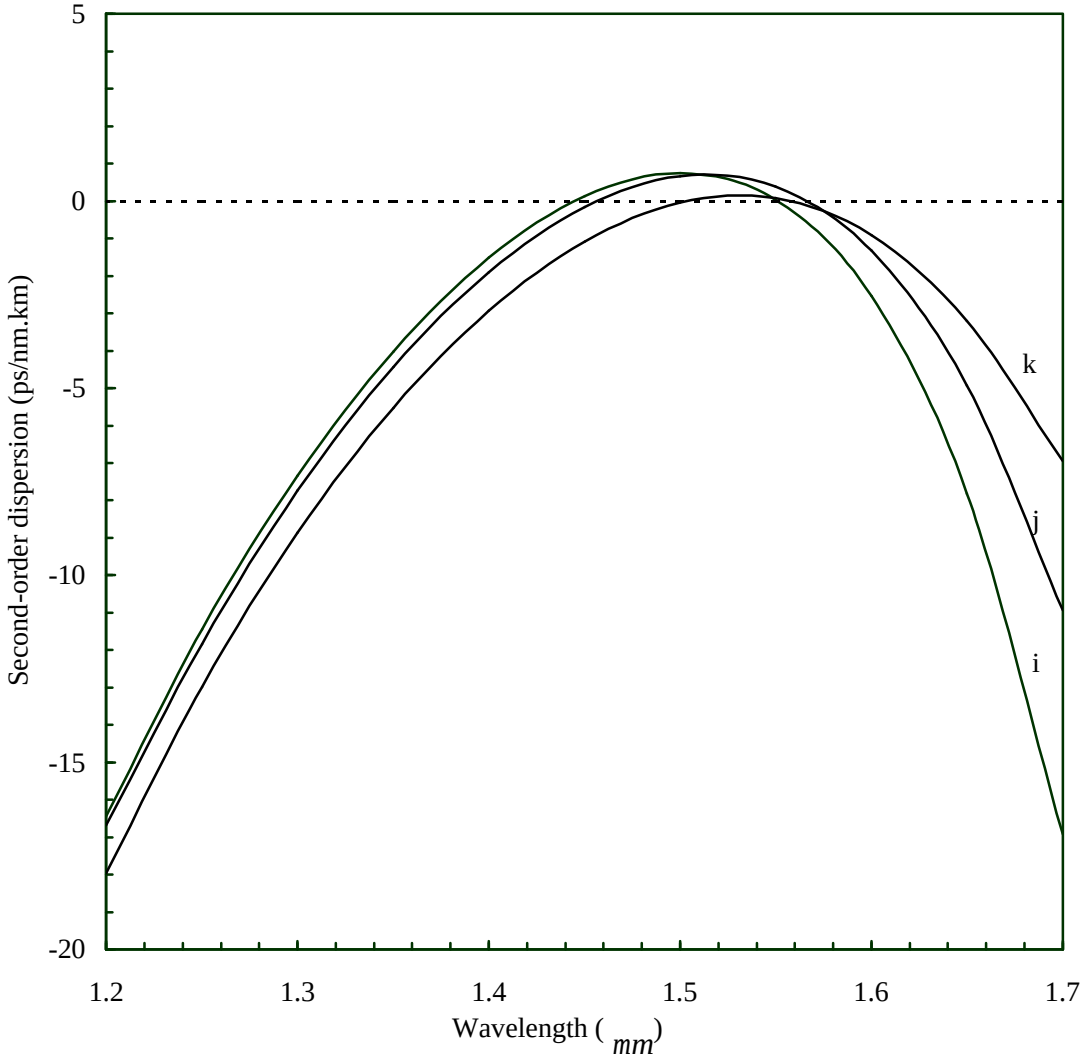

Figure 4.10 Variations of second-order dispersion versus wavelength for fibers i, j and k.

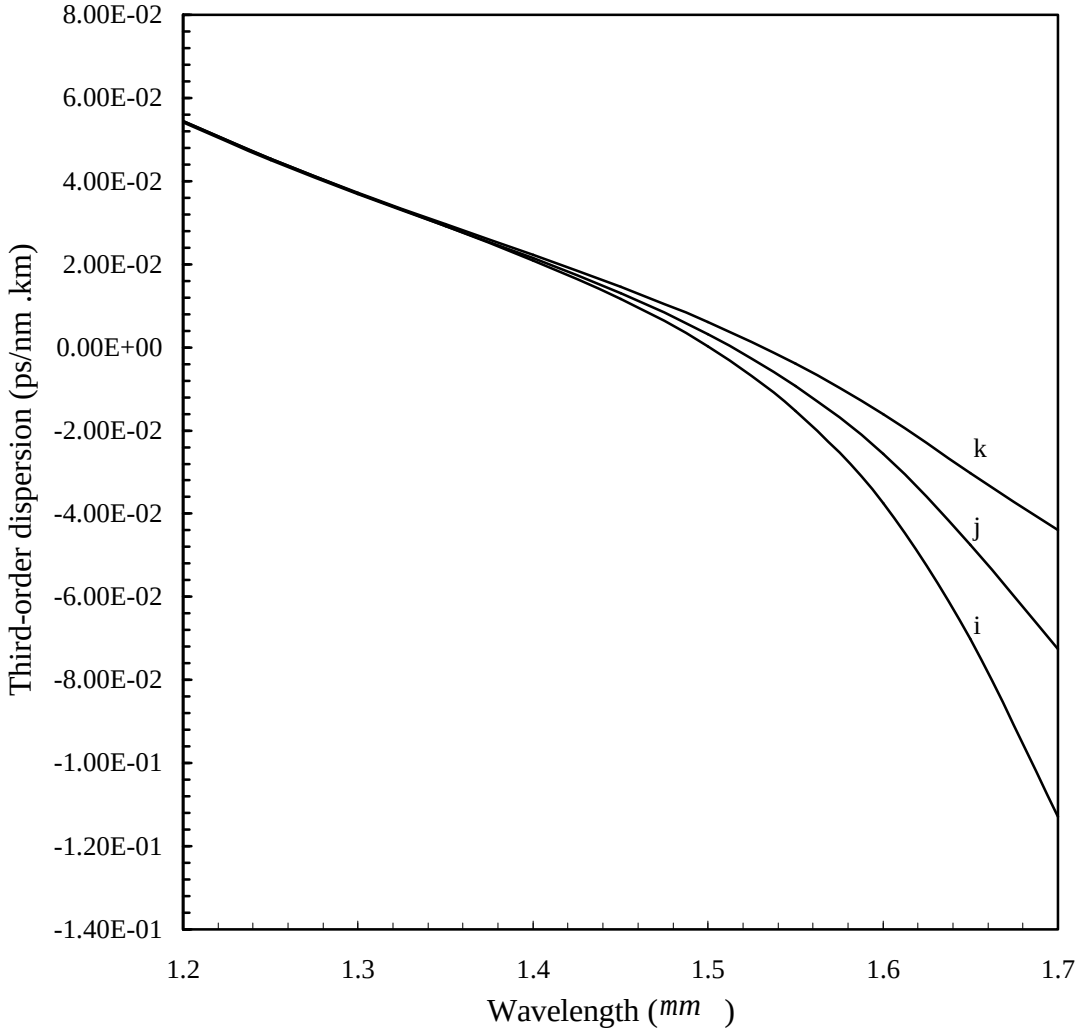

Figure 4.11 Variations of third-order dispersion versus wavelength for fibers i, j and k.

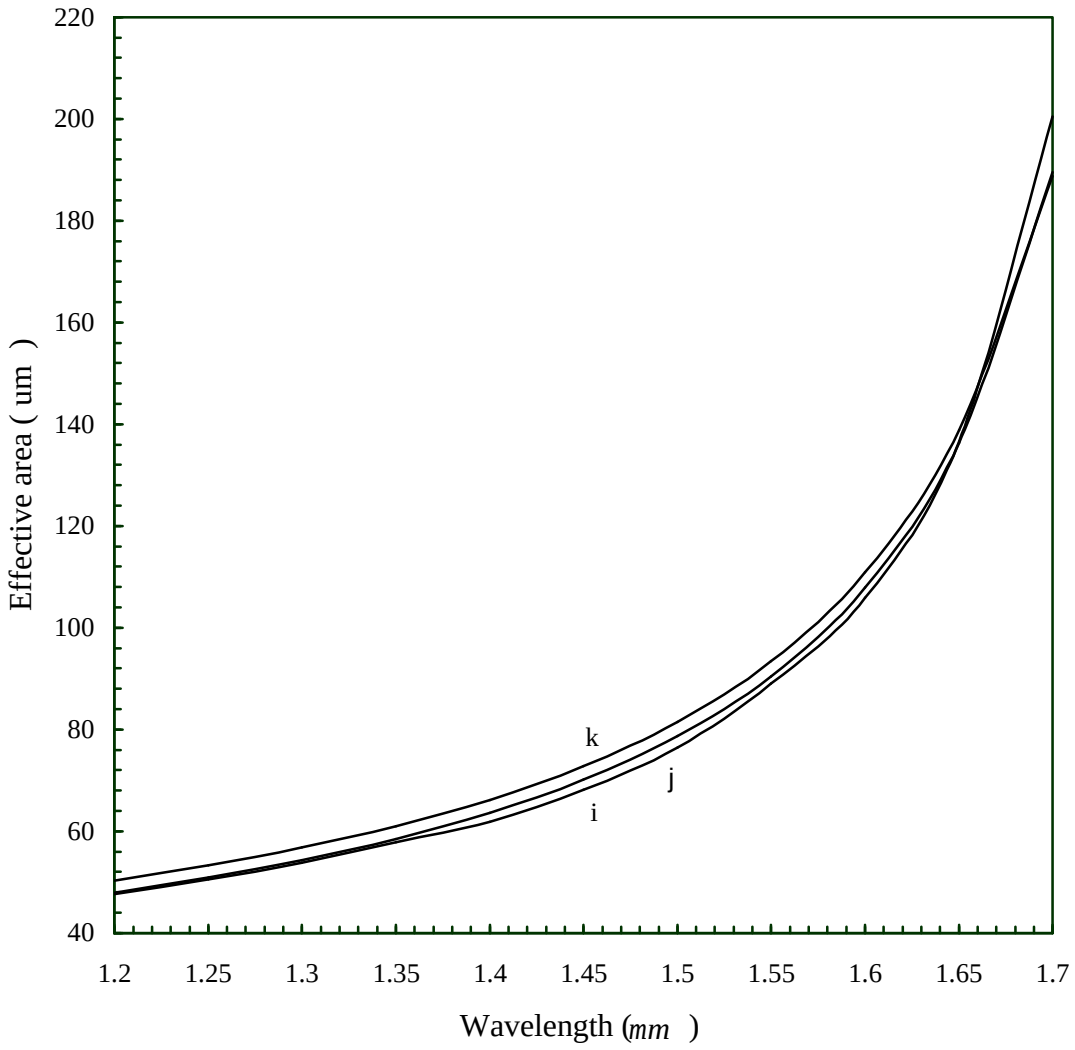

Figure 4.12 Variations of effective-area versus wavelength for fibers i, j and k.

Table 4.4- Material compositions and dimensions for dispersion-flattened fibers. Fibers i and j are four layer-fiber and fiber k is a five-layer fiber.

Fiber	Material compositions	Dimensions
i	$3.5\%\ B_2O_3, 96.5\%\ SiO_2\ (Chilled)$ $4.1\%\ GeO_2, 95.9\%\ SiO_2$ $13.5\%\ B_2O_3, 86.5\%\ SiO_2$ SiO_2	$a_1 = 1.0\ mm$ $a_2 = 3.0\ mm$ $a_3 = 6.2\ mm$
j	$3.5\%\ B_2O_3, 96.5\%\ SiO_2\ (Chilled)$ $4.1\%\ GeO_2, 95.9\%\ SiO_2$ $13.5\%\ B_2O_3, 86.5\%\ SiO_2$ SiO_2	$a_1 = 1.0\ mm$ $a_2 = 3.0\ mm$ $a_3 = 6.0\ mm$
k	$1.0\%\ F, 99.0\%\ SiO_2\ (Quenched)$ $4.1\%\ GeO_2, 95.9\%\ SiO_2$ $13.5\%\ B_2O_3, 86.5\%\ SiO_2$ $13.5\%\ GeO_2, 86.5\%\ SiO_2\ (Chilled)$ SiO_2	$a_1 = 1.0\ mm$ $a_2 = 3.1\ mm$ $a_3 = 4.8\ mm$ $a_4 = 6.0\ mm$

to 10.36, 10.45 and 10.48 mm, respectively. These values are within the range of tolerable values. [16] Figure 4.17 shows variations of bending losses versus bending radius for these three fibers. It is noted that these fibers present large bending losses, despite having tolerable values of mode-field-diameter. This clearly indicates that mode-field-diameter is not always a good indication of bending loss. On the other hand, tolerable bending losses can always be obtained if we work with a bending radius greater than a minimum radius. In the case of these dispersion-flattened fibers, a minimum radius of 100 mm provides low bending losses. It is widely known by fiber manufacturers that dispersion-flattened fibers usually exhibit high bending losses and are very sensitive to fabrication tolerances, being very difficult to be fabricated in practice.

4.3 Tradeoffs in the Design

The main advantage of the fiber designs presented here over conventional fibers is their larger effective-area. However, a larger effective-area comes at the expense of larger mode-field-diameter and, consequently higher bending loss. Bending loss is negligible if the bending radius is greater than a critical value. Kato et al. [16] have stated that tolerable bending losses can be achieved if the mode-field-diameter (d_o) is less than or equal a maximum value ($d_{\max}$), for a given bending radius. This maximum value is around 11 mm for a bending diameter of 30 mm. Based on this criterion, fibers a, b, c, i, j and k can be considered well designed and satisfactory. This is true for the dispersion-shifted fibers, but not for the dispersion-flattened fibers. The dispersion-flattened fibers exhibit large bending losses compared with dispersion-shifted fibers. A possible solution for this problem is to avoid bending these dispersion-flattened fibers with a radius less than 100 mm. However, this critical radius may be unsatisfactory for certain cable designs in which the fibers are bent in a smaller radius than this critical value.

Assuming that all other losses such as intrinsic and microbending losses are about the same for all fibers in Tables 4.1, 4.2 and 4.4, the performance of a design may be assessed in terms of a quality factor defined as $Q = A_{eff} / d_0^2$; the higher the quality factor, the better the design. Based on this criterion, the best design in Tables 4.1, 4.2 and 4.4 would be fibers d, g

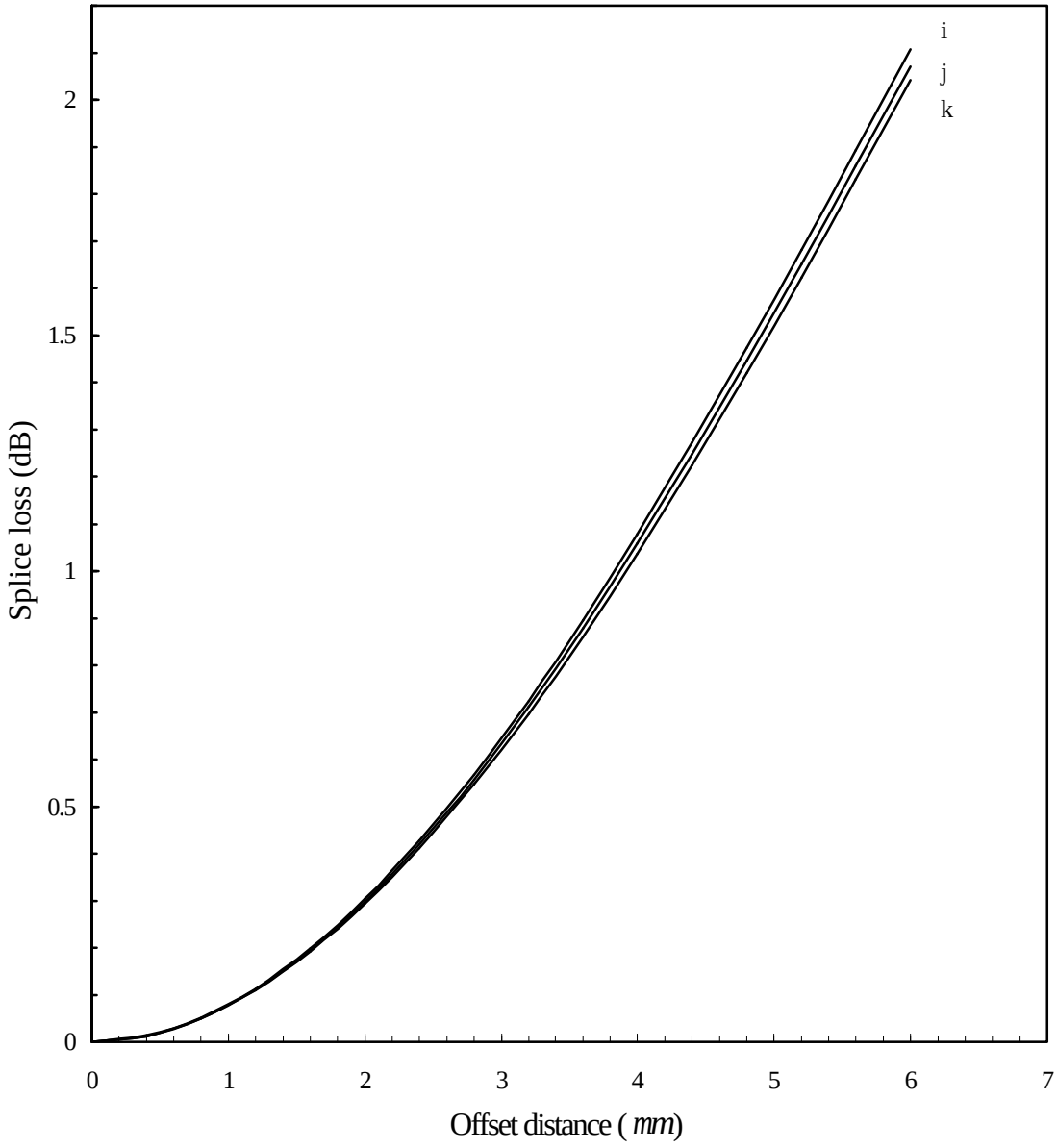

Figure 4.13 Variations of splice loss versus lateral displacement for fibers i, j and k, at 1.55 *mm* .

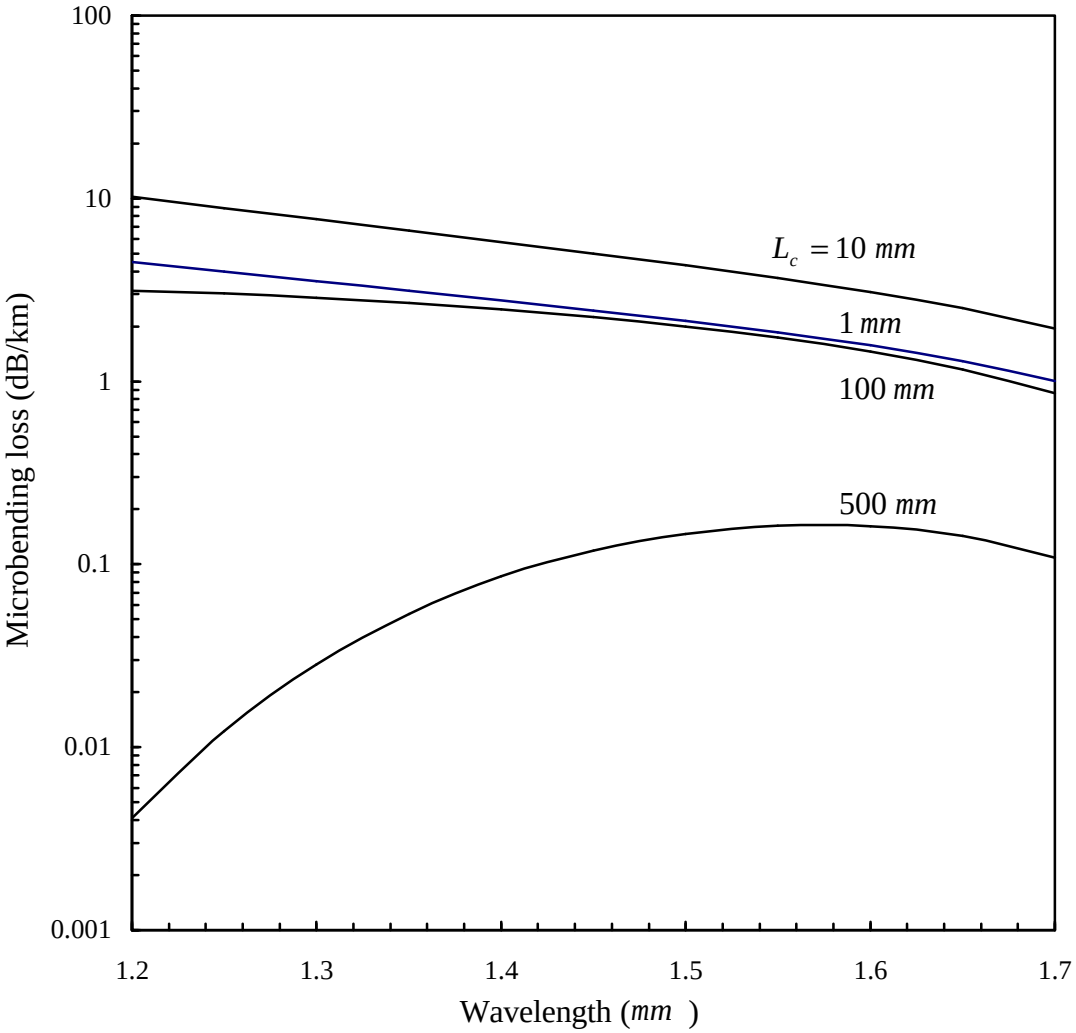

Figure 4.14 Variations of microbending loss versus wavelength for fiber i.

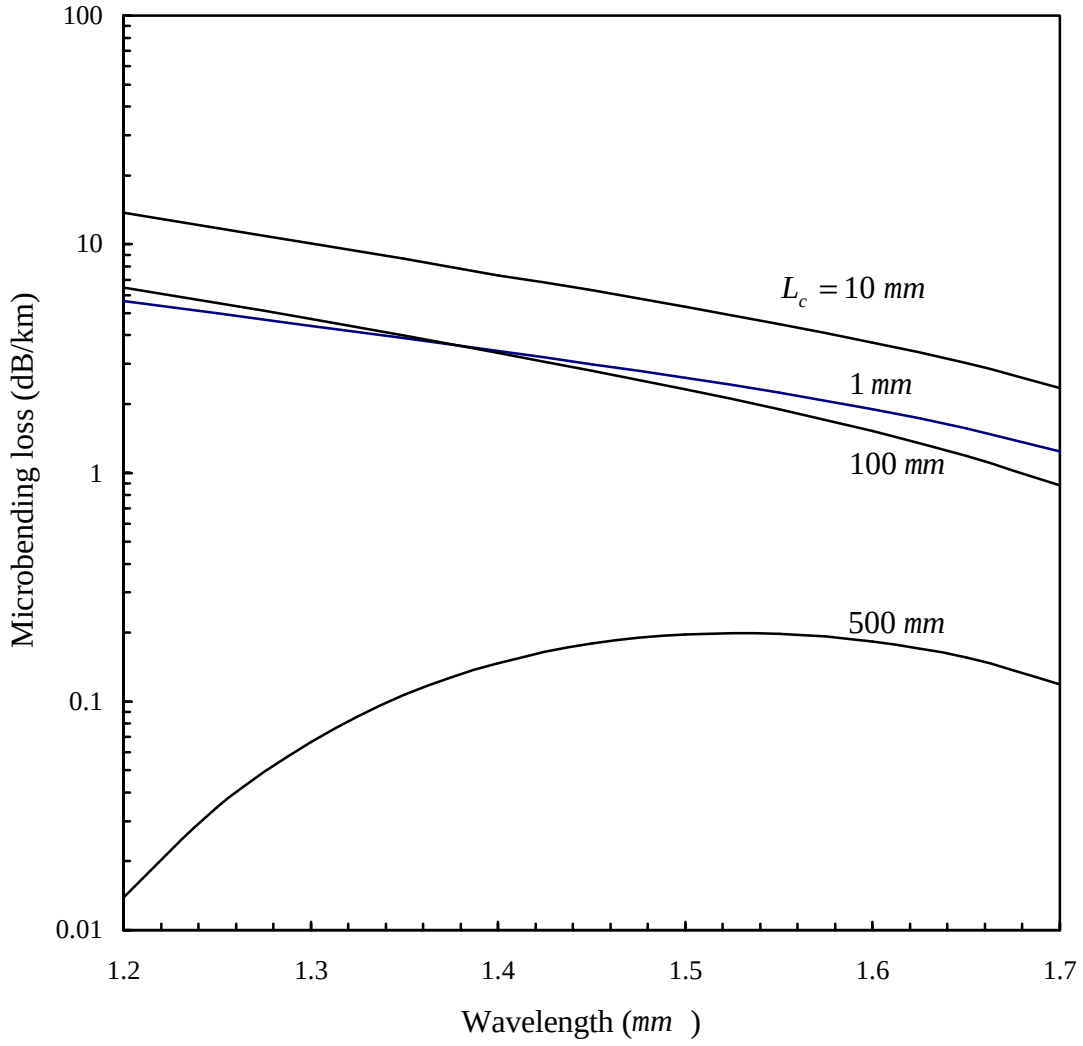

Figure 4.15 Variations of microbending loss versus wavelength for fiber k.

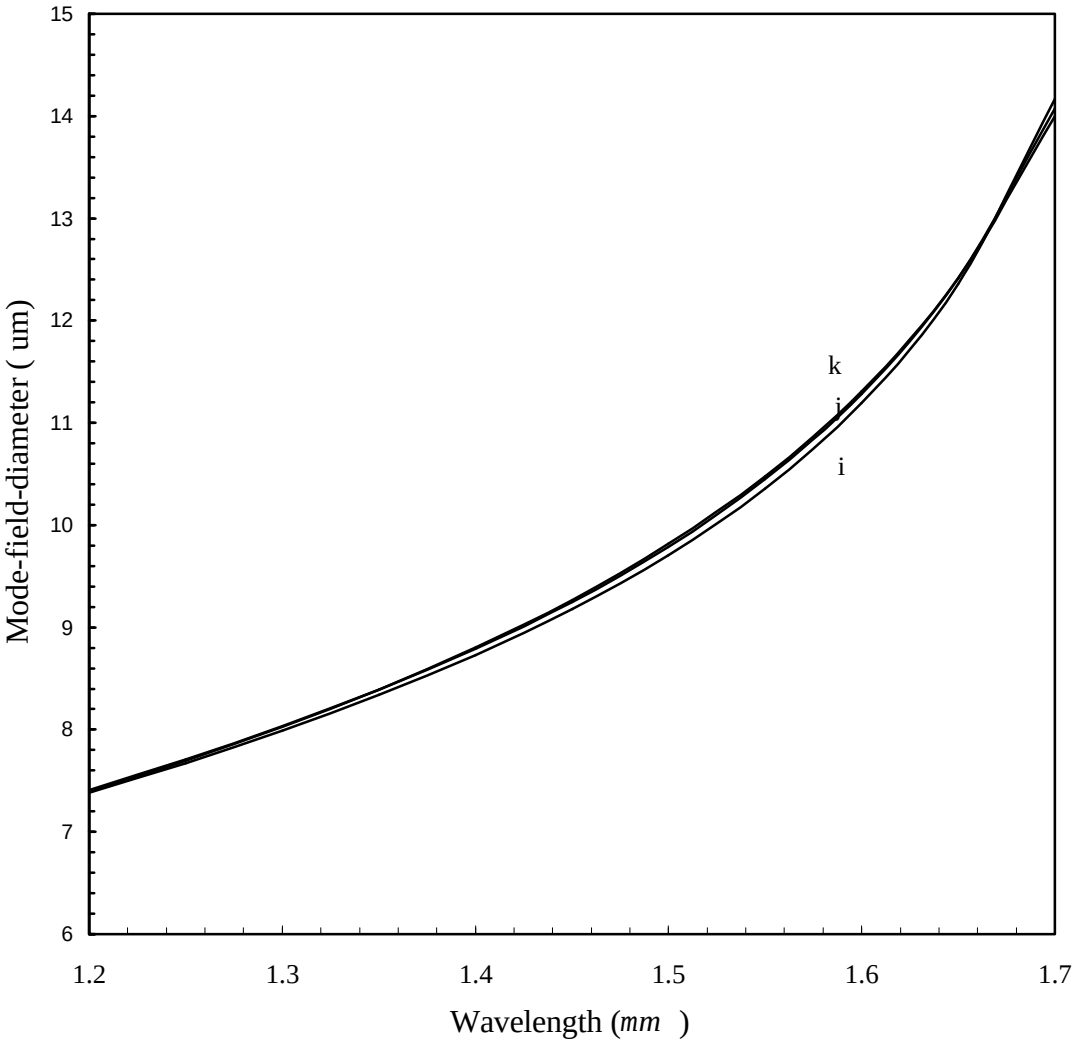

Figure 4.16 Variations of mode-field-diameter versus wavelength for fibers i, j and k.

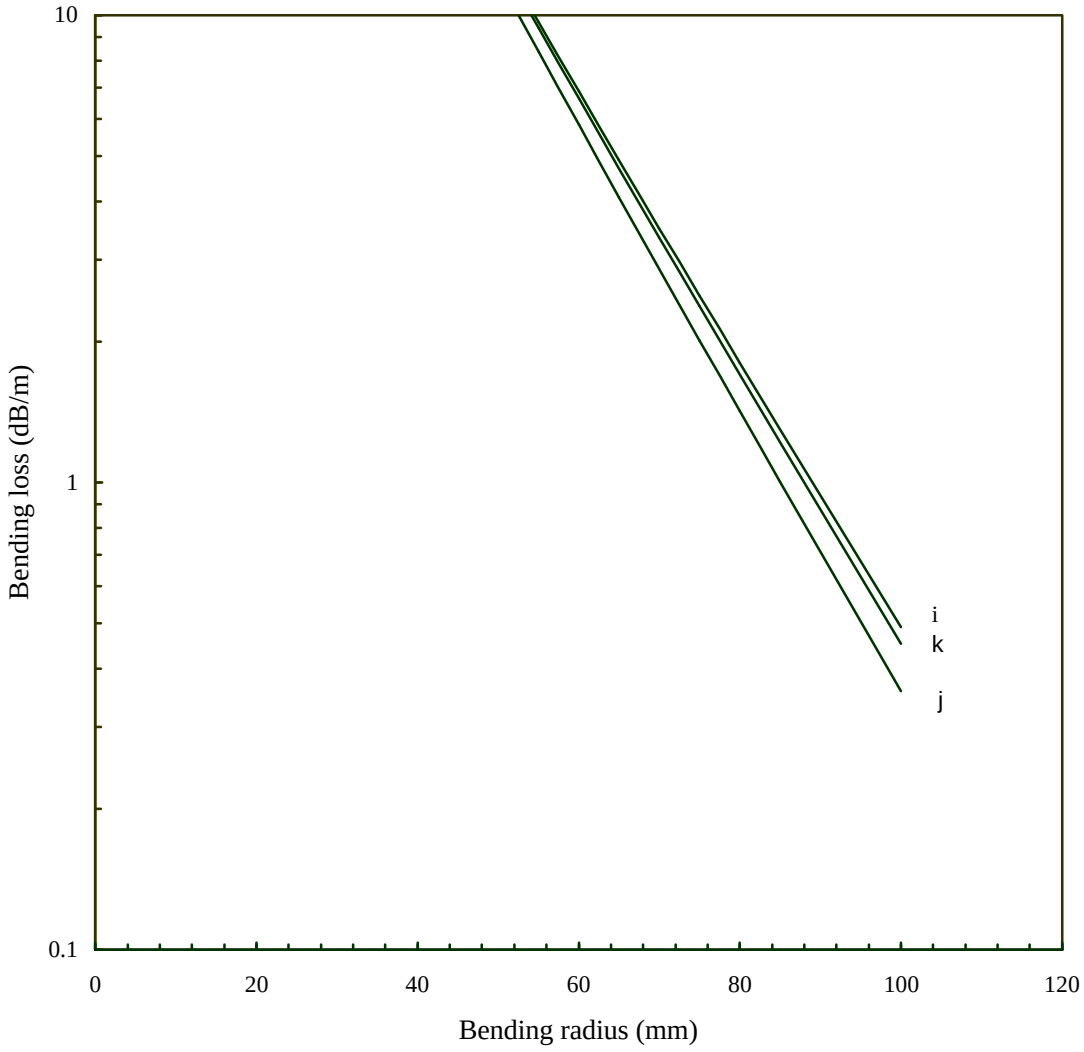

Figure 4.17 Variations of bending loss versus bending radius for fibers i to k, at 1.55 mm.

and k. However, if the mode-field-diameter is required to be less than or equal 11 mm, fiber d must be skipped and we must choose fiber c or the fiber in the row below to fiber c in Table 4.1 as the best design. For fibers in Table 4.1, Q varies from 0.764 for the reference W-fiber, until 1.09 for fiber d. Except for the reference W-fiber, all other fibers have a quality factor very near to 1.0. In Table 4.2, Q varies from 0.785, for fiber h to 1.13 for fiber g. This means that an adequate choice of materials and geometry can optimize the effective-area relative to the mode-field-diameter.

In Table 4.4, Q varies from 0.829 to 0.850. It is observed that, in general, the quality factors obtained for dispersion-shifted fibers are greater than those for dispersion-flattened fibers. This may suggest that low nonlinearity dispersion-flattened fibers are more complicated to design and, the maximization of effective-area with respect to the mode-field-diameter is a difficult task.

The Q parameter provides an idea of how well a fiber has been designed. However, actual calculations of bending loss are necessary. Examination of effective-area and bending loss, at a certain wavelength, indicates if the designed fiber has a large effective-area with tolerable bending loss. However, it is emphasized that the bending loss can be made negligible if the bending radius is greater than a critical value, no matter how the fiber has been designed. For example, the dispersion-shifted fibers a to c have small bending losses for radii greater than 25 mm, while fibers i to k can be considered to have small losses for bending radii greater than 100 mm.

The designed fibers have achieved values of Q as high as 1.13. However, there may be other designs with different index-profiles that result in a better performance than those presented here. Achieving the absolute best design is a very challenging task and requires a separate effort.

Chapter 5
Tolerance Analysis

In chapter 4, various designs for dispersion-shifted and dispersion-flattened fibers were presented. However, every design involves tolerances in the manufacturing process. These tolerances are important and determine if a given design is feasible or not. In this chapter, variations of second-order dispersion, effective-area and mode-field-diameter with respect to small changes in the radii and refractive indices will be analyzed. This analysis will establish that the proposed designs can indeed be manufactured, using the available fiber fabrication technology.

5.1 Tolerance Analysis for Dispersion-Shifted Fibers

Among the dispersion-shifted fibers presented in Chapter 4, fiber c is chosen as a representative case for tolerance analysis. This is because this fiber has a large effective-area and low bending loss. Besides, all designed fibers exhibit similar behavior versus variations of design parameters, and thus a representative case is sufficient for tolerance analysis.

Figures 5.1, 5.2 and 5.3 show variations of second-order dispersion versus wavelength when radii a_1, a_2 and a_3 from fiber c are varied, one at a time, by the amounts $\pm 1\%$ and $\pm 2\%$. It is noted from Fig. 5.3 that radius a_3 has less influence on dispersion than the other radii, while a_2 has the strongest influence. This means that special care should be taken with respect to a_2 in the manufacturing process. The largest variation in dispersion at 1.55 mm is –1.03 to 0.69 ps/nm.km, resulting from variation of a_2 from –2% to 2%.

Figures 5.4, 5.5 and 5.6 show variations of effective-area as a function of wavelength when radii a_1, a_2 and a_3 of fiber c are varied $\pm 1\%$ and $\pm 2\%$. Again, a_2 has the strongest influence on the effective-area, while a_3 has little effect. The largest variation in effective-area at 1.55 mm is from 110.4 to 117.30 mm^2 which results from variation of a_2 by –2% to +2%.

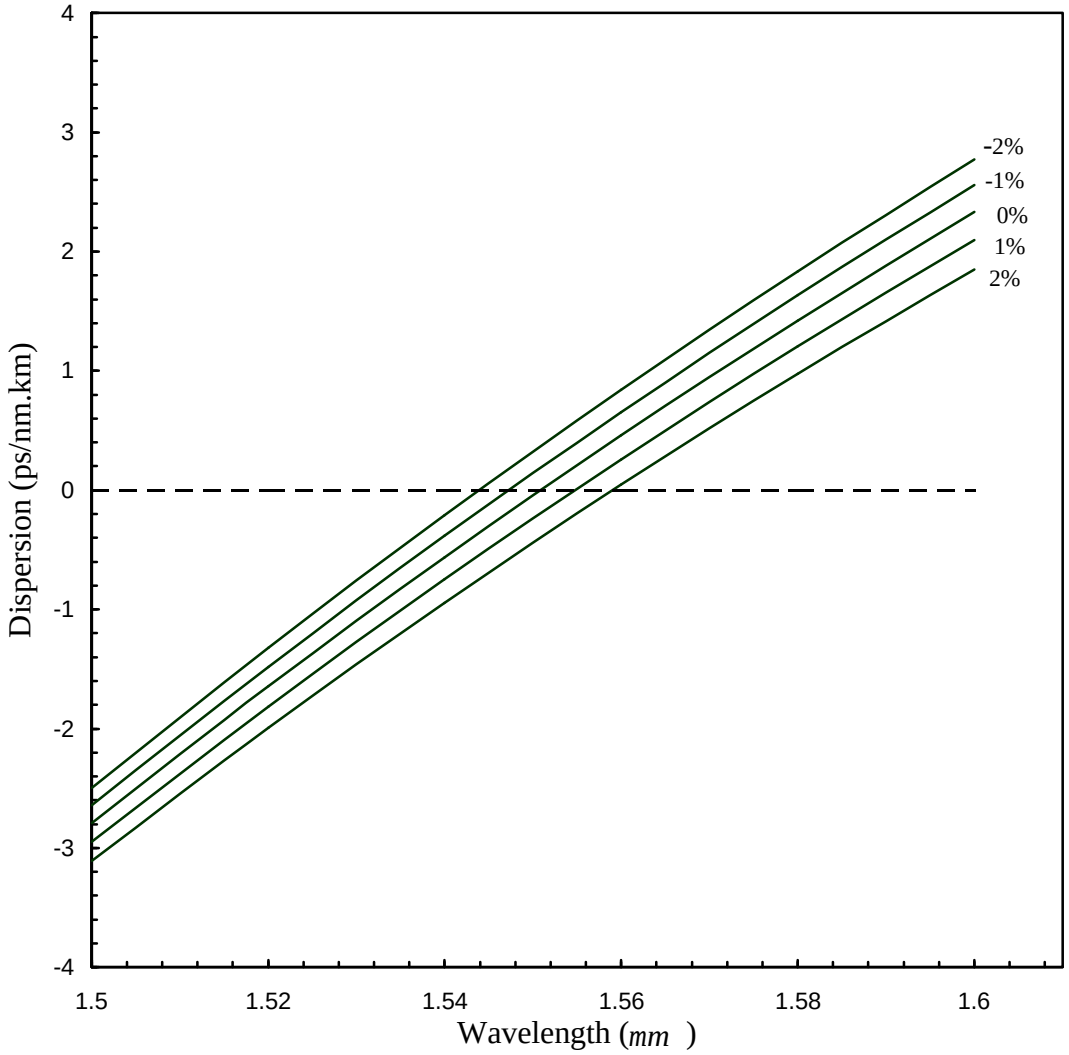

Figure 5.1 Variations of second-order dispersion versus wavelength for fiber c. Radius a_1 is varied $\pm 1\%$ and $\pm 2\%$.

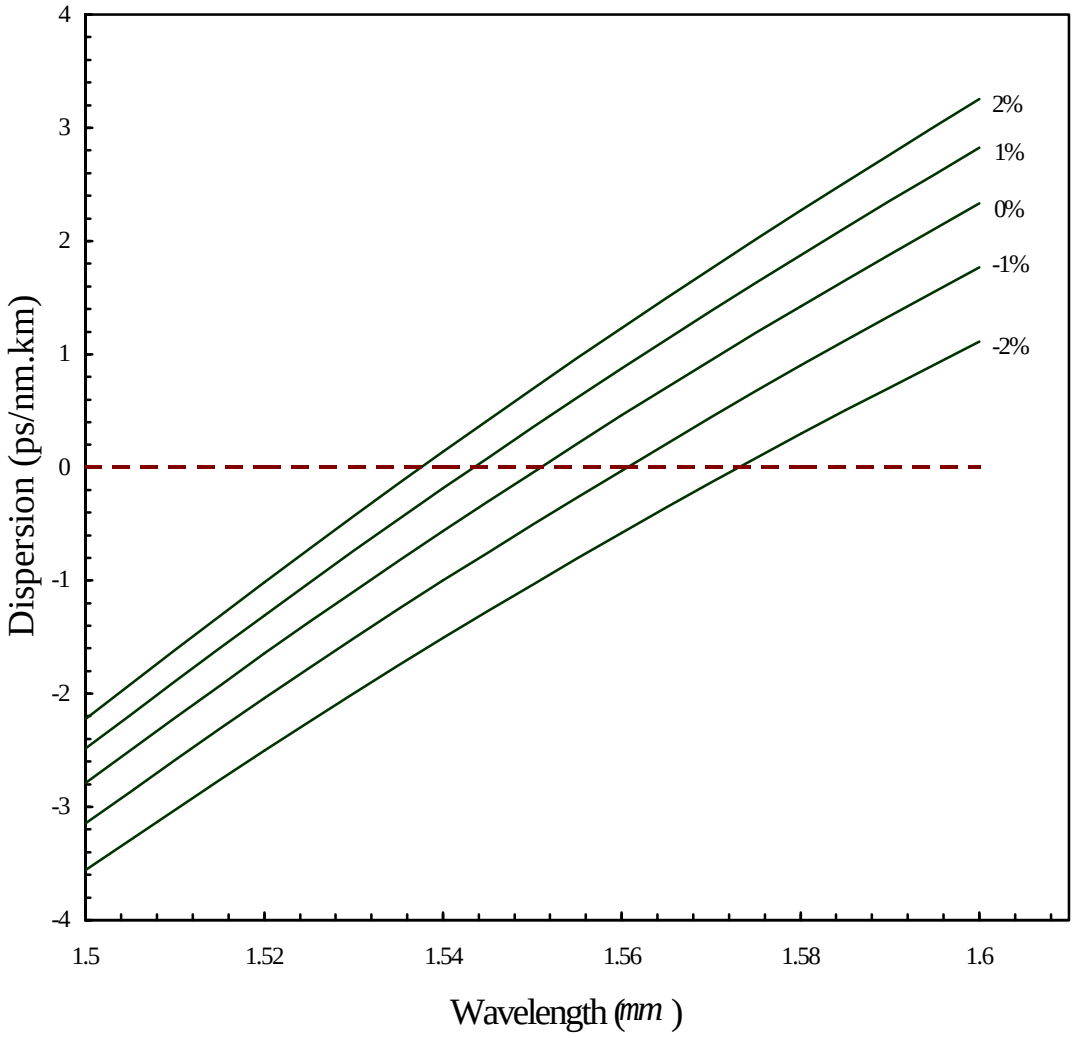

Figure 5.2 Variations of second-order dispersion versus wavelength for fiber c. Radius a_2 is varied $\pm 1\%$ and $\pm 2\%$.

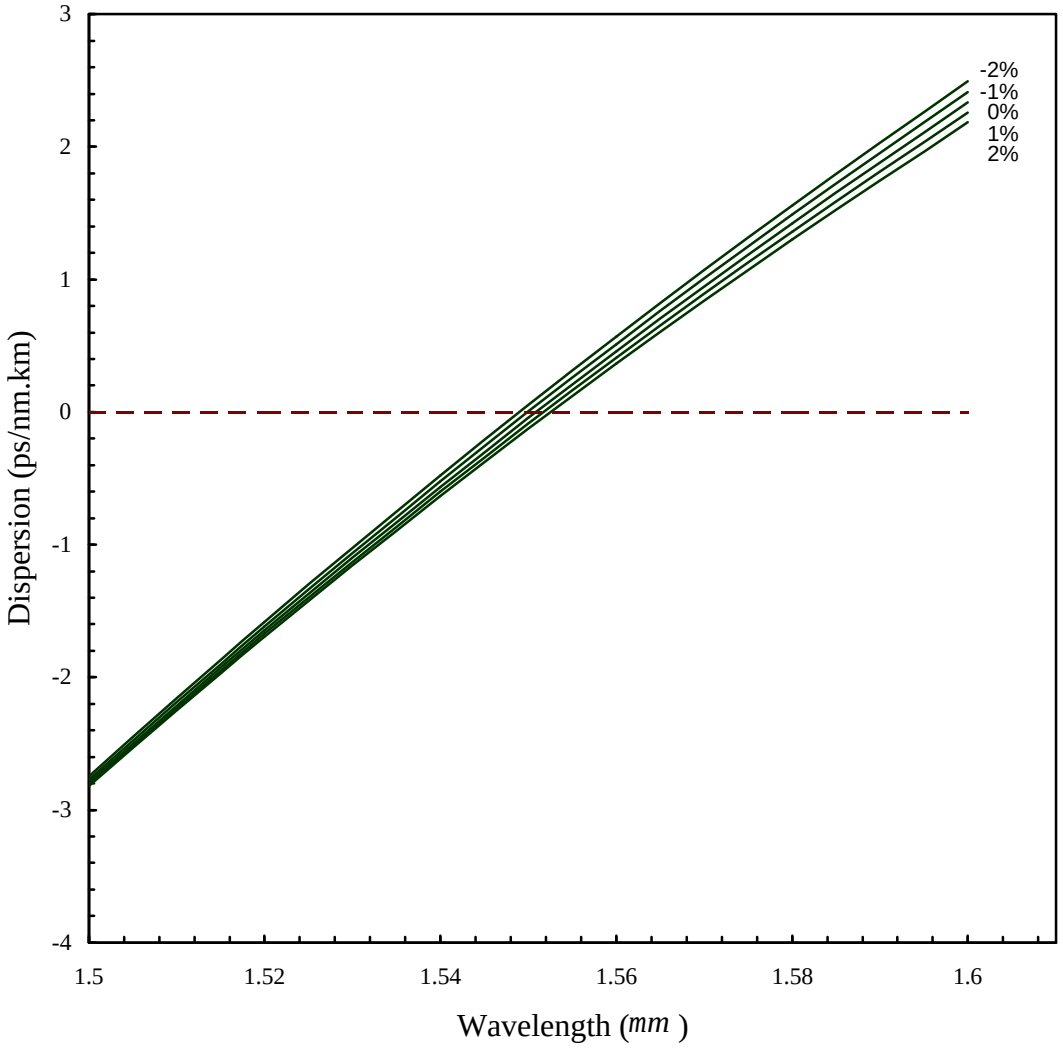

Figure 5.3 Variations of second-order dispersion versus wavelength for fiber c. Radius a_3 is varied $\pm 1\%$ and $\pm 2\%$.

Figures 5.7, 5.8 and 5.9 show variations of mode-field-diameter as a function of wavelength for variations of a_1, a_2 and a_3 for fiber c ($\pm 1\%$ and $\pm 2\%$). The same conclusions can be deduced in this case too. The largest variation in the mode-field-diameter at 1.55 mm is from 10.03 to 10.63 mm. Again, this variation is due to changes in a_2 by +2% and –2%. In summary, it is concluded that the most sensitive radius is a_2 and the least sensitive is a_3. This is expected because the fields at the most outer layer are much smaller than in the inner layers.

Next, we examine the effects of varying the refractive indices on the second-order dispersion, effective-area and mode-field-diameter. For the sake of brevity, only n_2 is varied. This is because variations of n_2 cause the greatest changes in transmission properties of fibers. This refractive index will be changed ± 0.01 %, typical variations that may occur in an actual fiber manufacturing process. Figures 5.10, 5.11 and 5.12 show variations of dispersion, effective-area and mode-field-diameter versus wavelength. It is noted from Fig. 5.10 that variations of the refractive index cause only a slight change in dispersion. Similar behaviors are also observed for effective-area and mode-field-diameter as noted in Figs. 5.11 and 5.12, respectively.

5.2 Tolerance Analysis for Dispersion-Flattened Fibers

As the designed dispersion-flattened fibers designed have similar characteristics, only one fiber (fiber i) is chosen as a representative example for tolerance analysis. As in the case of dispersion-shifted fibers, first the radii and then the highest refractive index n_2 are varied and the effects on transmission properties are assessed. The properties to be examined are second-order dispersion, effective-area and mode-field-diameter.

Fiber i includes three radii, a_1, a_2 and a_3, that are varied systematically one at a time by the amounts $\pm 2\%$ and $\pm 1\%$. The resulting changes in dispersion, effective-area, and mode-field-diameter are shown in Figures 5.13, 5.14 and 5.15, respectively. As expected, transmission properties are most sensitive to a_2 and least sensitive to a_3. It is noted from these figures that variations of dispersion with radii are fairly large and the maximum value of dispersion can reach as much as 3.40 ps/nm.km, and for certain values of a_2, even the zero dispersion is never

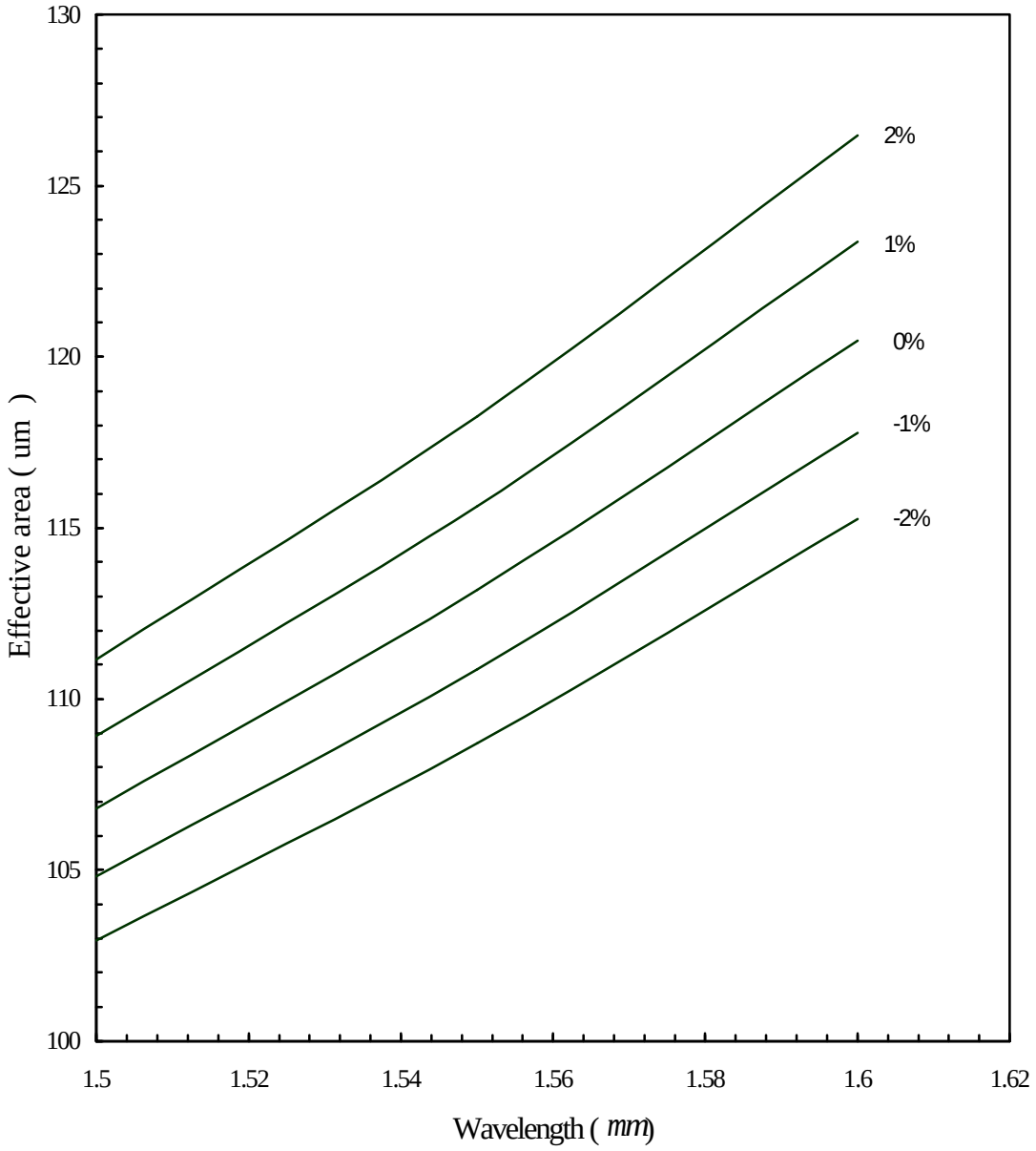

Figure 5.4 Variations of effective-area versus wavelength for fiber c. The radius a_1 is varied $\pm 1\%$ and $\pm 2\%$.

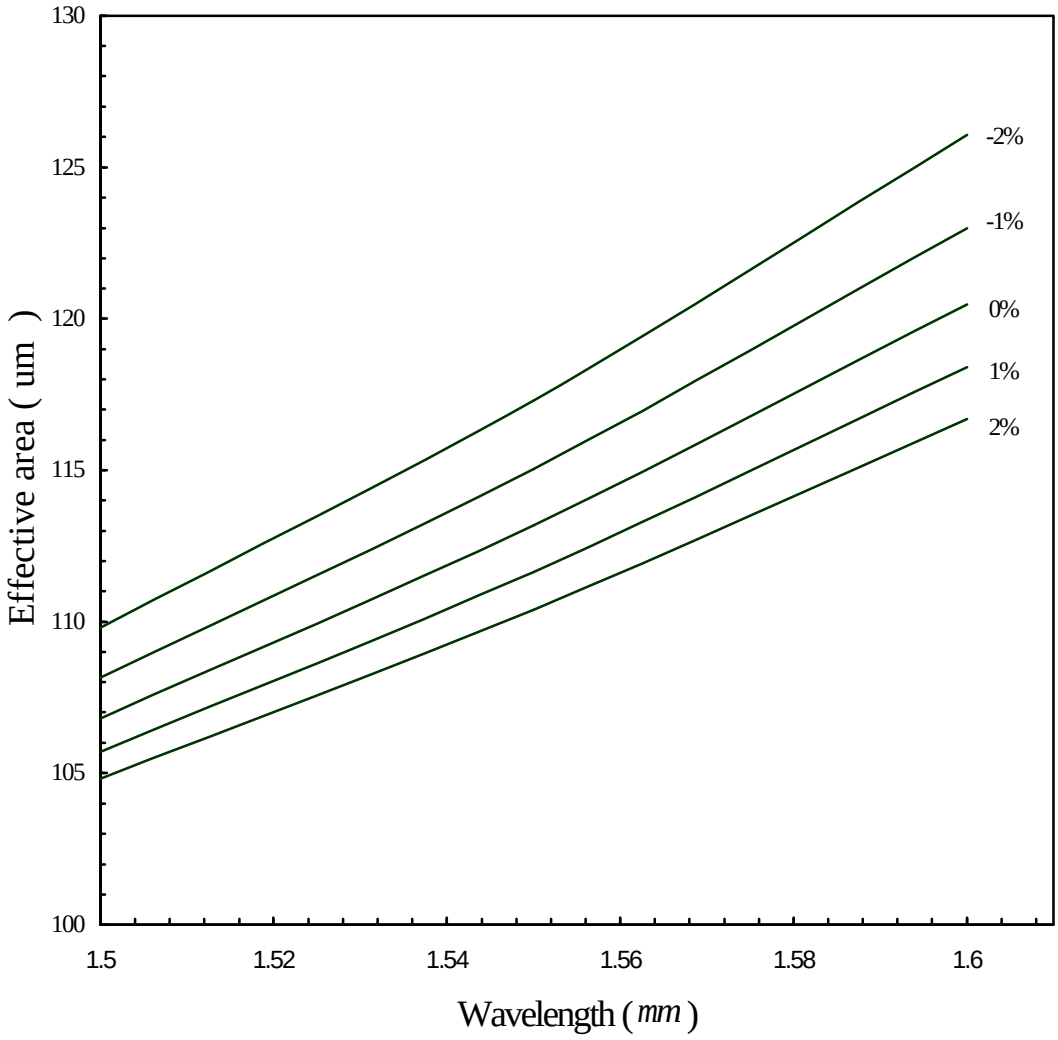

Figure 5.5 Variations of effective-area versus wavelengths for fiber c. The radius a_2 is varied $\pm 1\%$ and $\pm 2\%$.

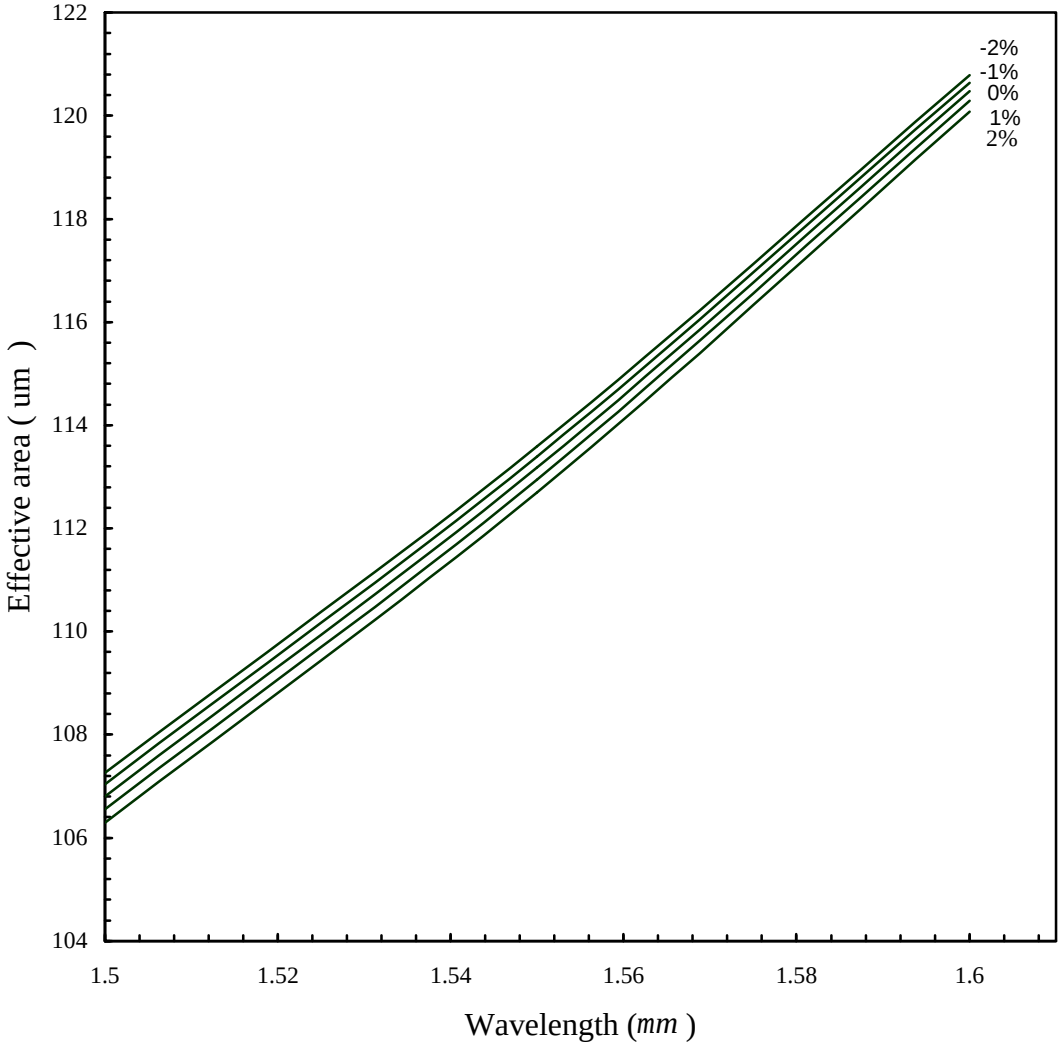

Figure 5.6 Variations of effective-area versus wavelengths for fiber c. The radius a_3 is varied $\pm 1\%$ and $\pm 2\%$.

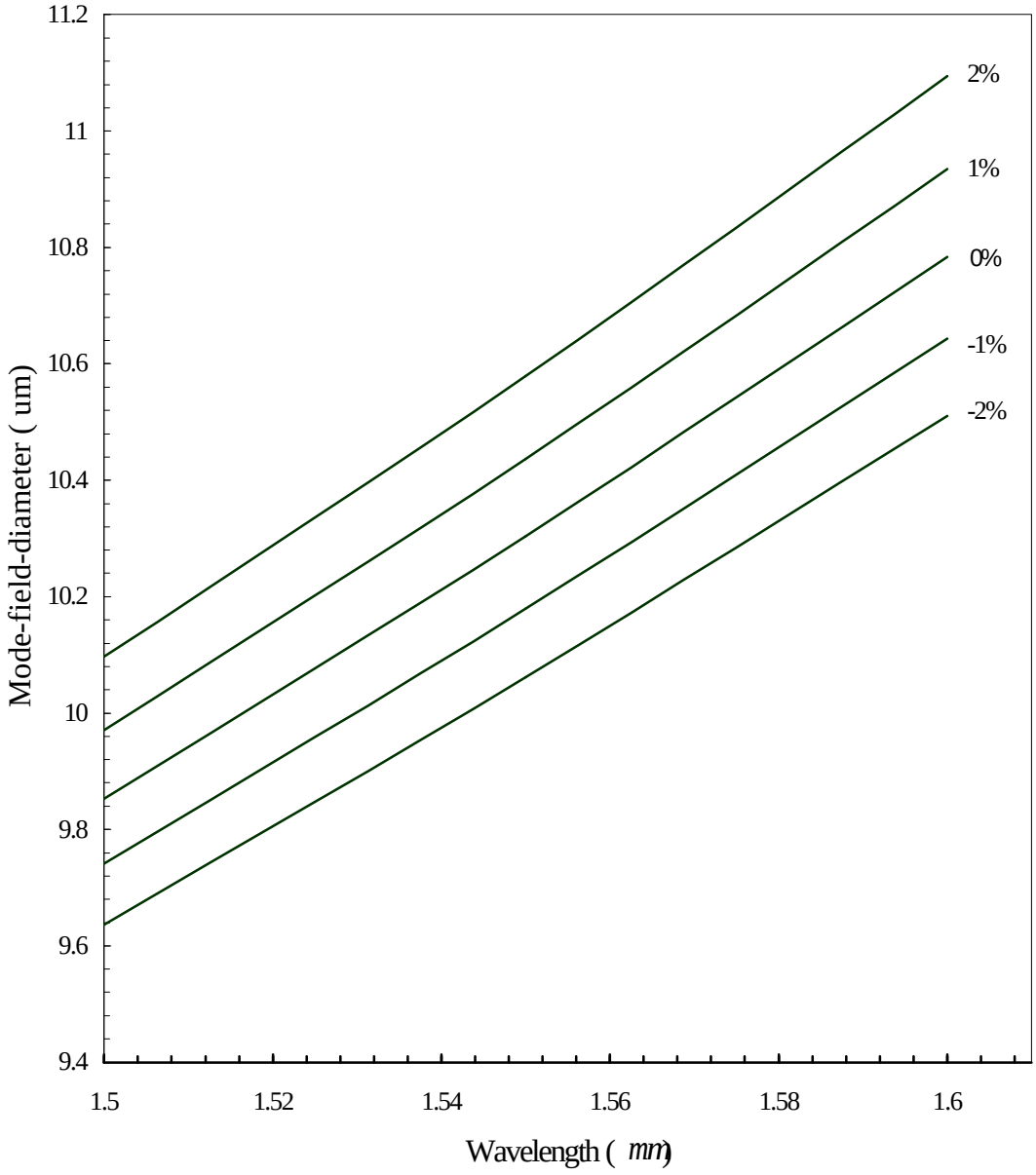

Figure 5.7 Variations of mode-field-diameter versus wavelengths for fiber c. The radius a_1 is varied $\pm 1\%$ and $\pm 2\%$.

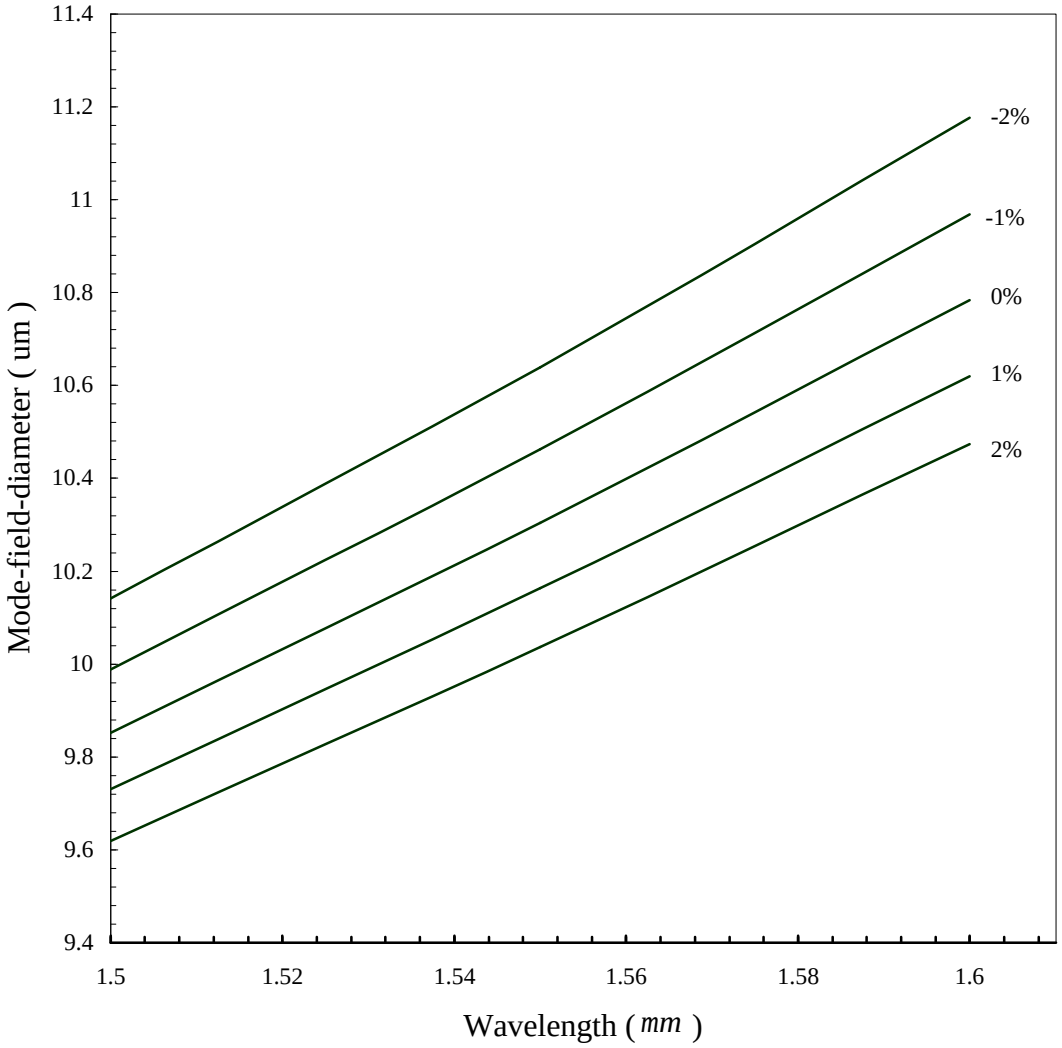

Figure 5.8 Variations of mode-field-diameter versus wavelengths for fiber c. The radius a_2 is varied $\pm 1\%$ and $\pm 2\%$.

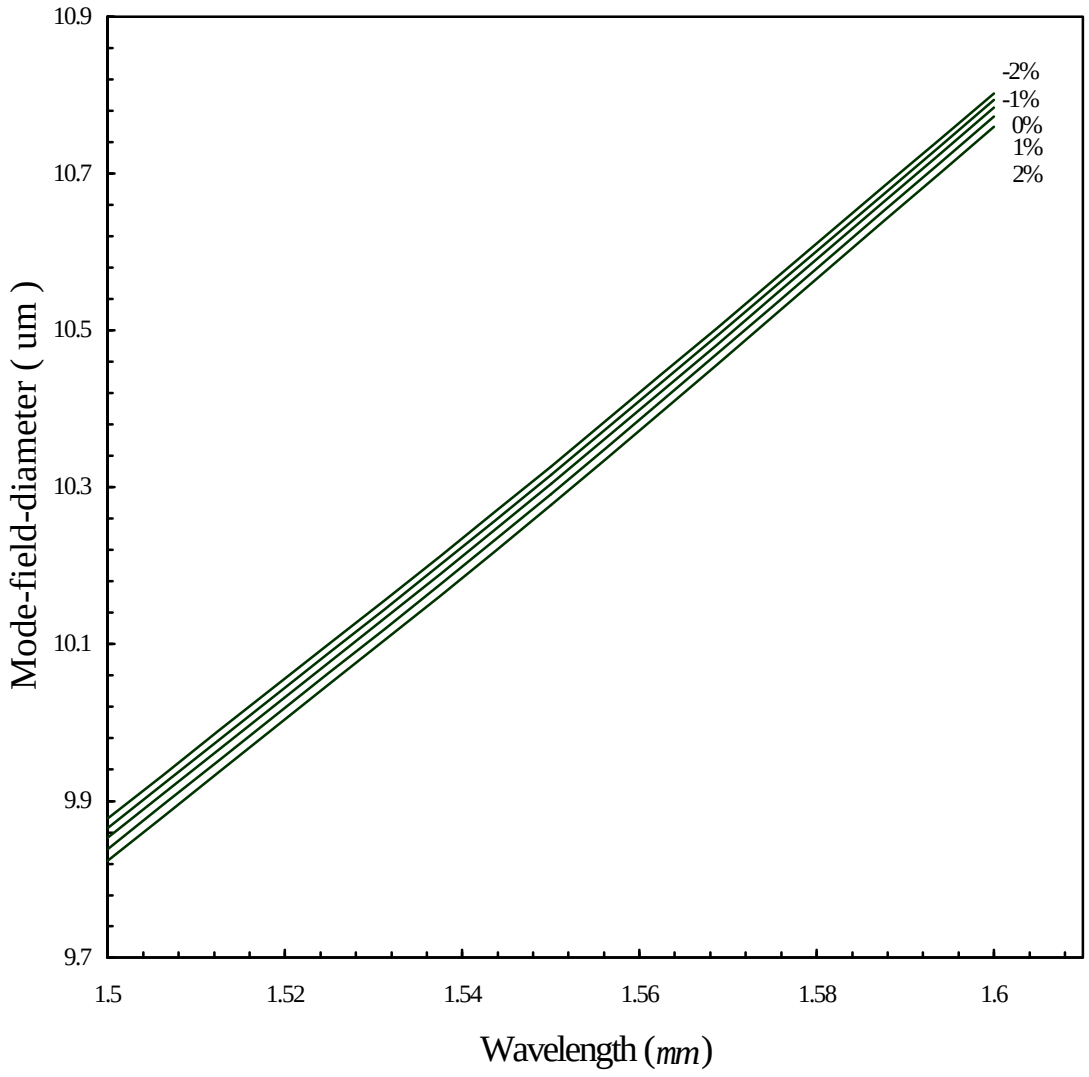

Figure 5.9 Variations of mode-field-diameter versus wavelength for fiber c. Radius a_3 is varied $\pm 1\%$ and $\pm 2\%$.

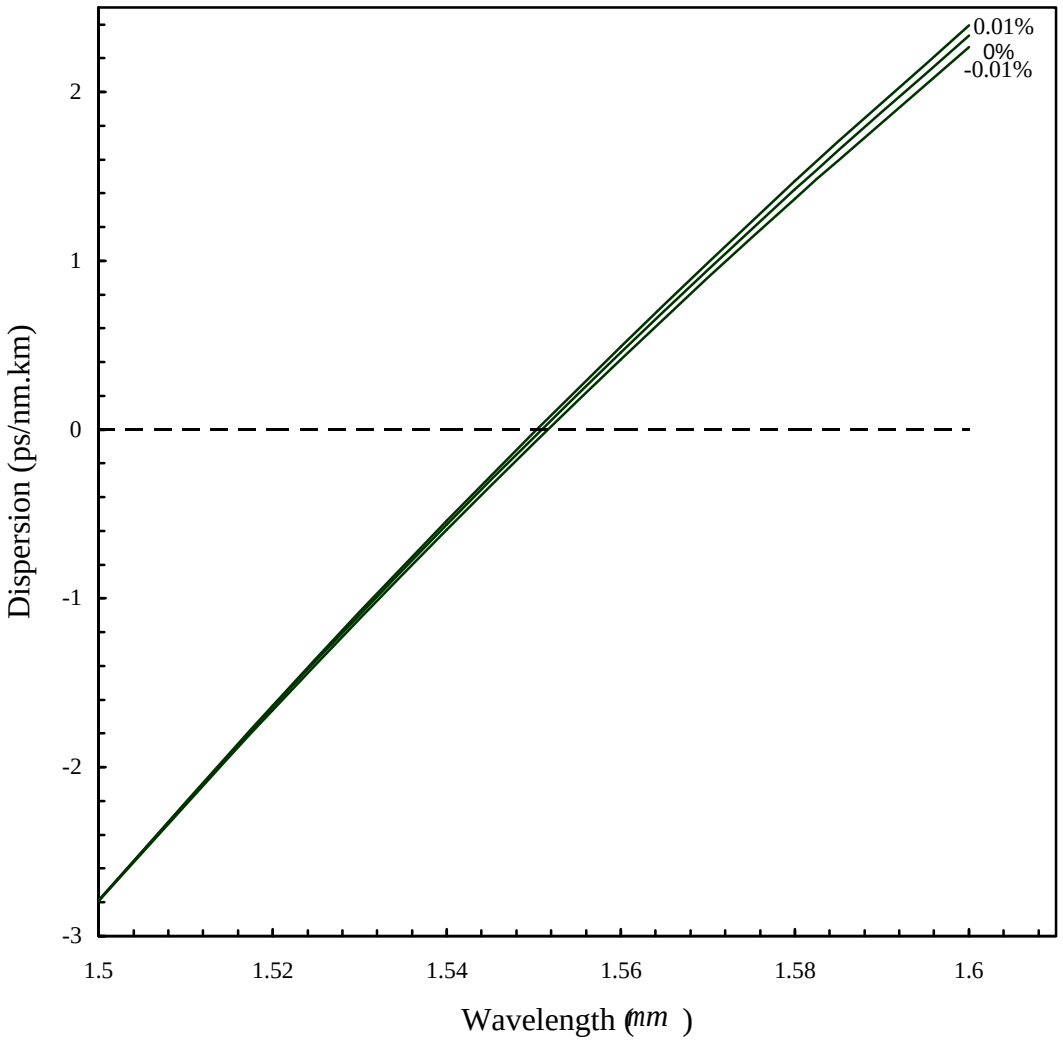

Figure 5.10 Variations of second-order dispersion versus wavelength for fiber c. Refractive index n_2 is varied $\pm 10^{-2}\%$.

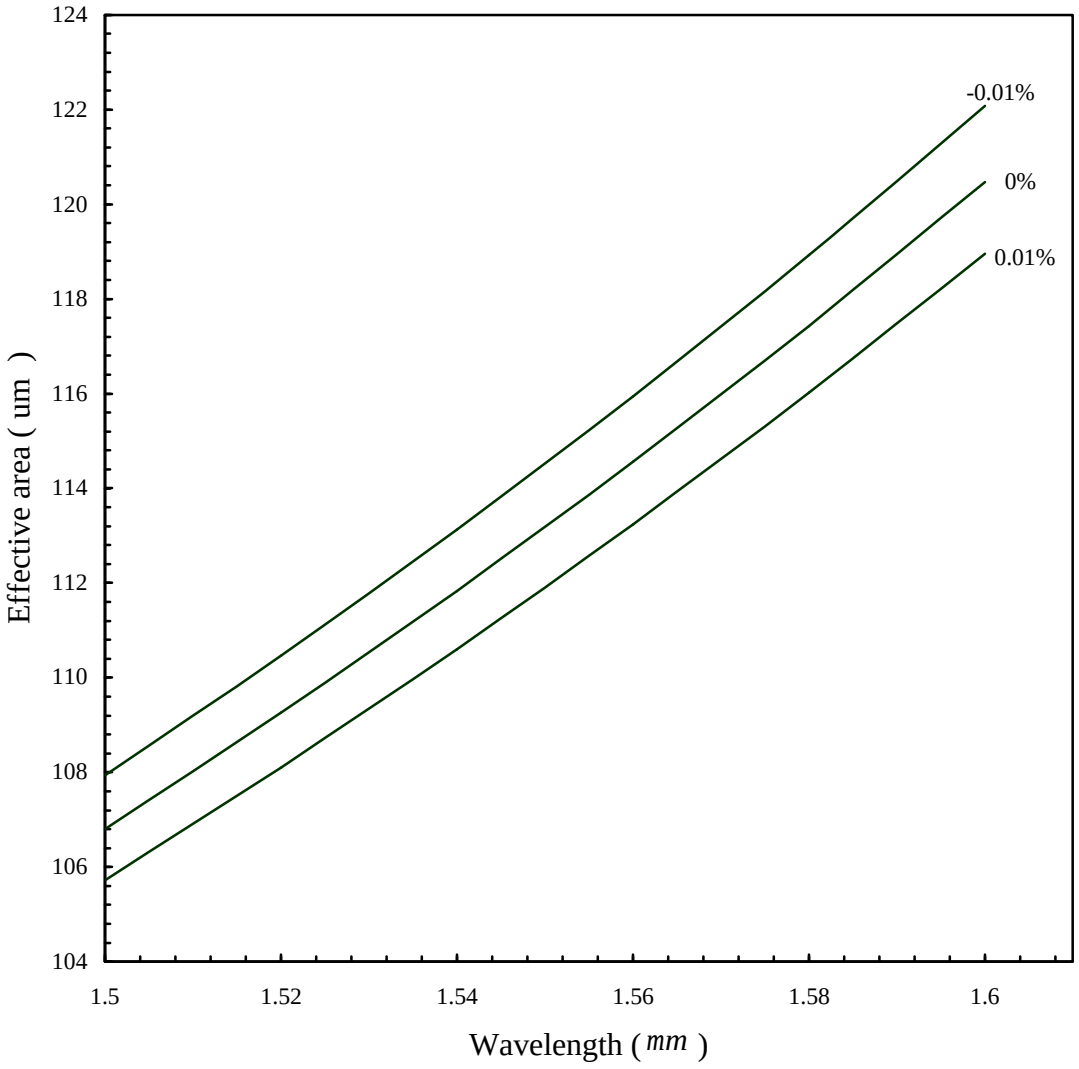

Figure 5.11 Variations of effective-area versus wavelengths for fiber c. Refractive index n_2 is varied $\pm 10^{-2}\%$.

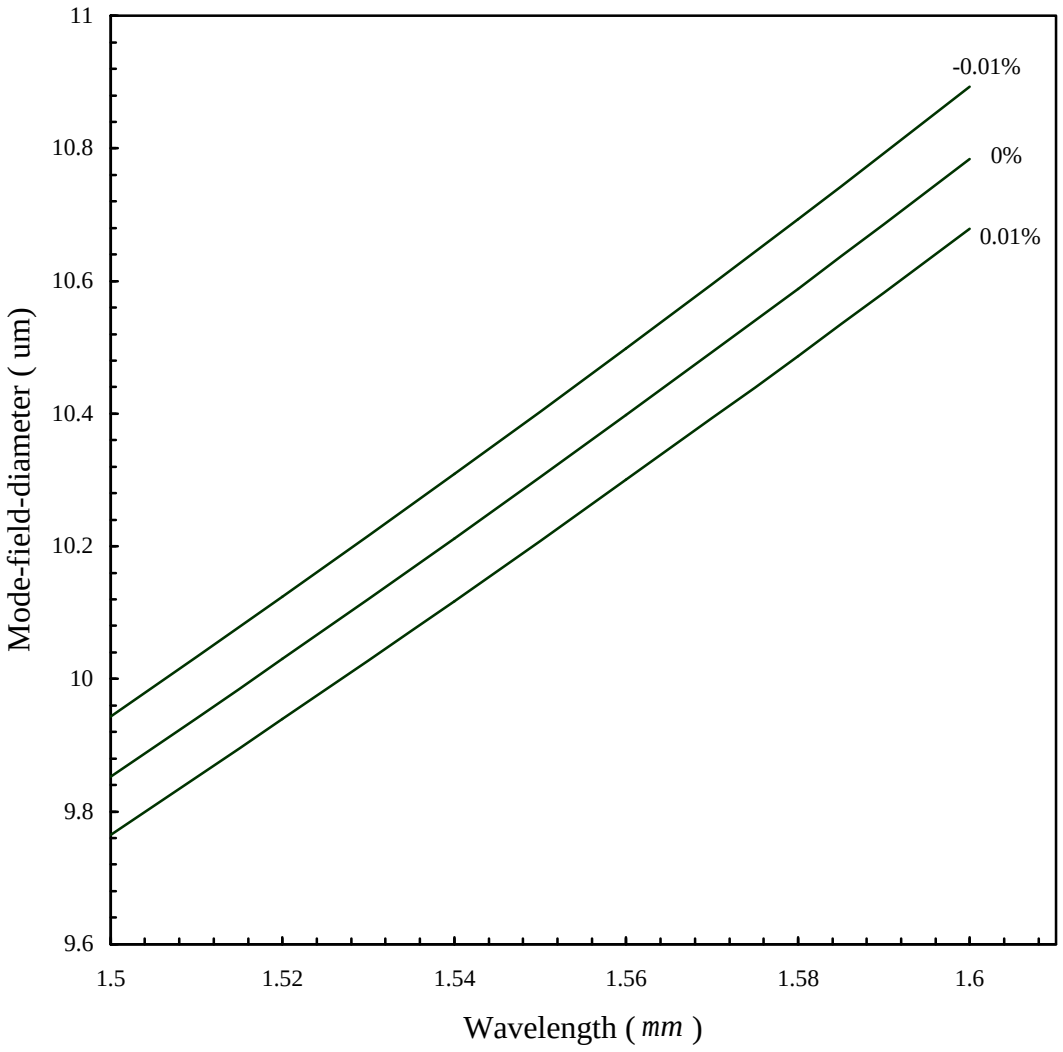

Figure 5.12 Variations of mode-field-diameter versus wavelengths for fiber c. Refractive index n_2 is varied $\pm 10^{-2}\%$.

achieved. It is further noted that the designed dispersion-flattened fibers are more sensitive to variations of radii than the dispersion-shifted fibers, particularly sensitivity to a_2 is more pronounced. It is known that commercial dispersion-flattened fibers are difficult to fabricate and the tolerance analysis given above is a good indication why this is the case.

Figures 5.16 to 5.18 illustrate variations of effective-area versus wavelength for changes in the fiber radii. The effective-area changes considerably for changes in a_1 and a_2. However, changes in a_2 are much more critical than changes in a_1. Variations in radius a_3 have an insignificant effect on the effective area. At $1.55\ mm$, the effective-area changes from 83.6 to $97.12\ mm^2$, when a_2 varies by –2% to +2%. It is a variation of nearly $\pm 8\%$ in the effective-area for a change of $\pm 2\%$ in the radius a_2.

Figures 5.19 to 5.21 show variations of mode-field-diameter versus wavelength for changes in the radii. It is observed that variations in radius a_2 cause significant changes in the mode-field-diameter, while changes in radius a_3 cause only small changes in this parameter. At $1.55\ mm$, the mode-field-diameter changes from 10.09 to $10.72\ mm$ when a_2 is varied from –2% to +2%.

The next step is to change the refractive indices. The most sensitive refractive index is n_2, and will be varied $\pm 0.01\%$. Figure 5.22 illustrates variations of dispersion versus wavelength for changes in n_2. It is noted that variations in this refractive index cause considerable variations in dispersion. When n_2 is reduced by 0.01%, zero dispersion is never achieved. Figures 5.23 and 5.24 show variations of effective-area and mode-field-diameter versus wavelength for changes in n_2, respectively. At $1.55\ mm$, the effective-area changes from 83.99 to $95.20\ mm^2$, while the mode-field-diameter changes from 10.1 to $10.66\ mm$.

In conclusion, dispersion-flattened fibers are more sensitive to changes in their radial dimensions and refractive indices than dispersion-shifted fibers. That is, manufacturing of large effective-area dispersion-flattened fibers should meet tighter tolerance requirements and need more accurately controllable processes than the dispersion-shifted fibers.

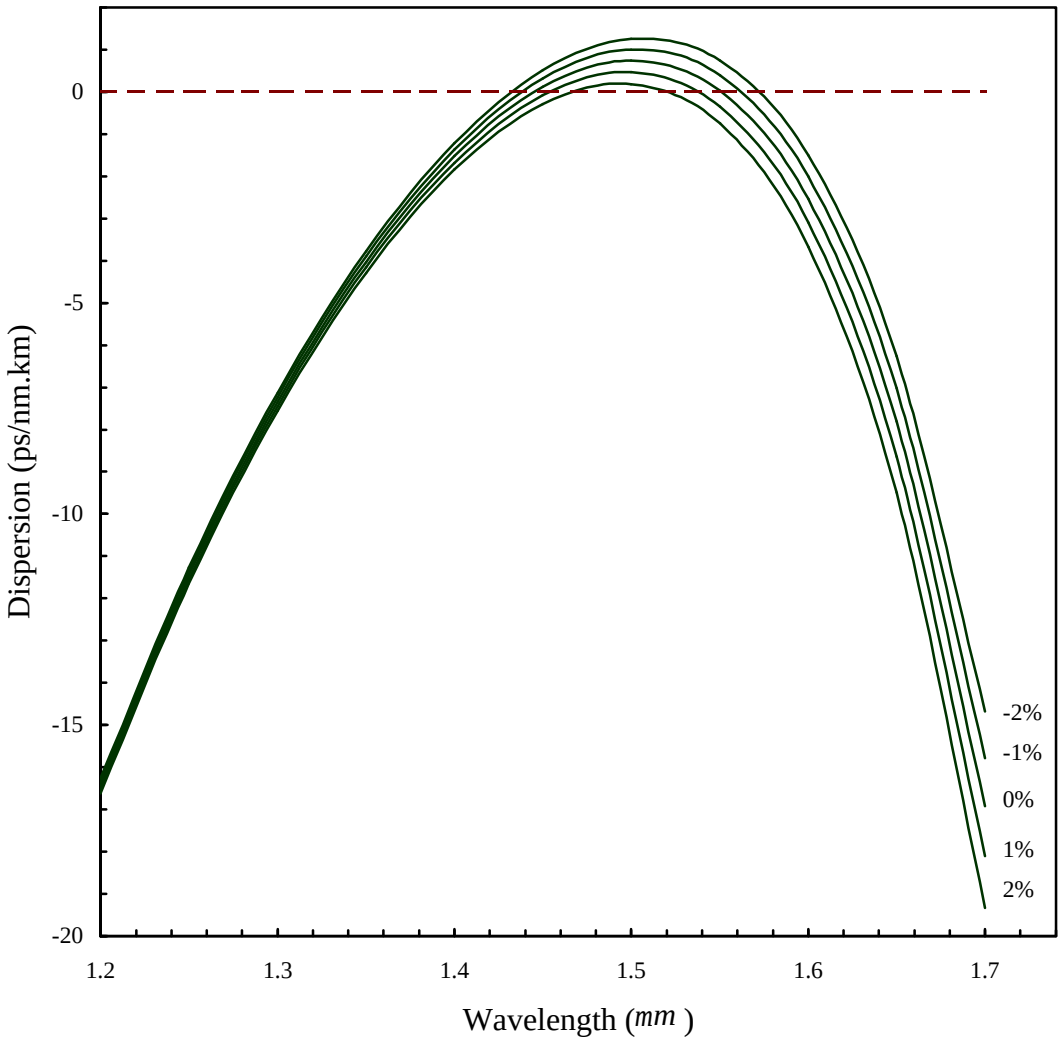

Figure 5.13 Variations of dispersion versus wavelength for fiber i. Radius a_1 is varied $\pm 1\%$ and $\pm 2\%$.

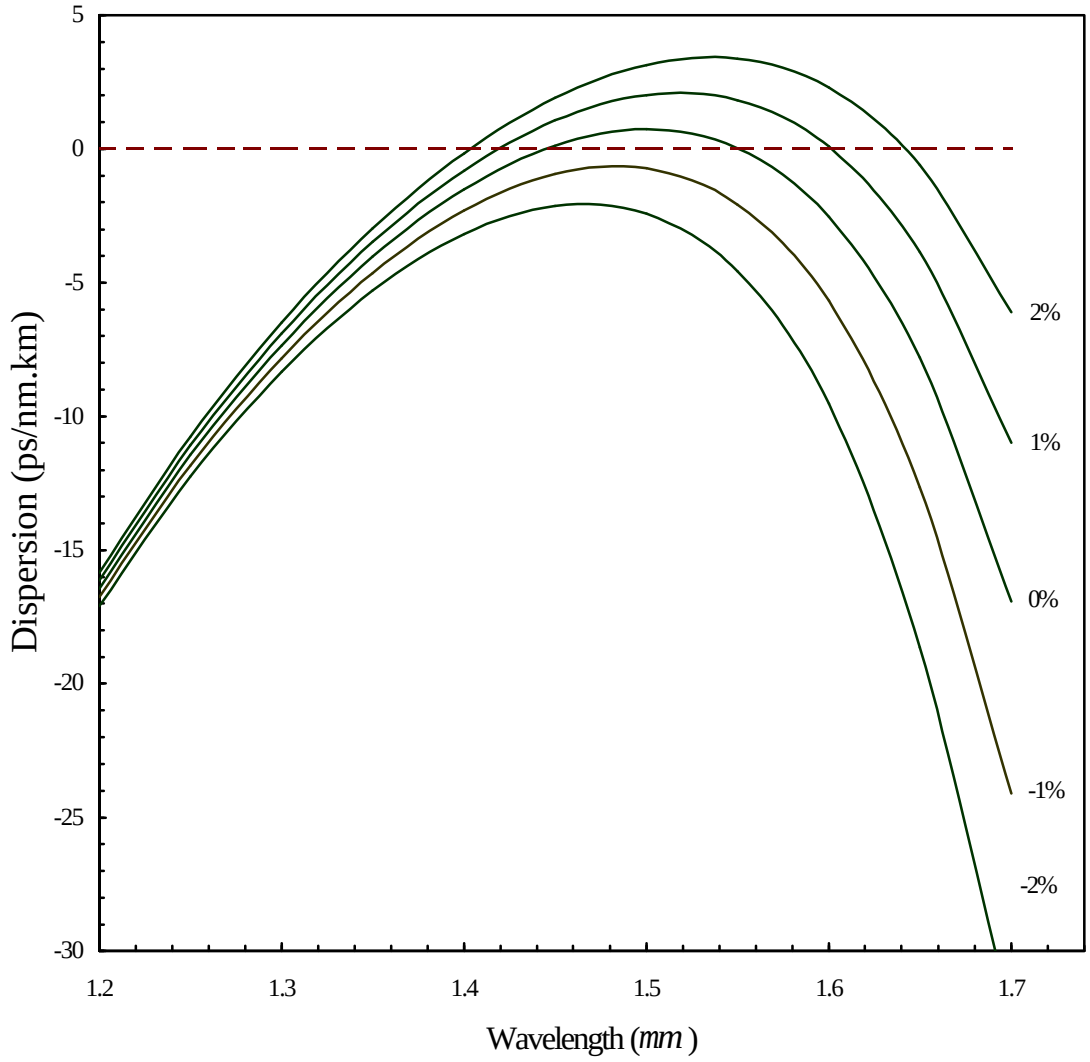

Figure 5.14 Variations of dispersion versus wavelength for fiber i. Radius a_2 is varied $\pm 1\%$ and $\pm 2\%$.

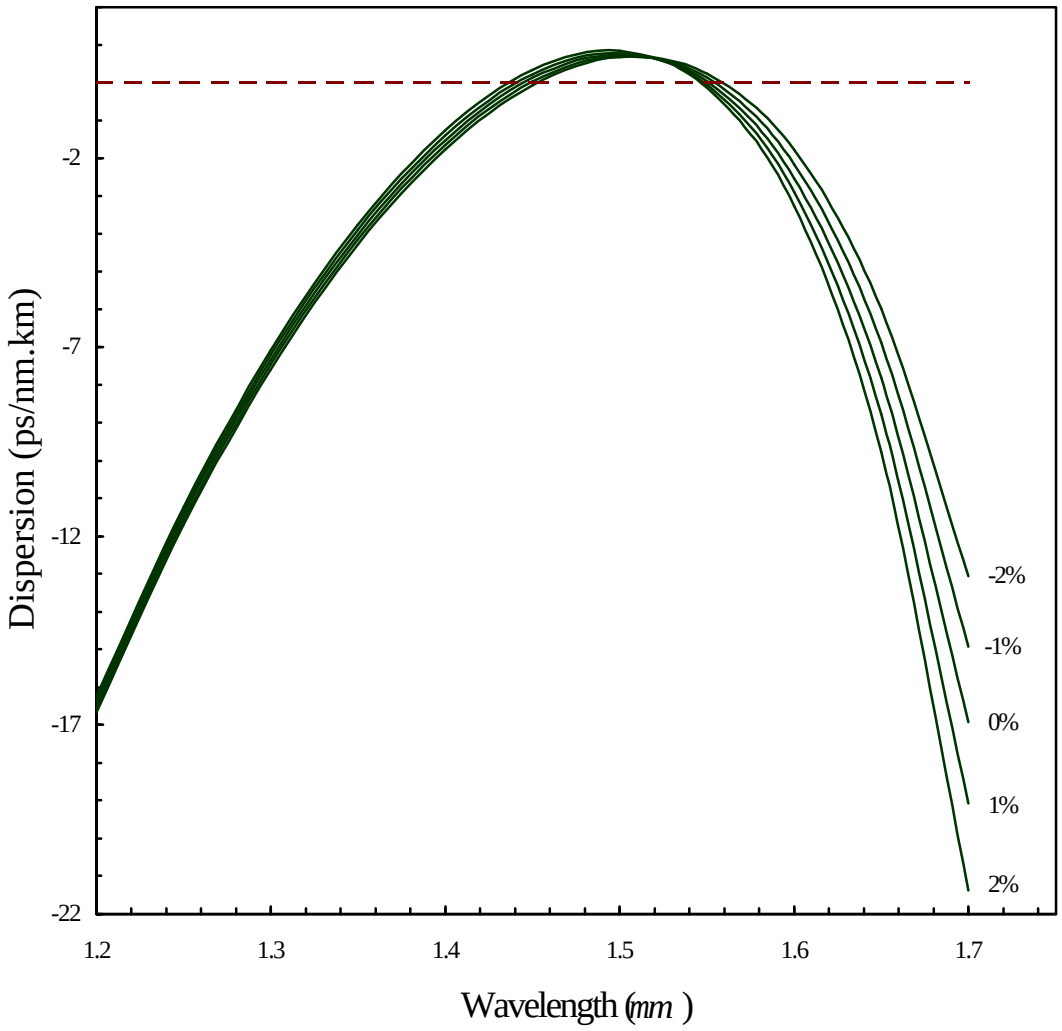

Figure 5.15 Variations of dispersion versus wavelength for fiber i. Radius a_3 is varied $\pm 1\%$ and $\pm 2\%$.

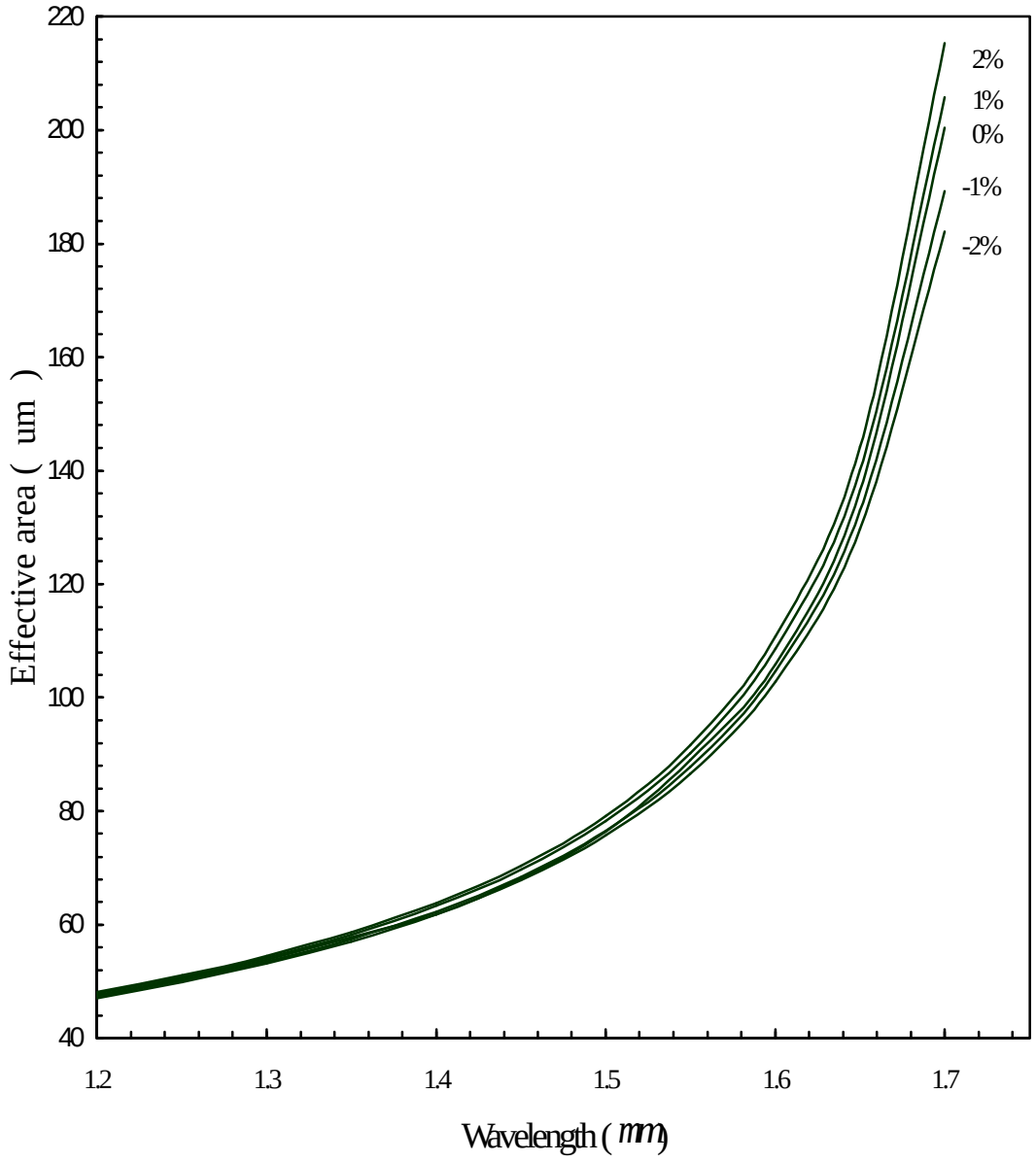

Figure 5.16 Variations of effective-area versus wavelength for fiber i. Radius a_1 is varied $\pm 1\%$ and $\pm 2\%$.

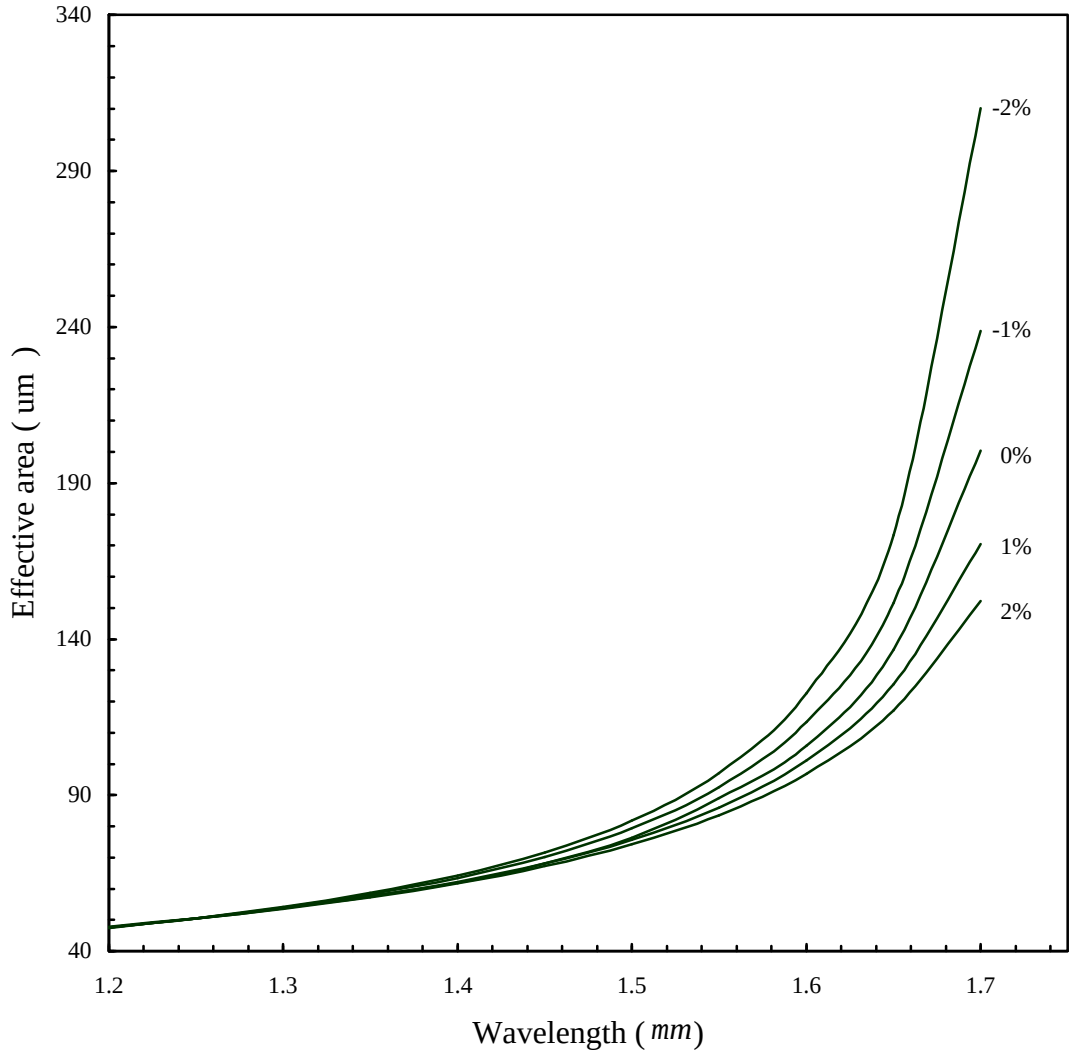

Figure 5.17 Variations of effective-area versus wavelength for fiber i. Radius a_2 is varied $\pm 1\%$ and $\pm 2\%$.

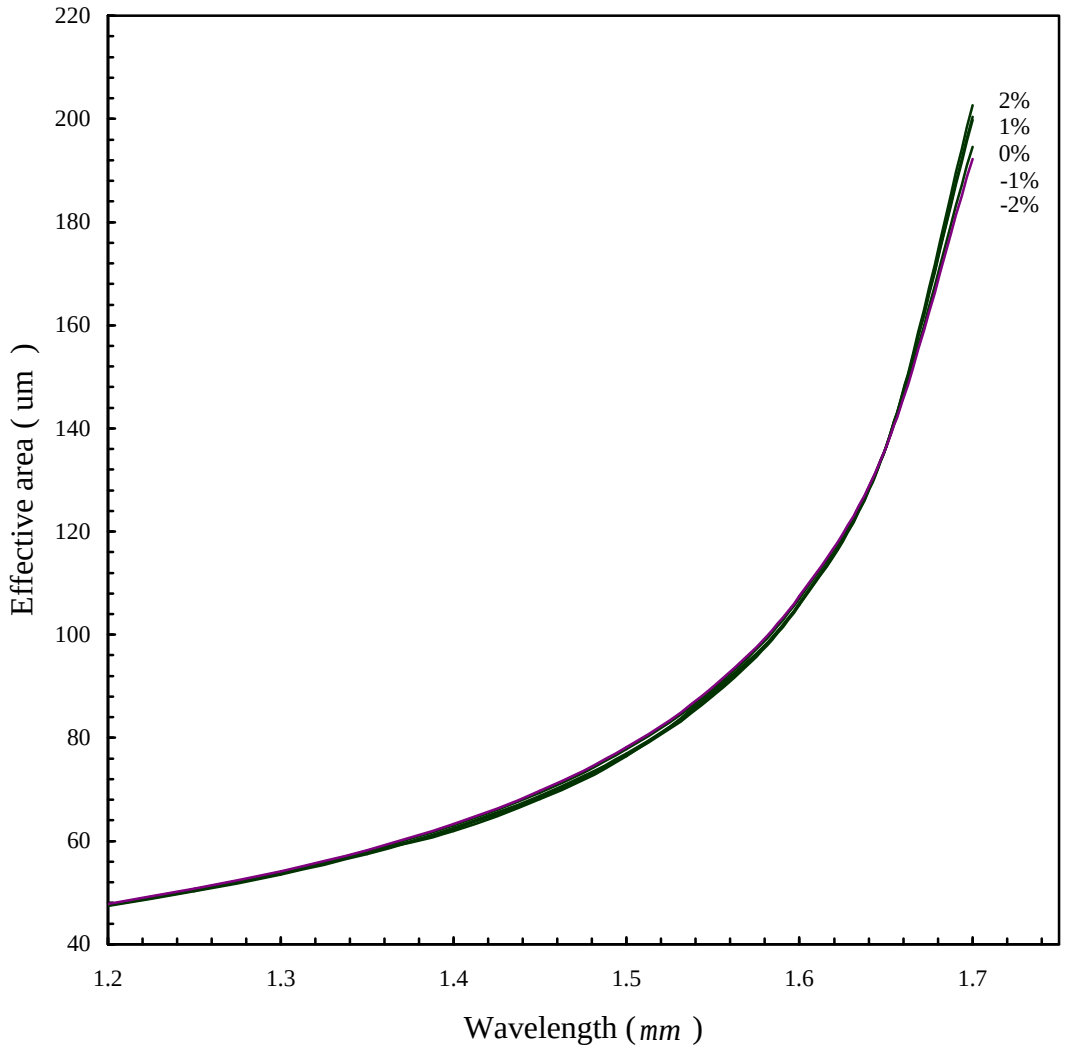

Figure 5.18 Variations of effective-area versus wavelength for fiber i. Radius a_3 is varied $\pm 1\%$ and $\pm 2\%$.

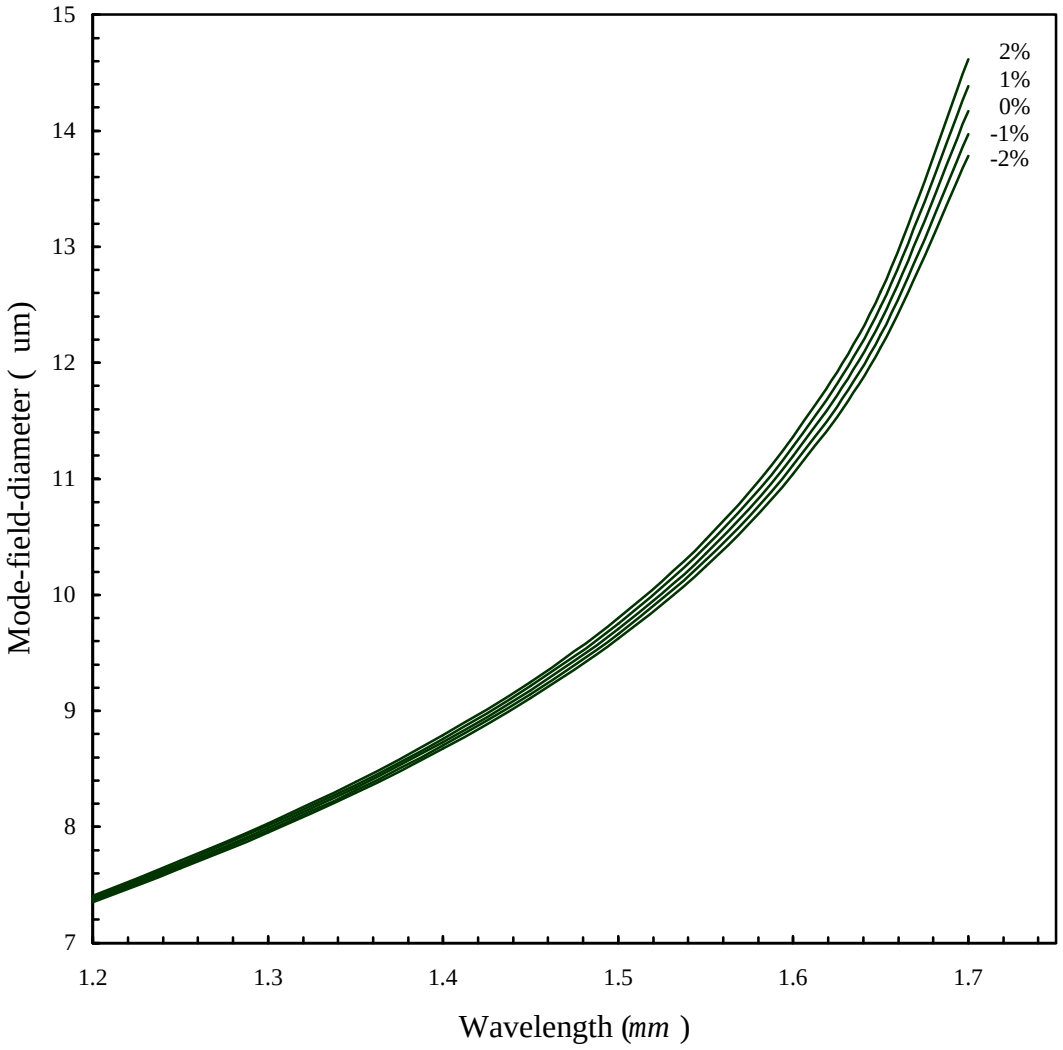

Figure 5.19 Variations of mode-field-diameter versus wavelength for fiber i. Radius a_1 is varied $\pm 1\%$ and $\pm 2\%$.

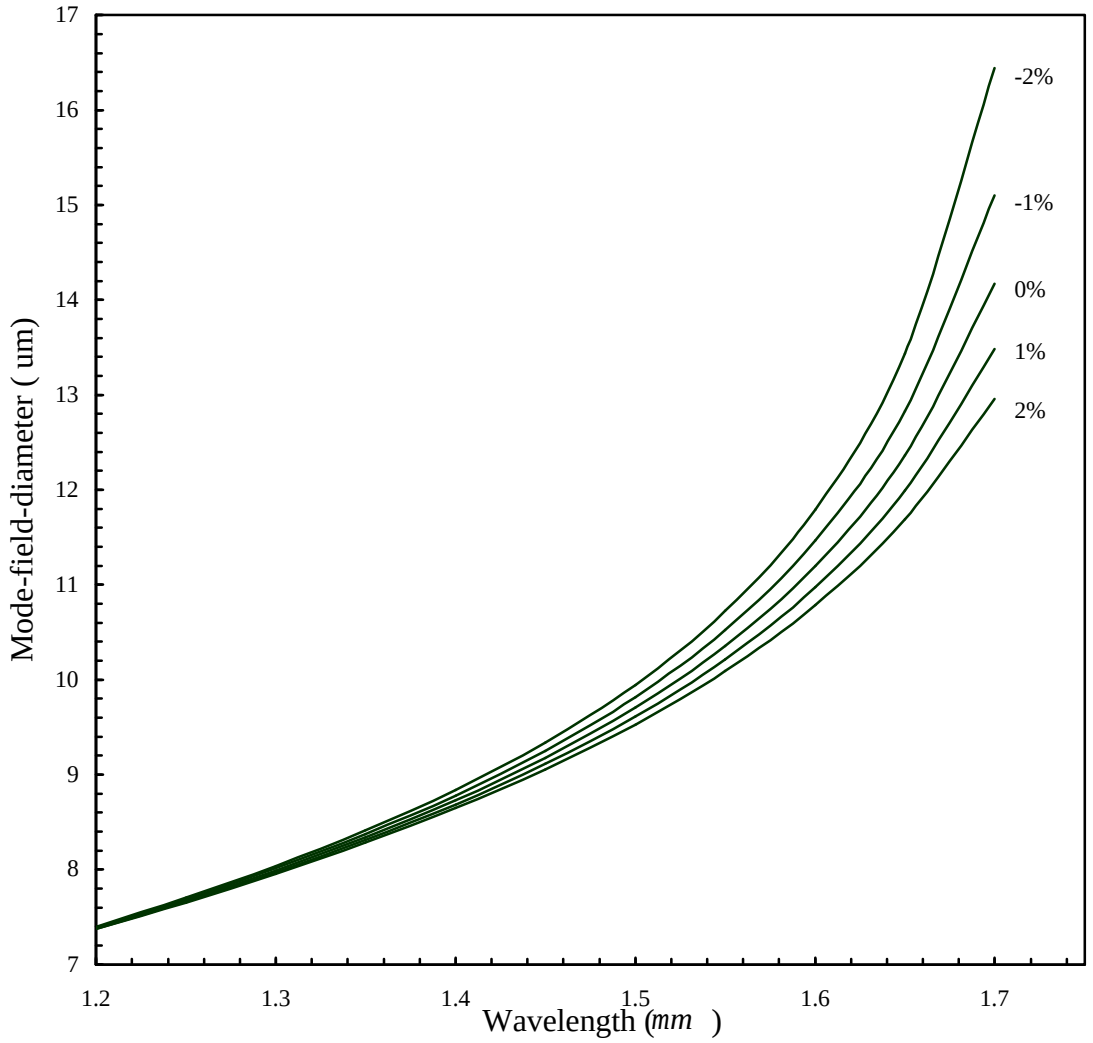

Figure 5.20 Variations of mode-field-diameter versus wavelength for fiber i. Radius a_2 is varied $\pm 1\%$ and $\pm 2\%$.

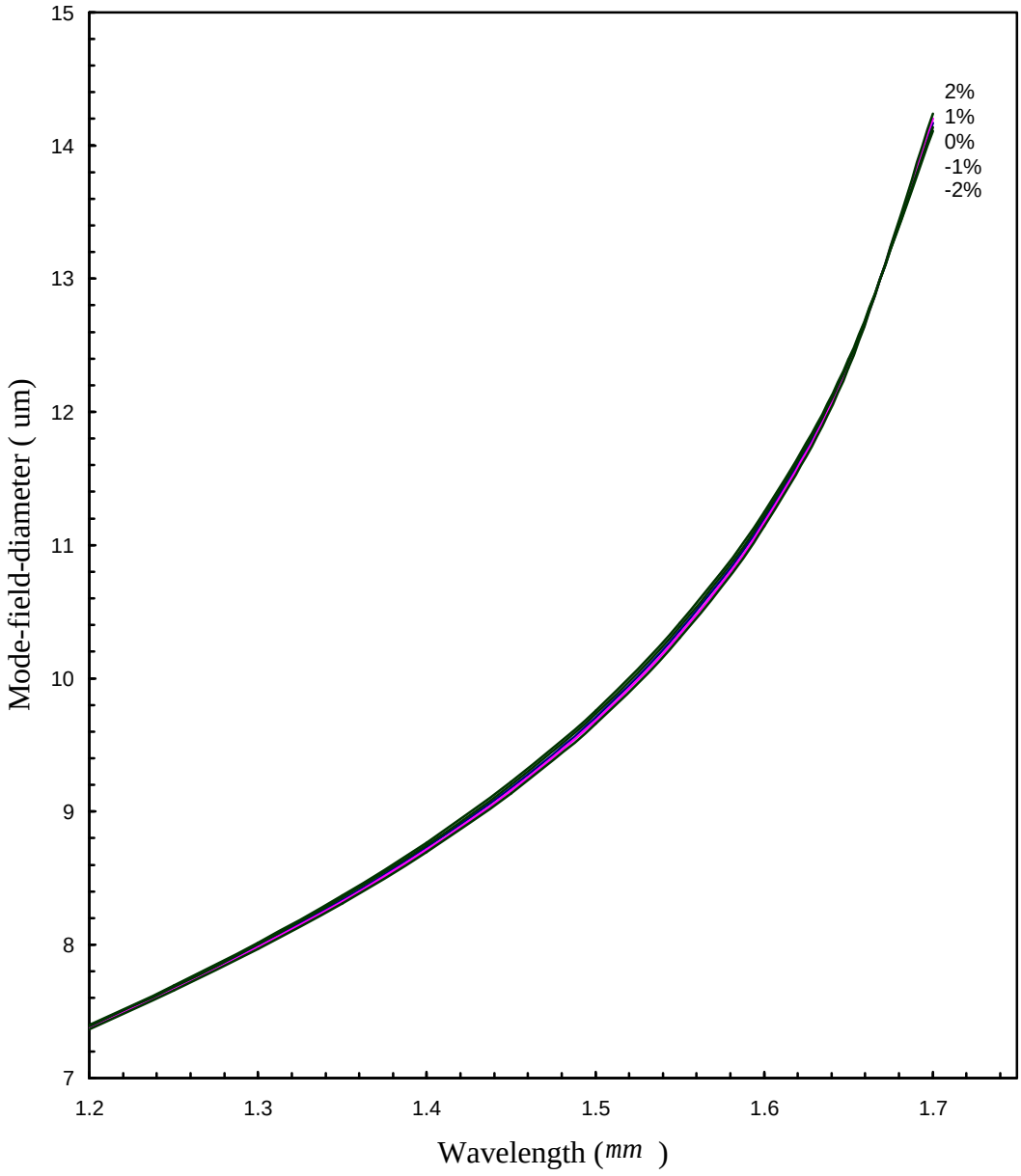

Figure 5.21 Variations of mode-field-diameter versus wavelength for fiber i. Radius a_3 is varied $\pm 1\%$ and $\pm 2\%$.

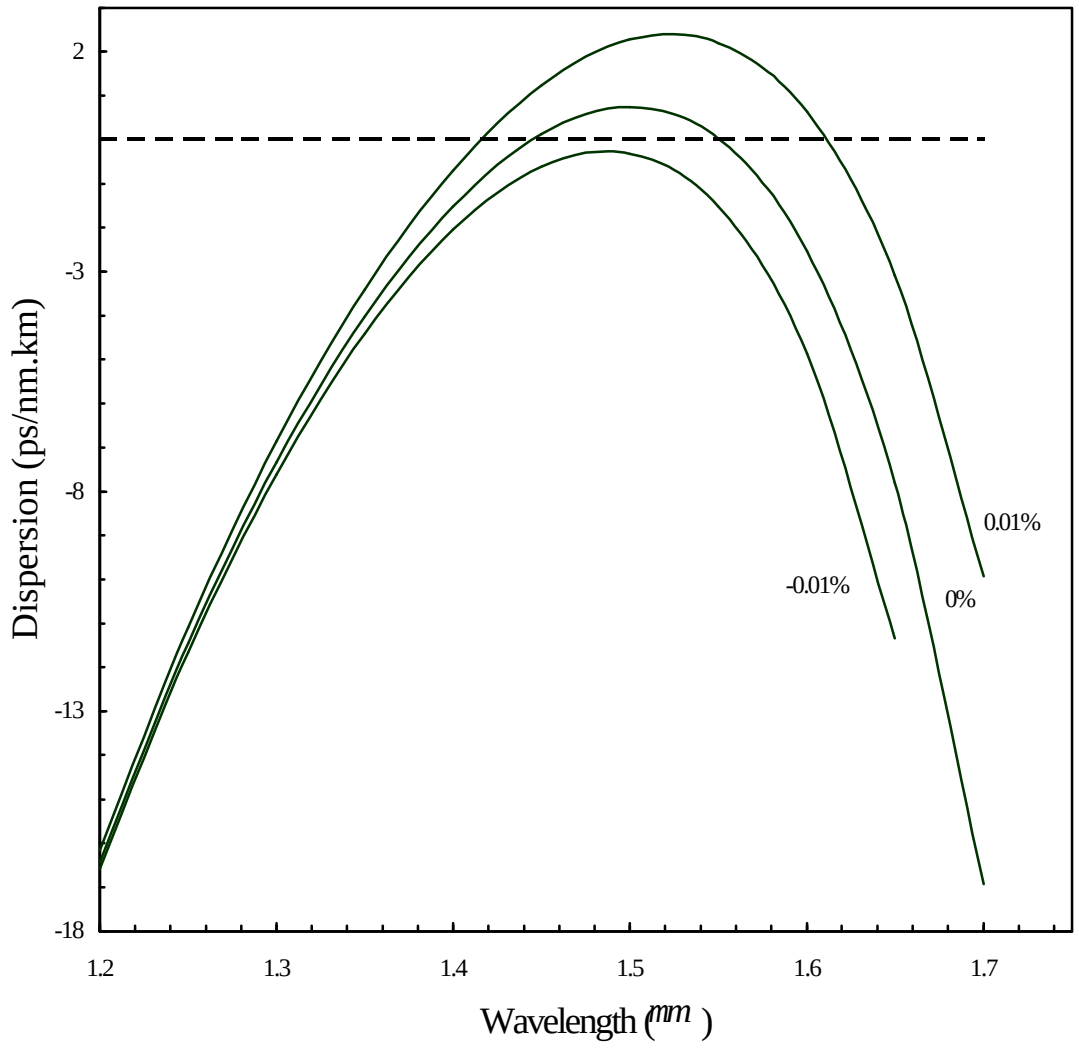

Figure 5.22 Variations of dispersion versus wavelength for fiber i. Refractive index n_2 is varied $\pm 0.01\%$.

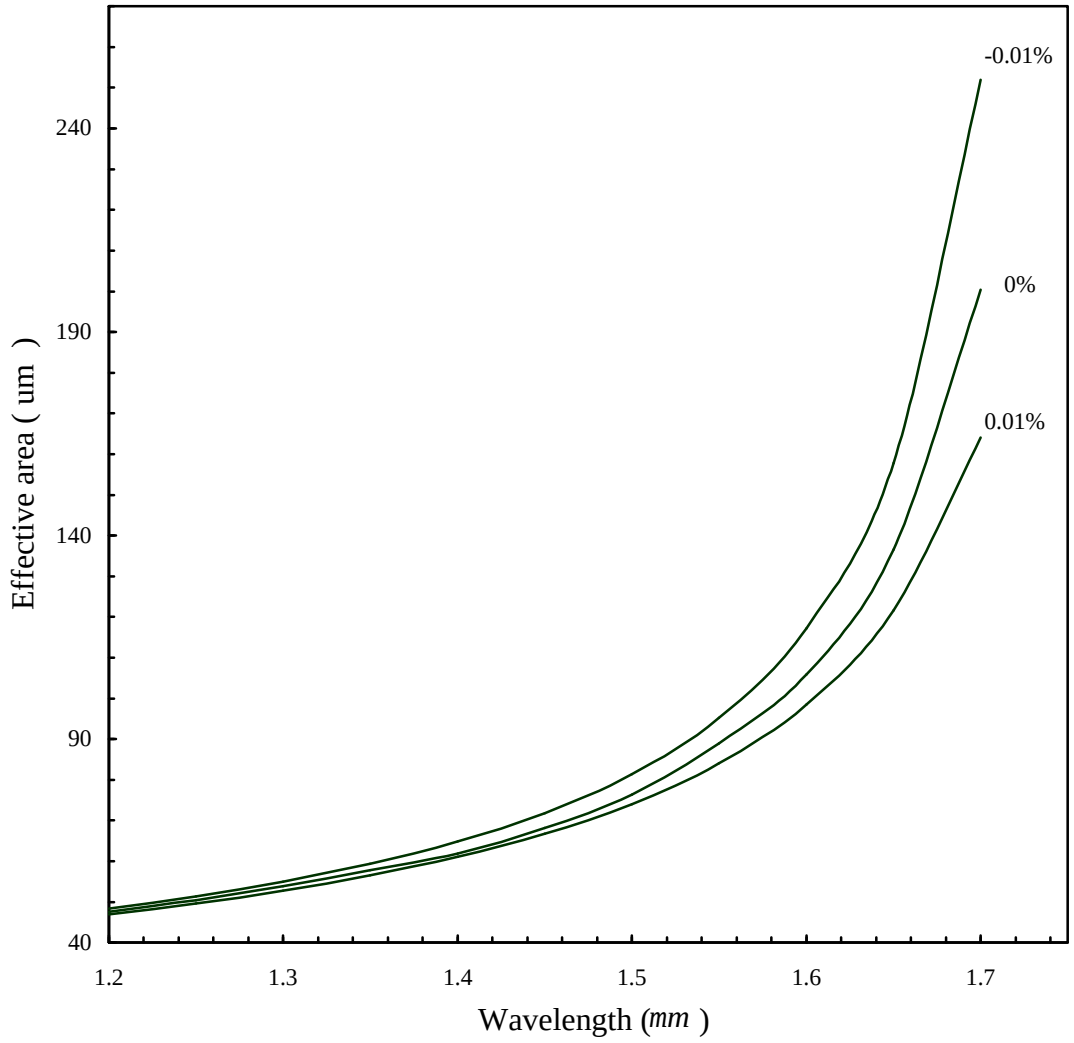

Figure 5.23 Variations of effective-area versus wavelength for fiber i. Refractive index n_2 is varied $\pm 0.01\%$.

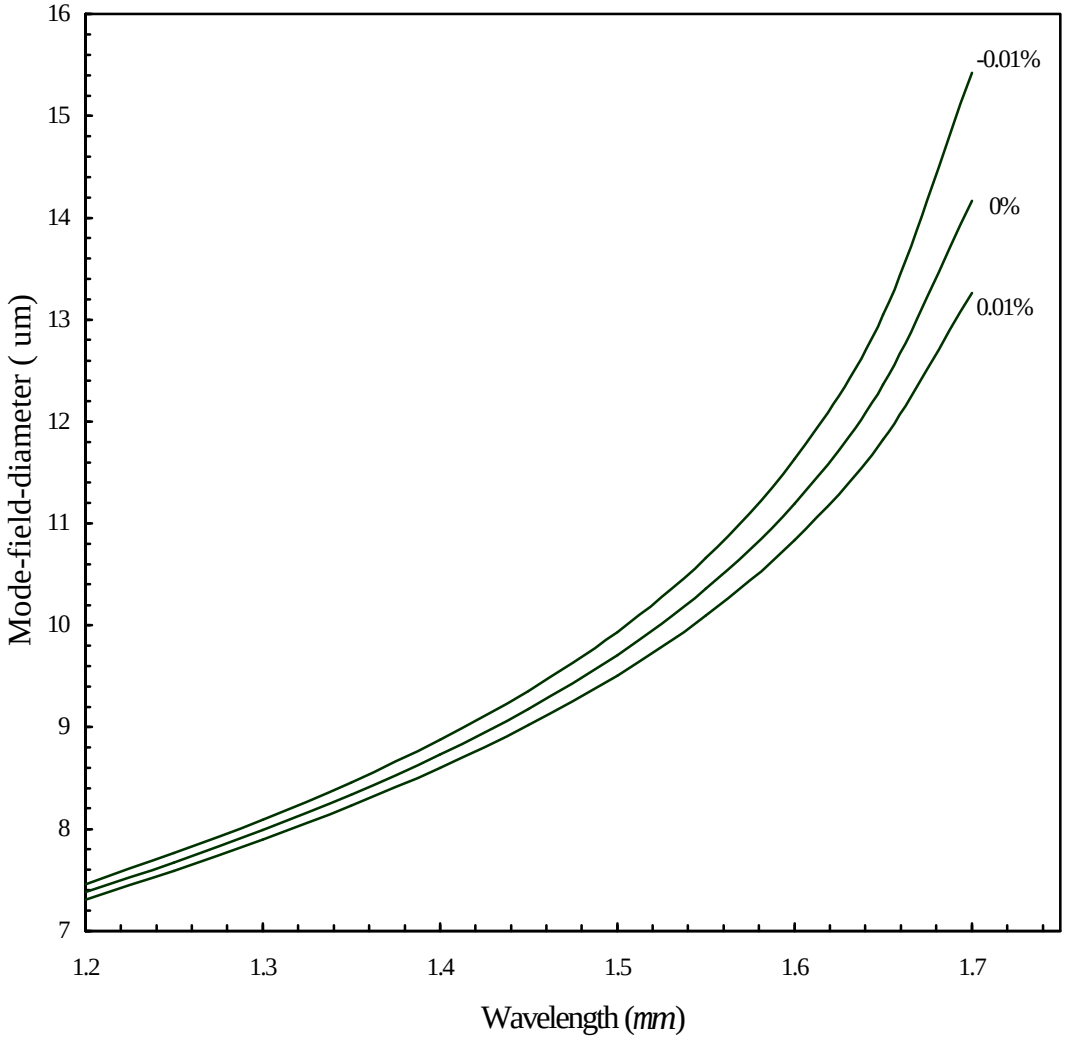

Figure 5.24 Variations of mode-field-diameter versus wavelength for fiber i. Refractive index n_2 is varied $\pm 0.01\%$.

Chapter 6

Analysis of Pulse Propagation in Nonlinear Optical Fibers

After designing low nonlinearity dispersion-shifted and dispersion-flattened fibers, one question may still arise: To what extent signal distortions due to nonlinearities are reduced in these fibers? To answer this question, pulse propagation in the designed fibers are examined and compared with that in a conventional dispersion-shifted fiber. First, the pseudo-random methods for solving the Schrödinger nonlinear equation are discussed. These methods employ the Fast-Fourier Transform (FFT) and are computationally efficient. The systems to be considered in this chapter employ NRZ (Non-Return-to-Zero), on-off shift-keying regime, carrying 2.5 Gb/s information and at 1.55 *mm* optical wavelength. The effects of both positive and negative dispersions systems are addressed.

6.1 Numerical Methods for Solving the Nonlinear Schrödinger Equation

Several methods can be employed to solve the nonlinear Schrödinger equation, including finite element, finite difference and pseudo-spectral methods. However, the first two methods are much slower than the pseudo-spectral methods that employ FFT. For this reason, pseudo-spectral methods are used in this analysis. Two different versions are discussed: one described by Hardin and Tappert [60] and another by Marcuse [53].

The first step is to re-express the nonlinear Schrödinger equation in a more appropriate format. We note that b_1 in (3.14a) is responsible only for propagation of the wave along the fiber and does not cause pulse distortion. By defining a new variable $T = t - b_1 z$, the nonlinear Schrödinger equation (3.14a) can be rearranged as [11]:

$$\frac{\partial A}{\partial z} - \frac{j}{2} b_2 \frac{\partial^2 A}{\partial T^2} - \frac{1}{6} b_3 \frac{\partial^3 A}{\partial T^3} + aA = -j \frac{2p}{l} \hat{n} |A|^2 A \qquad (6.1)$$

In the absence of dispersion, (6.1) has a simple solution. The wave is only attenuated and suffers a nonlinear phase shift. This solution can be expressed as,

$$A(z,T) = \exp(-az)\,A(0,T)\exp\left(-j\frac{2p}{l}\hat{n}\int_0^z \left|A(V,T)\right|^2 dV\right) \tag{6.2}$$

Next, assume that nonlinearity is not present. Defining the Fourier transform of the wave envelope as

$$f_1(z,\Omega) = \int_{-\infty}^{\infty} A(z,T)\exp(-j\Omega T)dT \tag{6.3a}$$

it is clearly seen that in the frequency domain,

$$f_1(z,\Omega) = f_1(0,\Omega)\exp(-az)\exp\left[-j\frac{\Omega^2}{2}\left(b_2 + \frac{\Omega}{3}b_3\right)z\right] \tag{6.3b}$$

Thus, given A(0,T), $f_1(0,\Omega)$ and subsequently $f_1(z,\Omega)$ can be easily found. And, by using the inverse Fourier transform, A(z,T) is determined for any z.

If nonlinearity and dispersion are both present, the problem becomes more involved. Following Hardin and Tappert's approach [60], the total length L is divided into small segments h. It is assumed that nonlinearity and dispersion act independently. This is an approximation accurate to second order in the step size h. For a segment starting at z= z_1, nonlinearities are assumed to be concentrated at z_1 +h/2, while dispersion acts in the whole segment. From z_1 to z_1 +h/2, dispersion acts alone and it is easier to work in the frequency domain. Because, if dispersion acts alone, $f_1(z_1 + h/2,\Omega)$ can be expressed in terms of $f_1(z_1,\Omega)$ by a simple multiplication by an exponential term. Exactly at z_1 +h/2, we go back to time domain, so that A(z_1 +h/2,T) is found by using the inverse Fourier transform. As nonlinearity in the whole segment is concentrated at this point, A(z_1 +h/2,T) is multiplied by $\exp\left(-j\,2p\hat{n}/l\,\left|A(z_1 + h/2,T)\right|^2 h\right)$. Finally, dispersion alone is considered again over the distance $z_1 + h/2$ to $z_1 + h$ and then A(z_1 +h,T) is found. This procedure is repeated until z=L is reached. It is emphasized that the direct and inverse Fourier transforms are not calculated exactly. These tasks are performed using FFT algorithms using Matlab software.

Marcuse [53] has also presented a pseudo-spectral method to analyze propagation of pulses in nonlinear fibers. However, his method is more involved. The basic theory was discussed in Chapter 3. A new variable $f(z,\Omega)$ is introduced as

$$A(z,T) = e^{-az}\int_{-\infty}^{\infty}\exp\left[-\frac{j}{2}\Omega^2\left(b_2+\frac{\Omega}{3}b_3\right)z\right]f(z,\Omega)e^{j\Omega T}d\Omega \tag{6.4}$$

where $f(z,\Omega)$ is

$$f(z,\Omega) = e^{az}\exp\left[\frac{j}{2}\Omega^2\left(b_2+\frac{\Omega}{3}b_3\right)\right]\int_{-\infty}^{\infty}A(z,T)e^{-j\Omega T}dT \tag{6.5}$$

As the Fourier transform is a linear operation, care must be taken to deal with the nonlinear term. This is accomplished by defining $G(z,\Omega)$ as,

$$G(z,\Omega) = e^{az}\exp\left[\frac{j}{2}\Omega^2\left(b_2+\frac{\Omega}{3}b_3\right)z\right]\int_{-\infty}^{\infty}|A(z,T)|^2A(z,T)e^{-j\Omega T}dT \tag{6.6}$$

Using (6.5) and (6.6) in (6.1), the following ordinary differential equation is obtained:

$$\frac{df(z,\Omega)}{dz} = -j\frac{2p}{l}\hat{n}\,G(z,\Omega) \tag{6.7}$$

The method employed to solve (6.7) is a predictor-corrector method. Again, the total length L is divided into small segments h. In order to calculate $f(z+h,\Omega)$ and $A(z+h,T)$, an intermediate variable $f_p(z+h)$ needs to be evaluated using the expression,

$$f_p(z+h,\Omega) = f(z,\Omega) - j\frac{2p}{l}\hat{n}\,G(z,\Omega)h \tag{6.8}$$

Using $f_p(z+h,\Omega)$, the term $A_p(z+h,T)$ can be evaluated from (6.4), which in turn allows us to calculate $G_p(z+h,\Omega)$ from (6.6). Then, $f(z+h,\Omega)$ is evaluated by using the following expression

$$f(z+h,\Omega) = f(z,\Omega) - j\frac{p}{l}\hat{n}\left[G(z,\Omega)+G_p(z+h,\Omega)\right]h \tag{6.9}$$

This procedure is repeated until the final segment is reached. In order to transform the Fourier integrals into fast Fourier transforms and inverse Fourier transforms, the approach presented in [53,Ch. 8] is employed. It is emphasized that in an N-point fast Fourier transform,

the maximum frequency spectrum occurs at N/2 point; data corresponding to the points N/2 to N represent merely a mirror reflection of the actual spectrum [53].

Both programs have been used to analyze pulse propagation in long distance fiber optic links. They provide the same results, but Agrawal's method is faster than Marcuse's method. The reason is that in Agrawal's method, fewer fast Fourier transforms need to be evaluated. Initially, the programs are tested to simulate pulse propagation in a dispersionless fiber. In this case, nonlinearity only introduces a phase shift and no distortion is observed.

6.2 System Considerations

The main goal in this chapter is to analyze nonlinear Kerr effect on pulse propagation in non-soliton systems. The bit rate is assumed to be 2.5 Gb/s and the pulse format is NRZ. The peak power of the transmitted signal is set equal to 10 or 25 mW. The laser source is assumed to be highly coherent so that the bandpass spectrum of the optical signal is only due to the modulating pulse sequence. It emits light at 1.55 mm. A fiber loss of 0.21 dB/km (typical loss at 1.55 mm) is assumed. There is one Erbium-doped fiber amplifier at every 100 km to exactly compensate the fiber attenuation. The fiber is not operated at the zero dispersion wavelength, in order to prevent noise buildup [7]. After traveling the fiber length, the optical signal enters in an ideal photodetector (unit quantum efficiency and no noise) and passes through a third-order analog Butterworth electric filter with cutoff frequency at 3 GHz. The sequence of pulses consists of 8 bits: 10011010. The block diagram of the system is shown in Figure 6.1. It is emphasized that noise is not accounted for here, because the main purpose is to analyze signal distortions caused by dispersion and nonlinearity in optical links and how a larger effective-area reduces such distortions.

In the absence of dispersion and noise, nonlinearity alone does not cause any pulse distortion, and only affects the phase of the optical carrier. The output signal of the fiber-optic link is converted to electric current by a photodetector. The photocurrent is proportional to the power carried by the optical wave [61] and is given by:

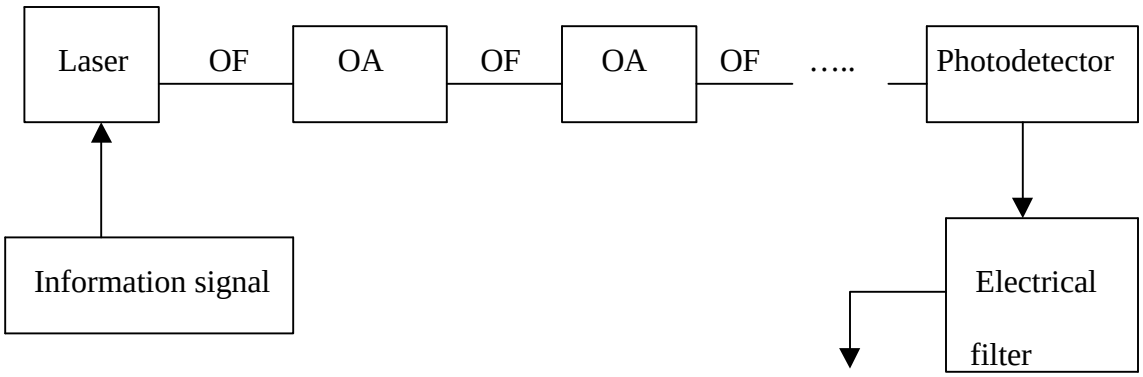

OF: Optical Fiber

OA: Optical Amplifier

Regenerated bit stream

Figure 6.1- Block diagram of an all-optical fiber-optic link.

$$i(t) = \frac{q\,l}{2hc}\sqrt{\frac{e_0}{m_0}}\left\langle nF^2(x,y)\right\rangle \left|A(t,L)\right|^2 \tag{6.10}$$

where i(t) is the photocorrent, q is the charge of electron, h is the Planck's constant, l is the wavelength of the light, c is the speed of light in free-space and e_0 and m_0 are the permittivity and permeability of free-space. The photocurrent is proportional to the instantaneous power of the optical signal and only the envelope of the optical wave is detected.

After detection, the signal passes through a third-order analog Butterworth filter with cutoff at 3.0 GHz. Clearly, the cutoff frequency satisfies the Nyquist criterion to minimize inter-symbol interference. Simulations have shown that nonlinearities tend to broaden the spectrum of the signal envelope, generating spikes in the received pulses, even in the absence of noise. To remove these high frequency components, a filter is needed at the receiver.

The maximum transmission distance is defined as the distance such that the transmitted pulses can still be recovered without error (in the absence of noise) despite the inter-symbol interference caused by dispersion and nonlinearities. Two cases corresponding to positive and negative dispersion are considered.

6.3 Nonlinear Optical Fiber Systems with Negative Dispersion

When a system operates under negative dispersion, fiber nonlinearities help dispersion to distort optical pulses. In other words, fiber nonlinearities and dispersion cause the broadening of optical pulses and consequently inter-symbol interference. This effect intensifies with the distance and can cause errors in correctly identifying the transmitted bits at the receiver end.

Generally, the second-order dispersion is the significant factor contributing to pulse distortion and the third-order dispersion has a minor effect. The maximum transmission distance for several values of second-order dispersion is provided in Table 6.1. Two peak powers were considered, 10 and 25 mW. In this simulation, fibers 1 and 2 have effective-areas of 210 mm^2 and 113 mm^2, respectively and correspond to fibers e and c in Table 4.1. Fiber 3 is a

conventional fiber with an effective-area of 50 mm^2. All three fibers are assumed to have the same dispersion.

Table 6.1 Comparison of maximum transmission distances for two large effective-area fibers (fibers 1 and 2) and a conventional single-mode fiber (fiber 3).

Dispersion / Power	-20 ps/nm.km	-1ps/nm.km	-0.1 ps/nm.km
Fiber 1, 10 mW	1030 km	6000 km	20 000 km
25 mW	800 km	3800 km	14 000 km
Fiber 2, 10 mW	850 km	4500 km	15 000 km
25 mW	650 km	2600 km	10 200 km
Fiber 3, 10 mW	650 km	2800 km	11 000 km
25 mW	420 km	1600 km	7 500 km

From Table 6.1, the advantages of maximizing the effective-area of a fiber are clearly observed. Longer distances can be reached for the same amounts of input power and dispersion. Of course, care must be taken with the bending losses so that they remain below a specified level.

Figures 6.2 and 6.3 show the output signal of the system shown in Fig. 6.1. In these figures, the dispersion is equal to -1 ps/nm.km for all fibers, the distance is equal to 4500 km and the peak transmitted power is 10 mW. Figure 6.2 (solid curve) shows the input sequence of pulses, while Figure 6.2 (dashed curve) shows the output signal when fiber 1 is employed. Figures 6.3 (solid) and (dashed) show the output signals when fibers 2 and 3 are used, respectively.

Setting the threshold at half the level of the "lowest" “1” bit, the original sequence would be correctly recovered when fiber 1 is used, but could be wrongly detected when fiber 2 is used (the "highest" zero level is nearly at the threshold).When fiber 3 is employed, the detected

sequence would be 1,0,1,0,0,1,1,0, clearly showing that errors occur in the detected signal. Thus, it is clear that a larger effective-area fiber reduces distortion in long optical fiber links with negative dispersion. This simulation demonstrates that the new designed optical fibers presented here are very useful in reducing the detrimental effects of nonlinearities in long-distance links.

6.4 Nonlinear Optical Fiber Systems with Positive Dispersion

When an optical fiber is operated in a positive dispersion regime, nonlinearities counteract dispersion in pulse broadening process. Various different phenomena may arise in this case: pulses may broaden, pulses may be compressed, and pulses may start to separate from each other (sometimes even leaving their bit slot). In general, positive dispersion and nonlinearities also cause distortions to optical pulses. Only, for picosecond soliton-like pulses, in which positive dispersion is perfectly compensated by nonlinearities, no distortion occurs.

Table 6.2 summarizes the maximum transmission distance for several values of positive dispersion and two values of peak powers (10 to 25 mW). From Tables 6.1 and 6.2, the following conclusions are obtained:

1- For a given transmitted peak power in a fiber, the greater the absolute value of the dispersion, the smaller will be the maximum distance. This is true in general, but an exception was found for fiber 3 when operated with peak power of 10 mW and positive dispersion. In this case, the maximum distances were 6000 km and 11000 km for dispersion values of 1 ps/nm.km and 20 ps/nm.km, respectively.

2- For a given dispersion in a fiber, it is advantageous to operate at lower powers so that nonlinearities are weaker. However, it is emphasized that noise always exists in optical fiber systems due to the spontaneous emission of optical amplifiers or due to the photodetection process, which also limit the performance of optical fiber systems. Therefore, there is a tradeoff between maximizing the power to get reduced influence of noise and minimizing the power to get reduced nonlinear effects. This problem becomes more complicated with WDM (Wavelength

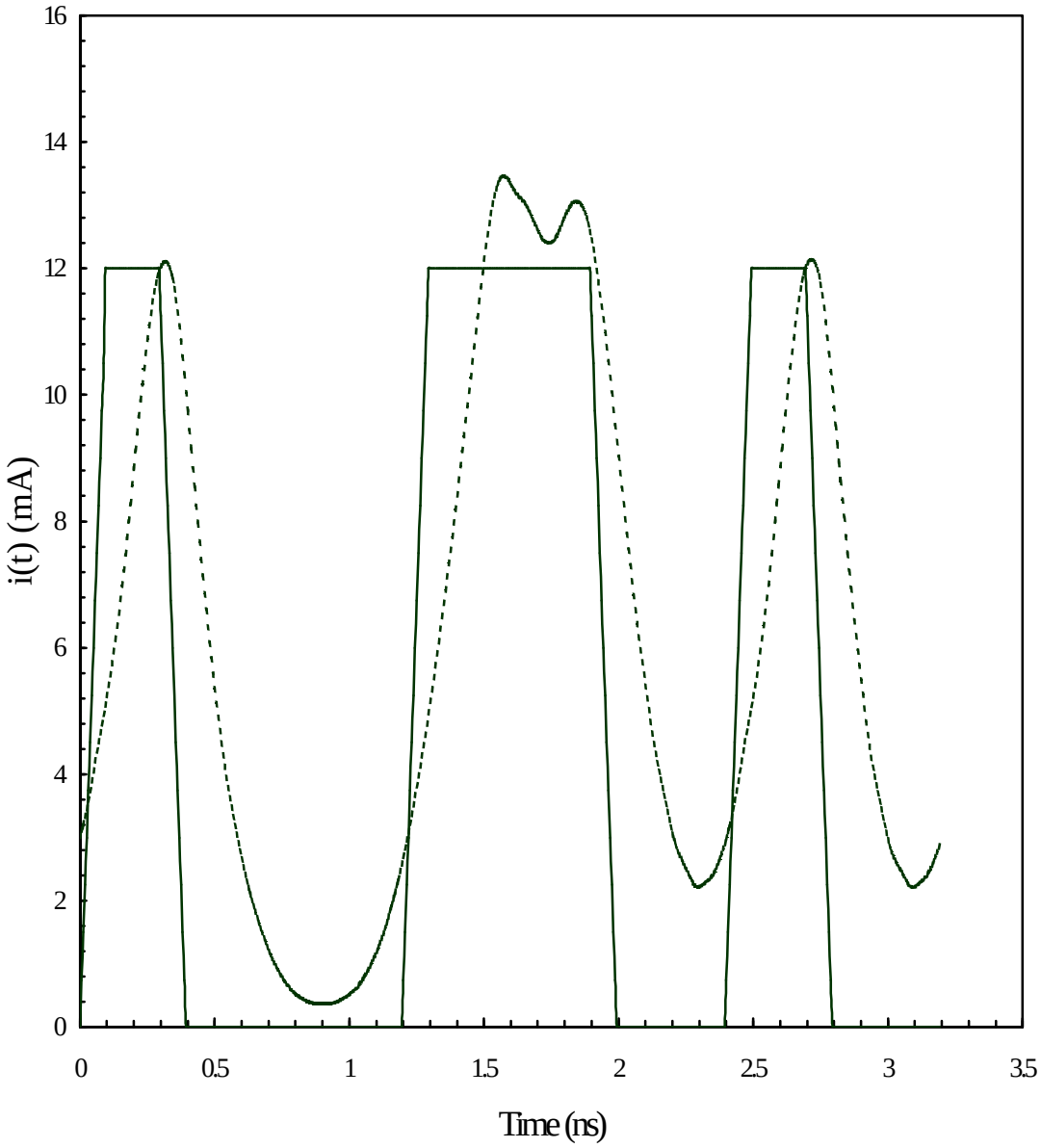

Figure 6.2 (—) Input and (---) output signals for a 4500 km link using fiber 1.

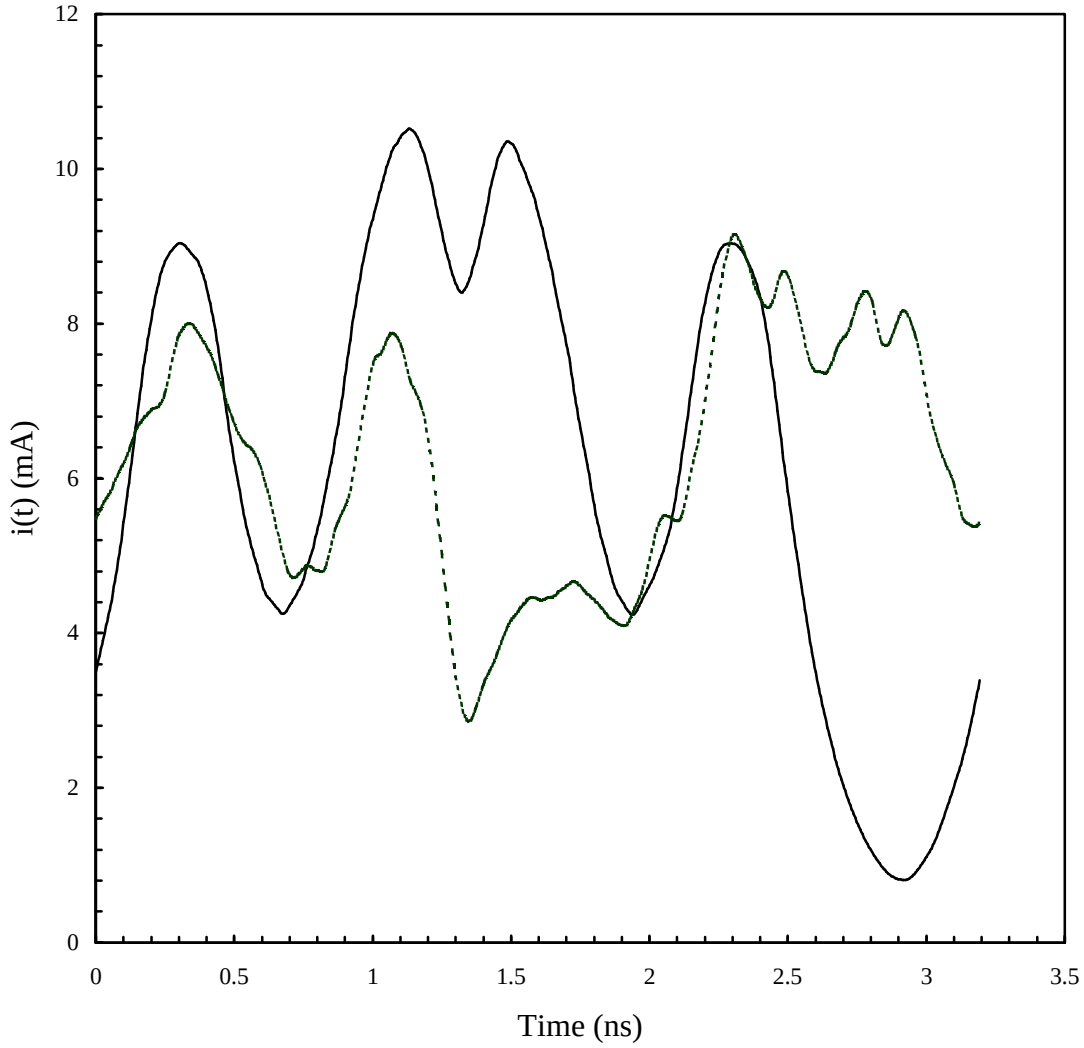

Figure 6.3 Output signals when fiber 2 (—) and fiber 3 (----) are used.

Division Multiplexing) systems, because the powers of all channels contribute to fiber nonlinearities.

3- The larger the effective-area, the longer the transmission distances. This is why the effective-area is so important in long-distance optical fiber systems. A rule of thumb was found for negative dispersion: increasing the effective-area by a factor n, increases the transmission distance by a factor of $\sqrt{n}$ (for moderate to high-transmitted powers). The situation is more complicated for positive dispersion and no simple rule was found. It should be remembered that the larger the effective-area, the larger are the bending losses. This trade-off must always be taken into account in optical fiber design.

Table 6.2- Maximum distances for a specified dispersion and peak power, but for fibers with different effective-areas.

Dispersion Power	20 ps/nm.km	1ps/nm.km	0.1 ps/nm.km
Fiber 1, 10 mW	1100 km	2700 km	> 30 000 km
25 mW	400 km	800 km	> 30 000 km
Fiber 2, 10 mW	3600 km	4400 km	> 30 000 km
25 mW	1100 km	2000 km	> 30 000 km
Fiber 3, 10 mW	11 000 km	6000 km	> 30 000 km
25 mW	2000 km	3800 km	> 30 000 km

4- When decreasing the power, the effective-area becomes less important. This is expected because for very low powers, the effects of nonlinearities on pulse propagation are negligible and, therefore, changes in the effective-area will not make much difference.

5- For moderate levels of transmitted power (below 10 mW), it is advantageous to operate under positive dispersion, in order to achieve longer transmission distances. This arises from the fact that nonlinearity and dispersion oppose to each other in this situation.

Figures 6.4 and 6.5 show the system output signals with a dispersion of 1 ps/nm.km for all fibers, a distance of 4400 km, and peak transmitted power of 10 mW. Figure 6.4 (solid curve) shows the input sequence of pulses, while Figure 6.4 (dashed curve) shows the output pulses when fiber 1 is employed. Figure 6.5 (solid) and (dashed) show the output signals when fibers 2 and 3 are used, respectively.

Setting the threshold at half the level of the "lowest" “1” bit, the original sequence would be correctly recovered when fiber 1 is used, but could be wrongly detected when fiber 2 is used (the "highest" zero level is nearly at the threshold). When fiber 3 is employed, the degree of distortion of the output signal clearly indicates that the original information has been completely lost.

A more thorough analysis of optical systems with nonlinearities is very involved and is out of the scope of this dissertation. Such analysis might include not only single-channel systems, but also WDM systems as well. Photodetector and optical amplifiers noises should be accounted for, the transmitted sequence should be long enough to simulate the transmission of a random sequence of pulses, etc. The purpose of this chapter has been to provide an understanding of the kind of distortions caused by dispersion and nonlinearities.

In summary, large effective-area fibers reduce distortions caused by dispersion and nonlinearity. The price to pay for a larger effective-area is an increase of the bending loss, which can be managed by keeping the bend radii above a specified limit. Certain fiber designs presented in Chapter 4 provide large effective-areas with tolerable bending losses. These fibers are expected to provide a significant improvement in long-distance optical fiber systems performance.

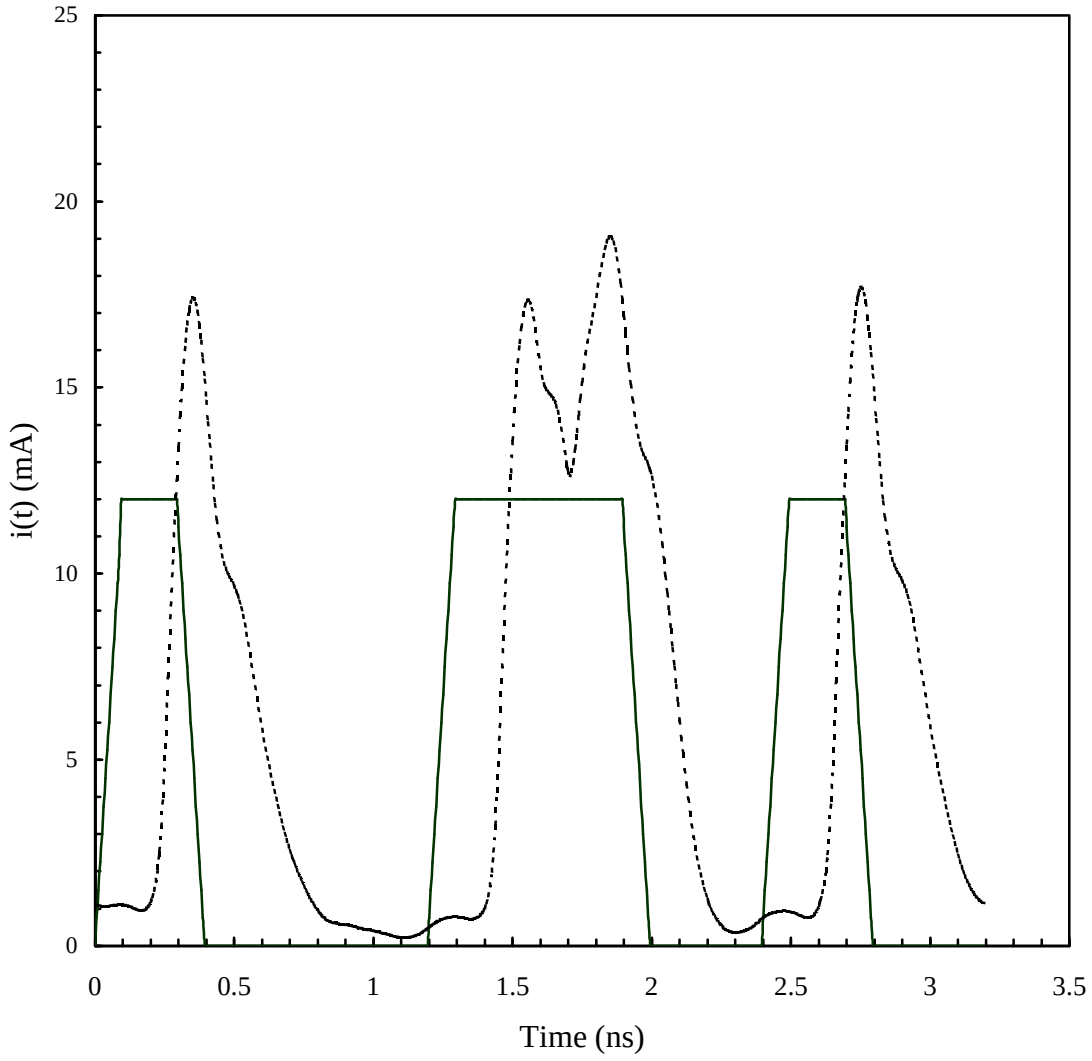

Figure 6.4 (──) Input and (----) output signals for a 4400 km link using fiber 1.

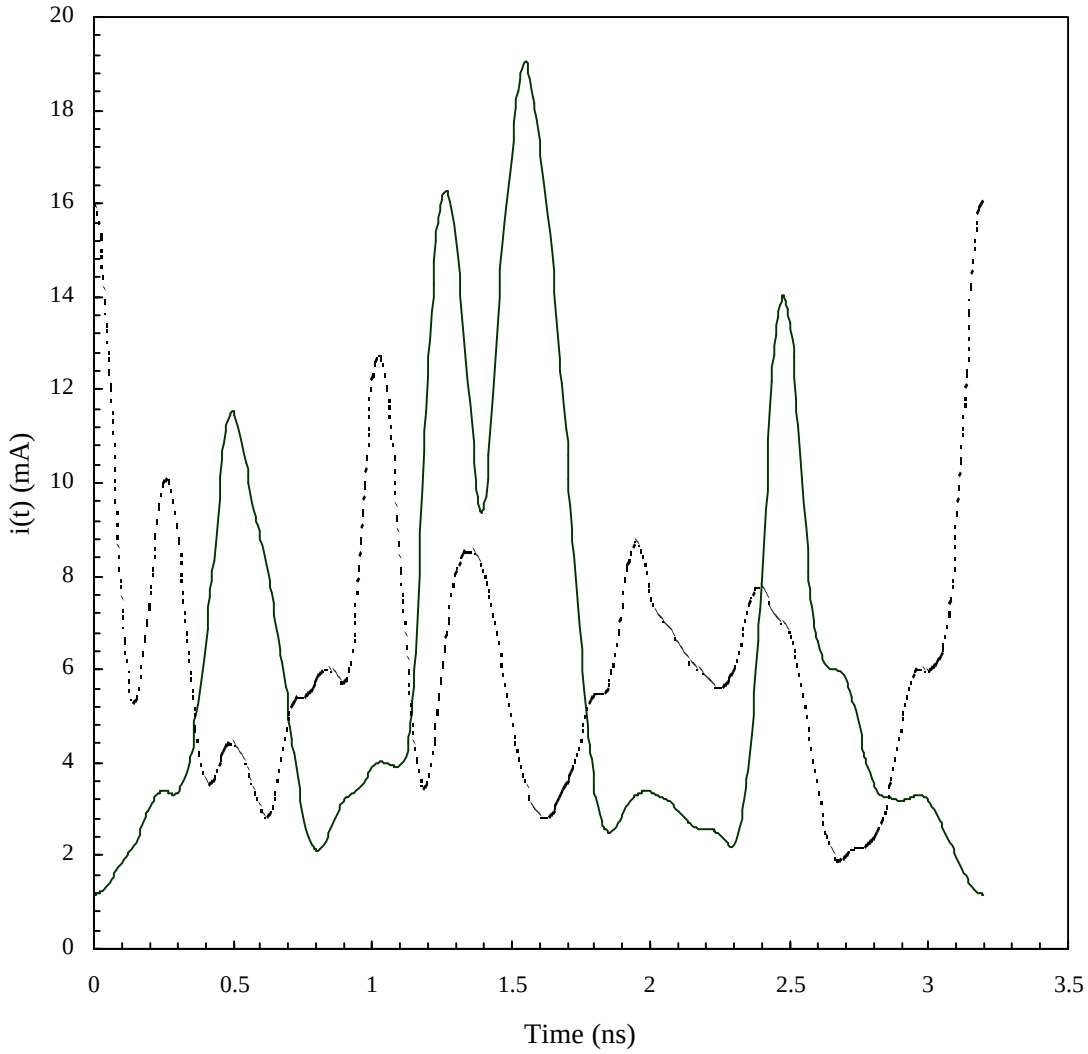

Figure 6.5 Output signals for (——) fiber 2, and (----) fiber 3.

Chapter 7
Conclusions and Suggestions of Future Work

7.1 Summary of the Work and Results

Optical fibers are the best means of transmitting large amounts of information over medium to long distances, because of their low losses and very large capacity. Moreover, Erbium-doped fiber amplifiers have rendered electronic repeaters unnecessary, creating the possibility of transmitting information optically over thousands of kilometers. However, in these long-distance applications, dispersion and nonlinearities are still two major sources of pulse distortion and must be avoided. The optical fibers that have been designed in this dissertation bring a satisfactory solution to these two problems by providing small dispersion and large effective-areas in the wavelength range of operation. Both dispersion-shifted and dispersion-flattened large effective-area fibers have been investigated.

The large effective-area dispersion-shifted and dispersion-flattened fibers designed here employed multi-clad and multi-step index profiles. The formulation and the necessary programs to numerically calculate the transmission properties of these fibers (dispersion, dispersion slope, cutoff wavelength, effective-area, mode-field-diameter, and splice, microbending and splice losses) were developed. Complete field solutions, dispersion relation, and expressions for effective-area, mode-field-diameter, and extrinsic losses were derived for the fundamental LP_{01} mode in a five-layer fiber with arbitrary step-index profile.

A systematic approach to the design of low nonlinearity depressed-core dispersion-shifted fibers was introduced. Based on this approach, large effective-area dispersion-shifted fibers were designed with effective-areas in the range of 78 to 210 mm^2, dispersion less than 0.07 ps/nm.km, dispersion slope less than 0.06 ps/nm^2.km, mode-field-diameters from 8.94 mm to 14.94 mm (values at 1.55 mm), cutoff wavelength well below 1.55 mm, and microbending losses comparable to conventional fibers. In these designs, a larger effective-area implies a lower

splice loss. However, a larger effective-area also implies a higher bending loss, thus a trade-off between nonlinear signal distortion and attenuation due to bending loss. Although bending losses can be made as low as desired by increasing the bending radius, some cable designs require the fibers to be bent and thus tolerable bending losses need to be met by the designs. In order to address the performance of the low nonlinearity fibers with respect to effective-area and bending loss, a quality factor (Q), defined as the ratio of effective-area over the mode-field-diameter squared was introduced. The quality factor for conventional fibers is about 0.74, while the designed large effective-area dispersion-shifted fibers have Q in the range of 0.785 to 1.13.

The large effective-area dispersion-flattened designs provided effective-areas in the range of 75 to 100 mm^2, a mode-field-diameter of 9.56 mm to 10.92 mm and dispersion less than 0.7 ps/nm.km in the 1.55 mm window, say 1.48 $mm < l <$ 1.58 mm. These designs, however, presented a higher bending loss than in conventional dispersion-shifted fibers.

A comprehensive tolerance analysis to examine the sensitivity of transmission properties of designed fibers to variations of radii and refractive indices was carried out. The designed dispersion-shifted fibers exhibited low sensitivity to variations in index and radii. Considering fiber c as a design example of dispersion-shifted fiber, a variation in the radius of the inner most cladding (a_2) by $\pm$ 2% resulted in variations of dispersion from –1.0 ps/nm.km to +0.69 ps/nm.km, effective-area from 110 mm^2 to 117 mm^2, and mode-field-diameter from 10.03 mm to 10.64 mm (values at 1.55 mm). On the other hand, dispersion-flattened fibers were considerably more sensitive to variations in some dimensions, particularly to a_2. Considering fiber i as a design example of dispersion-flattened fiber, a variation in a_2 by $\pm$ 2% resulted in variations of dispersion changed from –4.58 ps/nm.km to 3.38 ps/nm.km, effective-area from 84 mm^2 to 97 mm^2, and mode-field-diameter from 10.09 mm to 10.72 mm (values at 1.55 mm).

Simulations of pulse propagation clearly indicated that large effective-area dispersion-shifted fibers reduced the amount of distortion caused by nonlinearities and dispersion. These simulations were based on split-step Fourier methods. The results of these simulations indicated that a larger effective-area fiber allowed the error-free transmission of information over longer distances. It was observed that for negative dispersion and moderate powers, an increase of

effective-area by a factor n resulted in an increase of the maximum transmission distance by a factor $\sqrt{n}$. For positive dispersion, no simple rule was found for increase in the larger transmission distance. For example, for a dispersion of 1 ps/nm.km and peak power of 10 mW, the maximum distance is 2700 km for a conventional fiber with 50 mm^2 effective-area, while for a 210 mm^2 fiber this value becomes 6000 km. These simulations clearly indicated that large effective-area fibers have important applications in high capacity and long-distance terrestrial and submarine systems.

It is expected that large effective-area fibers will have the same manufacturing cost as conventional dispersion-shifted fibers, because the complexity of index profiles for both types of fibers is about the same.

7.2 Suggestions of Future Work

Large effective-area dispersion-shifted and dispersion-flattened fibers are the state-of-the-art of optical fiber design. This dissertation has significantly contributed to the design, analysis, and understanding of transmission properties of these fibers. However, further improvement in the designs and further investigation in nonlinear effects in these fibers need to be pursued. Some suggestions of future work are summarized below.

1. The designs presented here are based on step-index profiles. The possibility of improved designs using graded-index profiles, which might result in higher quality factors, is worth pursuing.
2. Although small index differences between neighboring layers imply small intrinsic losses, a quantitative examination of these losses is very useful and should be done in order to have a more accurate assessment of the losses for the designed fibers.
3. It is known that dispersion-flattened fibers are difficult to manufacture and generally have high bending losses. A novel design for dispersion-flattened fibers with large effective-area, satisfactory fabrication tolerances, and low bending loss would be a breakthrough.

4. The work presented here is solely theoretical. Fabrication of designed fibers and measurement of their properties are necessary tasks to be carried out. A collaborative effort with a fiber manufacturing company appears to be essential in performing this task.

5. The simulation of pulse propagation presented here does not account for noise. Future simulations of pulse propagation should include noise generated in the laser, optical fiber amplifiers and photodetector. The simulation can also be extended to multi-channel (WDM) systems. For WDM systems analysis, effects such as four-wave mixing and cross-phase modulation must also be included in the simulations.

Appendix A

Expressions for h_i; i= 1, 2, …, 17 in (2.6)

$$h_1 = x_{11}\frac{I_n'(x_{11})}{I_n(x_{11})},\ if\ \bar{b} > n_1,\quad \text{otherwise } x_{11}\frac{J_n'(x_{11})}{J_n(x_{11})} \tag{A.1}$$

$$h_2 = x_{21}\frac{I_n'(x_{21})}{I_n(x_{21})},\ if\ \bar{b} > n_2,\quad \text{otherwise } x_{21}\frac{J_n'(x_{21})}{J_n(x_{21})} \tag{A.2}$$

$$h_3 = x_{21}\frac{K_n'(x_{21})}{K_n(x_{21})},\ if\ \bar{b} > n_2,\quad \text{otherwise } x_{21}\frac{Y_n'(x_{21})}{Y_n(x_{21})} \tag{A.3}$$

$$h_4 = x_{22}\frac{I_n'(x_{22})}{I_n(x_{22})},\ if\ \bar{b} > n_2,\quad \text{otherwise } x_{22}\frac{J_n'(x_{22})}{J_n(x_{22})} \tag{A.4}$$

$$h_5 = x_{22}\frac{K_n'(x_{22})}{K_n(x_{22})},\ if\ \bar{b} > n_2,\quad \text{otherwise } x_{22}\frac{Y_n'(x_{22})}{Y_n(x_{22})} \tag{A.5}$$

$$h_6 = x_{32}\frac{I_n'(x_{32})}{I_n(x_{32})},\ if\ \bar{b} > n_3,\quad \text{otherwise } x_{32}\frac{J_n'(x_{32})}{J_n(x_{32})} \tag{A.6}$$

$$h_7 = x_{32}\frac{K_n'(x_{32})}{K_n(x_{32})},\ if\ \bar{b} > n_3,\quad \text{otherwise } x_{32}\frac{Y_n'(x_{32})}{Y_n(x_{32})} \tag{A.7}$$

$$h_8 = x_{33}\frac{I_n'(x_{33})}{I_n(x_{33})},\ if\ \bar{b} > n_3,\quad \text{otherwise } x_{33}\frac{J_n'(x_{33})}{J_n(x_{33})} \tag{A.8}$$

$$h_9 = x_{33}\frac{K_n'(x_{33})}{K_n(x_{33})},\ if\ \bar{b} > n_3,\quad \text{otherwise } x_{33}\frac{Y_n'(x_{33})}{Y_n(x_{33})} \tag{A.9}$$

$$h_{10} = x_{43}\frac{I_n'(x_{43})}{I_n(x_{43})},\ if\ \bar{b} > n_4,\quad \text{otherwise } x_{43}\frac{J_n'(x_{43})}{J_n(x_{43})} \tag{A.10}$$

$$h_{11} = x_{43}\frac{K_n'(x_{43})}{K_n(x_{43})},\ if\ \bar{b} > n_4,\quad \text{otherwise } x_{43}\frac{Y_n'(x_{43})}{Y_n(x_{43})} \tag{A.11}$$

$$h_{12} = x_{44}\frac{I_n'(x_{44})}{I_n(x_{44})}, if\ \bar{b} > n_4, \quad \text{otherwise } x_{44}\frac{J_n'(x_{44})}{J_n(x_{44})} \tag{A.12}$$

$$h_{13} = x_{44}\frac{K_n'(x_{44})}{K_n(x_{44})},\ if\ \bar{b} > n_4, \quad \text{otherwise } x_{44}\frac{Y_n'(x_{44})}{Y_n(x_{44})} \tag{A.13}$$

$$h_{14} = x_{54}\frac{K_n'(x_{54})}{K_n(x_{54})} \tag{A.14}$$

$$h_{15} = \frac{K_n(x_{22})I_n(x_{21})}{I_n(x_{22})K_n(x_{21})},\ if\ \bar{b} > n_2, \quad \text{otherwise } \frac{Y_n(x_{22})J_n(x_{21})}{J_n(x_{22})Y_n(x_{21})} \tag{A.15}$$

$$h_{16} = \frac{K_n(x_{33})I_n(x_{32})}{I_n(x_{33})K_n(x_{32})},\ if\ \bar{b} > n_3, \quad \text{otherwise } \frac{Y_n(x_{33})J_n(x_{32})}{J_n(x_{33})Y_n(x_{32})} \tag{A.16}$$

$$h_{17} = \frac{K_n(x_{43})I_n(x_{44})}{I_n(x_{43})K_n(x_{44})},\ if\ \bar{b} > n_4, \quad \text{otherwise } \frac{Y_n(x_{43})J_n(x_{44})}{J_n(x_{43})Y_n(x_{44})} \tag{A.17}$$

where n_i, $x_{ij} = a_j\sqrt{\left|k_o^2 n_i^2 - b^2\right|}$, i=1,..,5, j = i, i-1 (j>0), and a_j , j=1, … 5, n_i, i=1, …, 5, b, k_o, J_n, I_n, Y_n, and K_n have been defined in section 2.1.

Appendix B

B.1 Expressions for c_i, i=1, …4, in (2.8):

$$c_1 = \ln\left(\frac{n_2}{n_1}\right)\left[A_2 J_0(x_{21}) + \overline{A}_2 Y_o(x_{21})\right]\left[-x_{21}A_2 J_1(x_{21}) - x_{21}\overline{A}_2 Y_1(x_{21})\right], \quad if\ \ \overline{b} < n_2$$

or (B.1)

$$\ln\left(\frac{n_2}{n_1}\right)\left[A_2 I_0(x_{21}) + \overline{A}_2 K_0(x_{21})\right]\left[x_{21}A_2 I_1(x_{21}) - x_{21}\overline{A}_2 K_1(x_{21})\right], \quad if\ \ \overline{b} > n_2$$

$$c_2 = \ln\left(\frac{n_3}{n_2}\right)\left[A_2 J_0(x_{22}) + \overline{A}_2 Y_o(x_{22})\right]\left[-x_{22}A_2 J_1(x_{22}) - x_{22}\overline{A}_2 Y_1(x_{22})\right], \quad if\ \ \overline{b} < n_2$$

or (B.2)

$$\ln\left(\frac{n_3}{n_2}\right)\left[A_2 I_0(x_{22}) + \overline{A}_2 K_0(x_{22})\right]\left[x_{22}A_2 I_1(x_{22}) - x_{22}\overline{A}_2 K_1(x_{22})\right], \quad if\ \ \overline{b} > n_2$$

$$c_3 = \ln\left(\frac{n_4}{n_3}\right)\left[A_3 J_0(x_{33}) + \overline{A}_3 Y_o(x_{33})\right]\left[-x_{33}A_3 J_1(x_{33}) - x_{33}\overline{A}_3 Y_1(x_{33})\right], \quad if\ \ \overline{b} < n_3$$

or (B.3)

$$\ln\left(\frac{n_4}{n_3}\right)\left[A_3 I_0(x_{33}) + \overline{A}_3 K_0(x_{33})\right]\left[x_{33}A_3 I_1(x_{33}) - x_{33}\overline{A}_3 K_1(x_{33})\right], \quad if\ \ \overline{b} > n_3$$

$$c_4 = -\ln\left(\frac{n_5}{n_4}\right)\overline{A}_5^{\,2} K_0(x_{54})x_{54}K_1(x_{54}) \tag{B.4}$$

B.2 Expression for P in (2.8):

$$P = \sum_{i=1}^{5} P_i = \int_0^{\infty} \left|y_1(r)\right|^2 r dr \tag{B.5}$$

where:

$$P_1 = A_1^2 a_1^2\left[I_0^2(x_{11}) - I_1^2(x_{11})\right]/2, \quad if\ \ \overline{b} > n_1, \text{ or}$$

$$P_1 = A_1^2 a_1^2\left[J_0^2(x_{11}) + J_1^2(x_{11})\right]/2, \quad if\ \ \overline{b} \le n_1 \tag{B.6}$$

$$P_2 = A_2^2\left\{\frac{a_2^2}{2}\left[J_0^2(x_{22}) + J_1^2(x_{22})\right] - \frac{a_1^2}{2}\left[J_o^2(x_{21}) + J_1^2(x_{21})\right]\right\} +$$
$$A_2\overline{A}_2\left\{a_2^2\left[J_0(x_{22})Y_0(x_{22}) + J_1(x_{22})Y_1(x_{22})\right] - a_1^2\left[J_0(x_{21})Y_0(x_{21}) +\right.\right.$$
$$\left.\left.J_1(x_{21})Y_1(x_{21})\right] + \overline{A}_2^2\left\{\frac{a_2^2}{2}\left[Y_0^2(x_{22}) + Y_1^2(x_{22})\right] - \frac{a_1^2}{2}\left[Y_0^2(x_{21}) + Y_1^2(x_{21})\right]\right\},$$

if $\overline{b} < n_2$, or

$$P_2 = A_2^2\left\{\frac{a_2^2}{2}\left[I_0^2(x_{22}) - I_1^2(x_{22})\right] - \frac{a_1^2}{2}\left[I_o^2(x_{21}) - I_1^2(x_{21})\right]\right\} +$$
$$A_2\overline{A}_2\left\{a_2^2\left[I_0(x_{22})K_0(x_{22}) + I_1(x_{22})K_1(x_{22})\right] - a_1^2\left[I_0(x_{21})K_0(x_{21}) +\right.\right.$$
$$\left.\left.I_1(x_{21})K_1(x_{21})\right] + \overline{A}_2^2\left\{\frac{a_2^2}{2}\left[K_0^2(x_{22}) - K_1^2(x_{22})\right] - \frac{a_1^2}{2}\left[K_0^2(x_{21}) - K_1^2(x_{21})\right]\right\},$$

if $\overline{b} > n_2$. (B.7)

$$P_3 = A_3^2\left\{\frac{a_3^2}{2}\left[J_0^2(x_{33}) + J_1^2(x_{33})\right] - \frac{a_2^2}{2}\left[J_o^2(x_{32}) + J_1^2(x_{32})\right]\right\} +$$
$$A_3\overline{A}_3\left\{a_3^2\left[J_0(x_{33})Y_0(x_{33}) + J_1(x_{33})Y_1(x_{33})\right] - a_2^2\left[J_0(x_{32})Y_0(x_{32}) +\right.\right.$$
$$\left.\left.J_1(x_{32})Y_1(x_{32})\right] + \overline{A}_3^2\left\{\frac{a_3^2}{2}\left[Y_0^2(x_{33}) + Y_1^2(x_{33})\right] - \frac{a_2^2}{2}\left[Y_0^2(x_{32}) + Y_1^2(x_{32})\right]\right\},$$

if $\overline{b} < n_3$, or

$$P_3 = A_3^2\left\{\frac{a_3^2}{2}\left[I_0^2(x_{33}) - I_1^2(x_{33})\right] - \frac{a_2^2}{2}\left[I_o^2(x_{32}) - I_1^2(x_{32})\right]\right\} +$$
$$A_3\overline{A}_3\left\{a_3^2\left[I_0(x_{33})K_0(x_{33}) + I_1(x_{33})K_1(x_{33})\right] - a_2^2\left[K_0(x_{32})I_0(x_{32}) +\right.\right.$$
$$\left.\left.I_1(x_{32})K_1(x_{32})\right] + \overline{A}_3^2\left\{\frac{a_3^2}{2}\left[K_0^2(x_{33}) - K_1^2(x_{33})\right] - \frac{a_2^2}{2}\left[K_0^2(x_{32}) - K_1^2(x_{32})\right]\right\},$$

if $\overline{b} > n_3$. (B.8)

$$P_4 = A_4^2\left\{\frac{a_4^2}{2}\left[J_0^2(x_{44}) + J_1^2(x_{44})\right] - \frac{a_3^2}{2}\left[J_o^2(x_{43}) + J_1^2(x_{43})\right]\right\} +$$
$$A_4\overline{A}_4\left\{a_4^2\left[J_0(x_{44})Y_0(x_{44}) + J_1(x_{44})Y_1(x_{44})\right] - a_3^2\left[J_0(x_{43})Y_0(x_{43}) +\right.\right.$$
$$\left.\left.J_1(x_{43})Y_1(x_{43})\right] + \overline{A}_4^2\left\{\frac{a_4^2}{2}\left[Y_0^2(x_{44}) + Y_1^2(x_{44})\right] - \frac{a_3^2}{2}\left[Y_0^2(x_{43}) + Y_1^2(x_{43})\right]\right\},$$

if $\bar{b} < n_4$, or

$$P_4 = A_4^2\left\{\frac{a_4^2}{2}\left[I_0^2(x_{44}) - I_1^2(x_{44})\right] - \frac{a_3^2}{2}\left[I_o^2(x_{43}) - I_1^2(x_{43})\right]\right\} +$$
$$A_4\bar{A}_4\left\{a_4^2\left[I_0(x_{44})K_0(x_{44}) + I_1(x_{44})K_1(x_{44})\right] - a_3^2\left[I_0(x_{43})K_0(x_{43}) +\right.\right.$$
$$\left.\left.I_1(x_{43})K_1(x_{43})\right] + \bar{A}_4^2\left\{\frac{a_4^2}{2}\left[K_0^2(x_{44}) - K_1^2(x_{44})\right] - \frac{a_3^2}{2}\left[K_0^2(x_{43}) - K_1^2(x_{43})\right]\right\},$$

if $\bar{b} > n_4$. (B.9)

$$P_5 = -\frac{a_4^2}{2}\bar{A}_5^2\left[K_0^2(x_{54}) - K_1^2(x_{54})\right] \quad \text{(B.10)}$$

Appendix C

Table C.1- Number designation for pure and doped silica glasses.

k	material	k	material
1	SiO_2	13	$7.9\,m\%\,GeO_2, 92.1\,m\%\,SiO_2$
2	$13.5\,m\%\,GeO_2, 86.5\,m\%\,SiO_2$	14	$3.0\,m\%\,B_2O_3, 97.0\,m\%\,SiO_2$
3	$7.0\,m\%\,GeO_2, 93.0\,m\%\,SiO_2$	15	$3.5\,m\%\,B_2O_3, 96.5\,m\%\,SiO_2$
4	$4.1\,m\%\,GeO_2, 95.9\,m\%\,SiO_2$	16	$3.3\,m\%\,GeO_2, 87.5\,m\%\,SiO_2, 9.2\,m\%\,B_2O_3$
5	$9.1\,m\%\,GeO_2, 83.2\,m\%\,SiO_2, 7.7\,m\%\,B_2O_3$	17	$2.2\,m\%\,GeO_2, 94.5\,m\%\,SiO_2, 3.3\,m\%\,B_2O_3$
6	$4.03\,m\%\,GeO_2, 86.27\,m\%\,SiO_2, 9.7\,m\%\,B_2O_3$	18	*Quenched* SiO_2
7	$0.1\,m\%\,GeO_2, 94.5\,m\%\,SiO_2, 5.4\,m\%\,B_2O_3$	19	$13.5\,m\%\,GeO_2, 86.5\,m\%\,SiO_2$
8	$13.5\,m\%\,B_2O_3, 86.5\,m\%\,SiO_2$	20	$9.1\,m\%\,P_2O_5, 90.9\,m\%\,SiO_2$
9	$13.5\,m\%\,GeO_2, 86.5\,m\%\,SiO_2\,(Chilled)$	21	$13.3\,m\%\,B_2O_3, 86.7\,m\%\,SiO_2$
10	$3.1\,m\%\,GeO_2, 96.9\,m\%\,SiO_2$	22	$1.0\,m\%\,F, 99.0\,m\%\,SiO_2$
11	$3.5\,m\%\,GeO_2, 96.5\,m\%\,SiO_2$	23	$16.9\,m\%\,Na_2O, 50.6\,m\%\,SiO_2, 32.5\,m\%\,B_2O_3$
12	$5.8\,m\%\,GeO_2, 94.2\,m\%\,SiO_2$		

Table C.2- Sellmeier's coefficients for the materials of Table C.1.

k	A_1	A_2	A_3	$l_1(mm)$	$l_2(mm)$	$l_3(mm)$
1	0.6961663	0.4079426	0.8974794	0.0684043	0.1162414	9.896161
2	0.73454395	0.42710828	0.82103399	0.08697693	0.11195191	10.846540
3	0.68698290	0.44479505	0.79073512	0.078087582	0.11551840	10.436628
4	0.68671749	0.43481505	0.89656582	0.072675189	0.11514351	10.002398
5	0.72393884	0.41129541	0.79292034	0.085826532	0.10705260	9.3772959
6	0.70420420	0.41289413	0.95238253	0.067974973	0.12147738	9.6436219
7	0.69681388	0.40865177	0.89374039	0.070555513	0.11765660	9.8754801
8	0.70724622	0.39412616	0.63301929	0.080478054	0.10925792	7.8908063
9	0.67626834	0.42213113	0.58339770	0.076053015	0.11329618	7.8486094
10	0.7028554	0.4146307	0.8974540	0.0727723	0.1143085	9.896161
11	0.7042038	0.4160032	0.9074049	0.0514415	0.1291600	9.896156
12	0.7088876	0.4206803	0.8956551	0.0609053	0.1254514	9.896162
13	0.7136824	0.4254807	0.8964226	0.0617167	0.1270814	9.896161
14	0.6935408	0.4052977	0.9111432	0.0717021	0.1256396	9.896154
15	0.6929642	0.4047468	0.9154064	0.0604843	0.1239609	9.896152
16	0.6958807	0.4076588	0.9401093	0.0665654	0.1211422	9.896140
17	0.6993390	0.4111269	0.9035275	0.0617482	0.1242404	9.896158
18	0.696750	0.408218	0.890815	0.069066	0.115662	9.900559
19	0.711040	0.451885	0.704048	0.064270	0.129408	9.425478
20	0.695790	0.452497	0.712513	0.061568	0.119921	8.656641
21	0.690618	0.401996	0.898817	0.061900	0.123662	9.098960
22	0.691116	0.399166	0.890423	0.068227	0.116460	9.993707
23	0.796468	0.497614	0.358924	0.094359	0.093386	5.999652

Appendix D

The expression for I_{co}, used in the evaluation of the bending loss, is given by:

$$I_{co} = -j\frac{(2p)^2}{l}\sqrt{\frac{e_o}{m_o}}\left[\sum_{p=1}^{4}\left(n_5^2 - n_p^2\right)\left(A_p F_p + \overline{A}_p \overline{F}_p\right)\right] \tag{D.1}$$

where $\overline{A}_1 = \overline{F}_1 = 0$ and the terms F_p and $\overline{F}_p$ are expressed as,

$$F_1 = \frac{1}{x_1^2 + x_5^2}\left[x_5 a_1 J_o(x_{11}) I_1(x_5 a_1) + x_{11} J_1(x_{11}) I_0(x_5 a_1)\right], \qquad \text{if } \bar{b} < n_1. \tag{D.2a}$$

$$F_1 = \frac{1}{x_1^2 - x_5^2}\left[-x_5 a_1 I_0(x_{11}) I_1(x_5 a_1) + x_{11} I_1(x_{11}) I_0(x_5 a_1)\right], \qquad \text{if } \bar{b} > n_1. \tag{D.2b}$$

$$\begin{aligned} F_2 = \frac{1}{x_2^2 + x_5^2}\Big[&x_5 a_2 J_0(x_{22}) I_1(x_5 a_2) + x_{22} J_1(x_{22}) I_0(x_5 a_2) + \\ &- x_5 a_1 J_0(x_{21}) I_1(x_5 a_1) - x_{21} J_1(x_{21}) I_0(x_5 a_1)\Big], \end{aligned}$$

if $\bar{b} < n_2$. (D.3a)

$$\begin{aligned} F_2 = \frac{1}{x_2^2 - x_5^2}\Big[&-x_5 a_2 I_0(x_{22}) I_1(x_5 a_2) + x_{22} I_1(x_{22}) I_0(x_5 a_2) + \\ &+ x_5 a_1 I_0(x_{21}) I_1(x_5 a_1) - x_{21} I_1(x_{21}) I_0(x_5 a_1)\Big], \end{aligned}$$

if $\bar{b} > n_2$. (D.3b)

$$\begin{aligned} \overline{F}_2 = \frac{1}{x_2^2 + x_5^2}\Big[&x_5 a_2 Y_0(x_{22}) I_1(x_5 a_2) + x_{22} Y_1(x_{22}) I_0(x_5 a_2) + \\ &- x_5 a_1 Y_0(x_{21}) I_1(x_5 a_1) - x_{21} Y_1(x_{21}) I_0(x_5 a_1)\Big], \end{aligned}$$

if $\bar{b} < n_2$. (D.4a)

$$\begin{aligned} \overline{F}_2 = \frac{1}{x_5^2 - x_2^2}\Big[&x_5 a_2 K_0(x_{22}) I_1(x_5 a_2) + x_{22} K_1(x_{22}) I_0(x_5 a_2) + \\ &- x_5 a_1 K_0(x_{21}) I_1(x_5 a_1) - x_{21} K_1(x_{21}) I_0(x_5 a_1)\Big], \end{aligned}$$

if $\bar{b} > n_2$. (D.4b)

$$\begin{aligned} F_3 = \frac{1}{x_3^2 + x_5^2}\Big[&x_5 a_3 J_0(x_{33}) I_1(x_5 a_3) + x_{33} J_1(x_{33}) I_0(x_5 a_3) + \\ &- x_5 a_2 J_0(x_{32}) I_1(x_5 a_2) - x_{32} J_1(x_{32}) I_0(x_5 a_2)\Big], \end{aligned}$$

if $\bar{b} < n_3$. (D.5a)

$$F_3 = \frac{1}{x_3^2 - x_5^2}\Big[-x_5 a_3 I_0(x_{33}) I_1(x_5 a_3) + x_{33} I_1(x_{33}) I_0(x_5 a_3) + \\ + x_5 a_2 I_0(x_{32}) I_1(x_5 a_2) - x_{32} I_1(x_{32}) I_0(x_5 a_2)\Big],$$

if $\bar{b} > n_3$. (D.5b)

$$\bar{F}_3 = \frac{1}{x_3^2 + x_5^2}\Big[x_5 a_3 Y_0(x_{33}) I_1(x_5 a_3) + x_{33} Y_1(x_{33}) I_0(x_5 a_3) + \\ - x_5 a_2 Y_0(x_{32}) I_1(x_5 a_2) - x_{32} Y_1(x_{32}) I_0(x_5 a_2)\Big],$$

if $\bar{b} < n_3$. (D.6a)

$$\bar{F}_3 = \frac{1}{x_5^2 - x_3^2}\Big[x_5 a_3 K_0(x_{33}) I_1(x_5 a_3) + x_{33} K_1(x_{33}) I_0(x_5 a_3) + \\ - x_5 a_2 K_0(x_{32}) I_1(x_5 a_2) - x_{32} K_1(x_{32}) I_0(x_5 a_2)\Big],$$

if $\bar{b} > n_3$. (D.6b)

$$F_4 = \frac{1}{x_4^2 + x_5^2}\Big[x_{54} J_0(x_{44}) I_1(x_{54}) + x_{44} J_1(x_{44}) I_0(x_{54}) + \\ - x_5 a_3 J_0(x_{43}) I_1(x_5 a_3) - x_{43} J_1(x_{43}) I_0(x_5 a_3)\Big],$$

if $\bar{b} < n_4$. (D.7a)

$$F_4 = \frac{1}{x_4^2 - x_5^2}\Big[-x_{54} I_0(x_{44}) I_1(x_{54}) + x_{44} I_1(x_{44}) I_0(x_{54}) + \\ + x_5 a_3 I_0(x_{43}) I_1(x_5 a_3) - x_{43} I_1(x_{43}) I_0(x_5 a_3)\Big],$$

if $\bar{b} > n_4$. (D.7b)

$$\bar{F}_4 = \frac{1}{x_4^2 + x_5^2}\Big[x_{54} Y_0(x_{44}) I_1(x_{54}) + x_{44} Y_1(x_{44}) I_0(x_{54}) + \\ - x_5 a_3 Y_0(x_{43}) I_1(x_5 a_3) - x_{43} Y_1(x_{43}) I_0(x_5 a_3)\Big],$$

if $\bar{b} < n_4$. (D.8a)

$$\bar{F}_4 = \frac{1}{x_5^2 - x_4^2}\Big[x_{54} K_0(x_{44}) I_1(x_{54}) + x_{44} K_1(x_{44}) I_0(x_{54}) + \\ - x_5 a_3 K_0(x_{43}) I_1(x_5 a_3) - x_{43} K_1(x_{43}) I_0(x_5 a_3)\Big],$$

if $\bar{b} > n_4$. (D.8b)

Bibliography

[1] E. Desurvire, *Erbium-Doped Amplifiers: Principles and Applications,* John Wiley and Sons, 1994.

[2] T. J. Whitley, "A Review of Recent System Demonstrations Incorporating 1.3-*mm* Praseodymium-Doped Fluoride Fiber Amplifiers," Journal of Lightwave Technology, **13**, pp. 744-760, May 1995.

[3] A. E. Willner, and S. M. Hwang, " Transmission of Many WDM Channels Through a Cascade of EDFA's in Long-Distance and Ring Networks," Journal of Lightwave Technology, **13**, pp. 802-816, May 1995.

[4] N. S. Bergano, and C. R. Davidson, "Circulating Loop Transmission Experiments for the Study of Long-Haul Transmission Systems Using Erbium-Doped Fiber Amplifiers," Journal of Lightwave Technology, **13**, pp. 879-888, May 1995.

[5] B. J. Ainslie and C. R. Day, "A Review of Single-Mode Fibers with Modified Dispersion Characteristics," Journal of Lightwave Technology, **4**, pp. 967-979, August 1986.

[6] A. R. Chraplyvy, "Limitations on Lightwave Communications Imposed by Optical-Fiber Nonlinearities," Journal of Lightwave Technology, **8**, pp. 1548-1557, October 1990.

[7] D. Marcuse, "Single-Channel Operation in Very Long Nonlinear Fibers With Optical Amplifiers at Zero Dispersion," Journal of Lightwave Technology, **9**, pp. 356-361, March 1991.

[8] D. Marcuse, A. R. Chraplyvy, and R. W. Tkach, "Effect of Fiber Nonlinearity on Long-Distance Transmission," Journal of Lightwave Technology, **9**, pp. 121-128, January 1991.

[9] T. Li, “The Impact of Optical Amplifiers on Long-Distance Lightwave Telecommunications,” Proceedings of the IEEE, **81**, pp. 1568-1579, November 1993.

[10] R. H. Stolen and C. Lin,” Self-Phase Modulation in Silica Optical Fibers,” Physical Review A, **17**, pp. 1448-1453, April 1978.

[11] G. P. Agrawal, *Nonlinear Fiber Optics*, Academic Press, Boston, 1989.

[12] P. Nouchi, P. Sansonetti, S. Landais, G. Barre, C. Brehm, J. Y. Boniort, B. Perrin, J. J. Girard, and J. Auge, “Low-Loss Single-Mode Fiber with High Nonlinear Effective Area,” OFC’95, San Diego, CA, Technical Digest, pp. 260-261, 1995.

[13] J. P. Hamaide, F. Pitel, P. Nouchi, B. Biotteau, J. Von Wirth, P. Sansonetti and J. Chesnoy,” Experimental 10 Gb/s Sliding Filter-Guided Soliton Transmission up to 19 Mm with 63 km Amplifier Spacing Using Large Effective-Area Fiber Management,” Proceedings of ECOC’ 95, Brussels, Belgium, pp. 991-994, 1995.

[14] Y. Liu, A. J. Antos, and M. A. Newhouse, “Large Effective Area Dispersion-Shifted Fibers with Dual-Ring Index Profiles,” OFC ’96, San Jose, CA, Technical Digest, pp. 165-166, 1996.

[15] S. Arai, Y. Akasaka, Y. Suzuki, and T. Kamyia, “Low Nonlinear Dispersion-Shifted Fiber,” OFC ’97, Dallas, TX, Technical Digest, pp. 65, 1997.

[16] T. Kato, S. Ishikawa, E. Sasaoka, and M. Nishimura, “Low Nonlinearity Dispersion-Shifted Fibers Employing Dual-Shaped Core Profile with Depressed Cladding”, OFC’ 97, Dallas, TX, Technical Digest, pp. 66, 1997.

[17] M. Kato, K. Kurukawa, and Y. Miyajima, “A New Design for Dispersion-Shifted Fiber with an Effective Core Area Larger Than 100 mm^2 and Good Bending Characteristics,” OFC’ 98, San Jose, CA, paper ThK1, 1998.

[18] Y. Akasaka, and Y. Suzuki, “ Enlargement of Effective Core Area on Dispersion-Flattened Fiber and its Low Nonlinearity,” OFC’98, San Jose, CA, paper ThK2, 1998.

[19] P. Nouchi, ”Maximum Effective Area for Nonzero Dispersion-Shifted Fiber,” OFC’98, San Jose, CA, paper ThK3, 1998.

[20] A. Safaai-Jazi and H. T. Hattori, “Low Nonlinearity Dispersion-Shifted Fibers,” PIERS 97, Boston, MA, pp. 43, 1997.

[21] H. T. Hattori and A. Safaai-Jazi, “Fiber Designs with Significantly Reduced Nonlinearity for Very Long Distance Transmission,” Applied Optics, To be Published, 1998.

[22] Y. Namihira, “Relationship Between Nonlinear Effective Area and Modefield Diameter for Dispersion-Shifted Fibers,” Electronics Letters, **30**, pp. 262-264, February 1994.

[23] V. Bhagavatula et al., “Dispersion-Shifted Single-Mode Fiber for High-Bit-Rate and Multiwavelength Systems,” OFC’ 95, San Diego, CA, Technical Digest, pp. 259-260, 1995.

[24] E. S. Georges, “ Experimental Study of Four-Wave Mixing on Dispersion-Shifted Fiber and Low Dispersion Fibers with a Dense Multiwavelength Source,” OFC’ 97, Dallas, TX, Technical Digest, pp.67-69, 1997.

[25] Y. S. Jang, Y. C. Chung, “Four-Wave Mixing of Spectrum-Sliced Fiber Amplifier Light Source in a Dispersion-Shifted Fiber,” OFC’97, Dallas, TX, Technical Digest, pp.71-72, 1997.

[26] A. Safaai-Jazi, and H. T. Hattori, “Large-Effective-Area Dispersion-Flattened Fiber”, Microwaves and Optical Technology Letters, **16**, pp.327-328, December 1997.

[27] D. Gloge, “Weakly Guiding Fibers,” Applied Optics, **10**, pp. 2252-2258, October 1971.

[28] A. W. Snyder, and J. D. Love, *Optical Waveguide Theory*, Chappman and Hall, London, 1983.

[29] C. A. Balanis, *Advanced Engineering Electromagnetics*, John Wiley and Sons, New York, 1989.

[30] R. E. Collin, *Field Theory of Guided Waves*, Mc Graw Hill, New York, 1960.

[31] M. J. Adams, *An Introduction to Optical Waveguides*, John Wiley and Sons, Chichester, 1981.

[32] J. W. Fleming, “Material Dispersion in Lightguide Glasses,” Electronics Letters, **14**, pp. 326-328, May 1978.

[33] D. Gloge, “Dispersion in Weakly Guiding Fibers,” Applied Optics, **10**, pp. 2442-2445, November 1971.

[34] D. Marcuse, “Pulse Distortion in Single-Mode Fibers,” Applied Optics, **19**, pp. 1653-1660, May 1980.

[35] G. P. Agrawal, *Fiber-Optic Communication Systems*, John Wiley and Sons, New York, 1992.

[36] D. L. Frazen, “Determining the Effective Cutoff Wavelength of Single-Mode Fibers: An Interlaboratory Comparison,” Journal of Lightwave Technology, **3**, pp. 128-134, February 1985.

[37] G. Keiser, *Optical Fiber Communications*, 2nd Edition, Mc Graw Hill, New York, 1991.

[38] A. Iino and J. Tamura, “Radiation Resistivity in Silica Optical Fibers,” Journal of Lightwave Technology, **6**, pp.145-149, February 1988.

[39] R. H. West, “A Local View of Radiation Effects in Fiber Optics,” Journal of Lightwave Technology, **6**, pp. 155-164, February 1988.

[40] R. Olshansky, “Propagation in Glass Optical Waveguides,” Reviews of Modern Physics, **51**, pp.341-367, April 1979.

[41] R. Maurer, ”Glass Fibers for Optical Communications,” Proceedings of the IEEE, **61**, pp. 452-462, April 1973.

[42] D. Marcuse, “Microdeformation Losses of Single-Mode Fibers,” Applied Optics, **23**, pp.1082-1091, April 1984.

[43] A. Bjarklev, “ Microdeformation Losses of Single-Mode Fibers With Step-Index Profiles”, Journal of Lightwave Technology, **4**, pp. 341-346, March 1986.

[44] K. Furuya and Y. Suematsu, “Random-Bend Loss in Single-Mode and Parabolic-Index Multimode Optical Fiber Cables,” Applied Optics, **19**, pp. 1493-1500, May 1980.

[45] K. Petermann, “Theory of Microbending Loss in Monomode Fibers with Arbitrary Refractive-Index Profiles,” Arch. Elek. Obertragung, pp. 337-342, 1976.

[46] K. Petermann, "Constraints for Fundamental-Mode Spot Size for Broadband Dispersion-Compensated Single-Mode Fibres”, Electronics Letters, **19**, pp. 712-714, September 1983.

[47] D. Gloge, " Bending Loss in Multimode Fibers with Graded and Ungraded Core Index," Applied Optics, **11**, pp. 2506-2513, November 1972.

[48] A. W. Snyder, I. White and D. J. Mitchell, "Radiation From Bent Optical Waveguides," Electronics Letters, **11**, pp. 332-333, July 1975.

[49] J. Sakai and T. Kimura, "Bending Loss of Propagation Modes in Arbitrary-Index Profile Optical Fibers," Applied Optics, **17**, pp. 1499-1506, May 1978.

[50] I. A. White, "Radiation From Bends in Optical Waveguides: the Volume-Current Method," Microwaves, Optics and Acoustics, **3**, pp. 186-188, September 1979.

[51] H. F. Taylor, "Bending Effects in Optical Fibers," Journal of Lightwave Technology, **2**, pp. 617-628, October 1984.

[52] D. Marcuse, "Field Deformation and Loss Caused by Curvature of Optical Fibers," Journal of the Optical Society of America, **66**, pp. 311-320, April 1976.

[53] D. Marcuse, *Theory of Dielectric Optical Waveguides, 2nd edition*, Academic Press, New York, 1991.

[54] A. Hasegawa and Y. Kodama, "Signal Transmission by Optical Solitons in Monomode Fiber, " Proceedings of the IEEE, **69**, pp. 1145-1150, September 1981.

[55] L. M. Mollenauer, J. P. Gordon, and M. N. Islam, "Soliton Propagation in Long Fibers with Periodically Compensated Loss," IEEE Journal of Quantum Electronics, **22**, pp. 157-173, January 1986.

[56] N. J. Doran and K. J. Blow, “Solitons in Optical Communications,” IEEE Journal of Quantum Electronics, **19**, pp. 1883-1888, December 1983.

[57**]** A. Safaai-Jazi, and L. J. Lu, “Evaluation of Chromatic Dispersion in W-Type Fibers,” Optics Letters, **14**, pp. 760-762, July 1989.

[58] L. G. Cohen, W. L. Mammel, and S. J. Jang, “ Low-Loss Quadruple-Clad Single-Mode Lightguides with Dispersion Below 2 ps/nm.km Over the 1.28-1.65 *mm* Wavelength Range,” Electronics Letters, **18**, pp. 1023-1024, November 1982.

[59] V. A. Bhagarvatula, M. S. Spotz, W. F. Love, and D. B. Keck, “Segmented-Core Single-Mode Fibres with Low Loss and Low Dispersion,” Electronics Letters, **19**, pp. 317-318, April 1983.

[60] R. H. Hardin and F. D. Tappert,” Applications of the Split-Step Fourier Method to the Numerical Solution of Nonlinear and Variable Coefficient Wave Equations,” SIAM Review Chronicle, **15**, pp. 423, 1973.

[61] A. Yariv, *Optical Electronics in Modern Communications,* 5^{th} edition, Oxford University Press, Oxford, 1997.

Vita

Haroldo Takashi Hattori was born in São José dos Campos, Brazil on October 22, 1965. He obtained a BS in Electrical Engineering from Instituto Tecnológico de Aeronáutica in 1988. Upon graduation, he joined Elebra Telecom as a design engineer. In 1991, he joined Alcatel where he designed optical line equipments, and also was pursuing his MS degree in Electrical Engineering at Instituto Tecnológico de Aeronáutica. Taking leave from Alcatel, Mr. Hattori enrolled in the Ph.D. program in Electrical Engineering at Virginia Tech. His research interests include optical communications, electromagnetics and wireless communications. Mr. Hattori is a member of the IEEE, Eta Kappa Nu and Phi Kappa Phi.